FRICTION-BASED MONOPILE SEA FASTENING

Analyzing and improving the standard for obtaining an accurate coefficient of friction

B. Schrijvers

TU Delft

TWD

Source of cover image: internal image DEME (2018)

FRICTION-BASED MONOPILE SEA FASTENING

Analyzing and improving the standard for obtaining an accurate coefficient of friction

By

B. Schrijvers

in partial fulfilment of the requirements for the degree of

Master of Science
in Structural Engineering

at the Delft University of Technology.

Thesis committee:	Dr. A. Cicirello	TU Delft
	Dr. A. Cabboi	TU Delft
	Dr. Ir. P. Van Der Male	TU Delft
	Ir. E. Sulollari	TU Delft
	Ir. J. Remmers	TWD
	Ir. G. Vletter	TWD

Preface

This thesis is the final work to complete my Master degree in Structural Engineering at Delft University of Technology. This research studies improvements to the standard used to determine friction coefficients for friction-based monopile sea fastening.

I would like to thank everyone who helped to realize this work. I am grateful that I was able to work with such a diverse committee with a great drive to help me ensure the success of this thesis. I would like to thank Alice Cicirello for chairing the committee and guarding the research methodology. The research tips and theoretical explanations of Alessandro Cabboi in the bi-weekly meetings were of great value. Therefore, I would like to express my gratitude to him. I would like to thank Pim van der Male for bringing his offshore engineering expertise to our meetings. I also want to thank Enxhi Sulollari for her feedback related to friction theories and research methodology. Special thanks are given to Joost Remmers, my daily supervisor at TWD. Thanks for showing that simple tests can already provide relevant insights, for honest and direct feedback and the tips to improve my writing. I also want to thank Guido Vletter for looking at the bigger picture and the overall quality of the work.

I want to thank TWD for the opportunity to graduate in such an innovative and inspiring environment. I would like to thank my colleagues for helping or distracting me whenever needed. Finally, I want to thank my family and friends for their support at all times.

Bart Schrijvers
Rotterdam, August 2022

Summary

Larger offshore wind turbines are being built to meet the increasing worldwide demand for offshore renewable energy. These larger turbines require larger monopiles, the most used foundations for offshore wind turbines. Sea fastening is required for safe transport of monopiles to offshore locations. The current monopile sizes extend the width of the vessels. This makes sea fastening with fixed constraints undesirable because off the high costs. Friction-based sea fastening is a good alternative, since it does not require large outboard structures. Support pads on the sea fastening structure function as friction interface with the monopile surface.

The current design standard prescribes either a static coefficient of friction for a limited set of materials or provides a very basic test standard to determine project specific static friction coefficients. Literature mentions several factors that affect friction which are not stated for the predetermined static friction coefficients (e.g. coating, temperature, pressure). This means that the predetermined static friction coefficients are either unsafe or conservative. Several factors to consider while testing friction are missing as well (e.g. temperature, rate of loading). Another problem with the test standard is that no test setup or methodology is specified. The design coefficient of friction is determined with a characteristic coefficient and a material factor. It is unknown what the safety factor should cover and if these measures are sufficient. This makes the current design standard not suitable for application.

Therefore, this research investigates how the current design standard should be improved, specifically for monopile sea fastening with polymers. Literature and results from tests performed previously to this research are investigated in order to obtain a complete overview of the factors that should be considered in the design standard. Additional tests are carried out on factors for which literature and previous test exercises are unconclusive. Friction test methods are compared to determine the best method for testing monopile sea fastening friction. The total test variability is analyzed to determine why safety measures are required. The validity of these measures is studied with a large set of test results. Finally, modelling as an alternative for testing is investigated.

Ten factors that affect friction follow from literature and results from previous test campaigns at the TWD lab: hardness of support pads (1), viscoelastic properties of support pads (2), monopile roughness (3), roughness of support pads (4), monopile coatings (5), applied pressure (6), lubrication (7), rate of loading (8), temperature (9) and consolidation time (10). These factors are visualized in a monopile sea fastening application in Figure I. The effect on friction of the factors pressure, lubrication and consolidation time could be extracted from both literature and previous test exercises. Literature and previous test exercises indicate an effect of hardness, monopile roughness, temperature and viscoelasticity on friction, but do not provide a coherent answer on these effects.

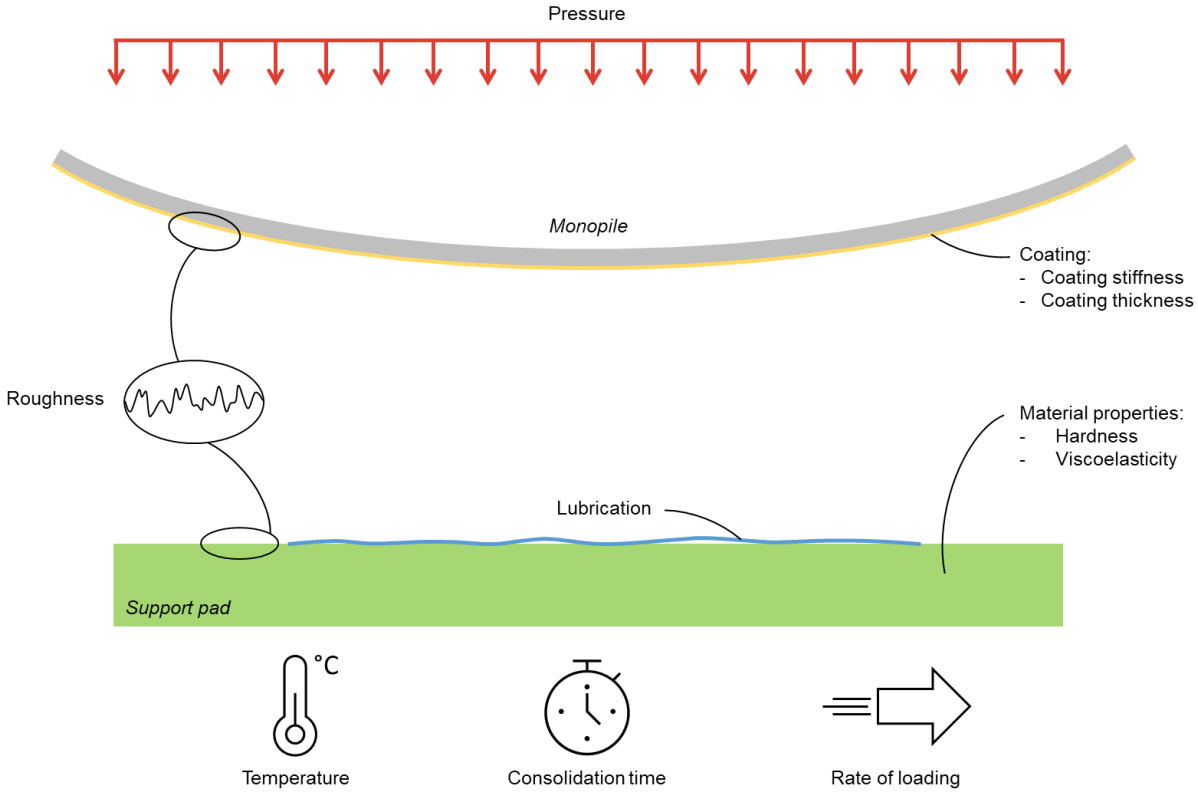

Figure I. Overview of factors affecting friction

A test campaign of 120 tests is performed to investigate the effects of hardness, monopile roughness, temperature and viscoelasticity. The friction increased with increasing hardness and increasing monopile roughness. The increase in friction for an increase in hardness can be related to an increase in local shear strength, which is dominant over the decrease in real contact area, the area of asperities in contact on a micro-scale level. For an increase in monopile roughness, the increase in real contact area explains the increase in friction. The results of temperature do not align with expectations, which might be caused by the way the PU samples are supported, loose samples in a holder or samples casted on a steel back plate. There are no conclusive results for the effect of viscoelastic properties on friction, since this research attempted to use the temperature dependency of the viscoelastic properties to determine the effect. Determining the viscoelastic properties was not possible, since the surface temperature could not be measured exactly. The test standard should specifically prescribe all ten factors to be represented in friction tests. Prescribed friction values are not advised, since it would be too extensive to cover all combinations of conditions.

The horizontal plane, vertical plane, inclined plane and the pin-on-disk test method are highlighted and compared. The criteria for the comparison are based on the ability to obtain a static friction coefficient, to obtain a force-displacement graph and to represent all factors that affect monopile sea fastening friction. The inclined plane method is not able to test with a constant pressure. The pin-on-disk method focusses on kinetic friction and is not able to accurately determine static friction coefficients. The

horizontal plane and vertical plane method meet all criteria and are thus the best methods for testing monopile sea fastening friction. The test standard should prescribe these methods for friction tests.

Modelling of pre-sliding displacements in a force-displacement graph is investigated with the Dahl model. Pre-sliding displacements can be used to determine the force distribution over the supporting cradles. The pre-sliding displacements are not included in a friction coefficient. Although the model fits very well with test data, no correlation is found between the model parameters and friction factors. It is not yet realistic to replace friction tests by a friction model.

A characteristic friction coefficient is selected from the friction coefficients measured in a test series. A material factor is applied to this value to obtain a design friction coefficient. The current test standard prescribes a material factor of 1.4 and a characteristic value that is the 5^{th} percentile of the test results. The effect of wear on friction and unexpected effects should be covered by the material factor. The current material factor is insufficient, because the differences between friction coefficients can already be larger than 1.4 when conditions are not considered. The difference between the friction coefficients measured at cold and room temperature is already larger, without even considering wear and unexpected effects. It is recommended to consider all conditions, rather than applying material factors to cover this. The 5^{th} percentile should cover the total test variability. It deems that the 5^{th} percentile is very conservative since the size of the cradle is much larger than the tested samples. Determining the characteristic friction coefficient as mean could be an alternative for the 5^{th} percentile.

Friction tests should be performed with the horizontal plane or vertical plane method, as these can represent the monopile sea fastening friction conditions. The representative materials should be tested considering hardness, viscoelastic properties, roughness and coating. Lubrication should be applied and a representative consolidation time minutes should be considered. For the pressure, rate of loading and temperature it is required to perform sensitivity tests to determine the conservative case. Considering these test conditions results in a safe and economical friction-based monopile sea fastening design.

Contents

1 Introduction

1.1 Background

The offshore wind industry is increasing. In 2020, offshore windfarms in Europe (belonging to countries within the EU) generated a total amount of 12 GW of energy. The European Commission aims to increase this capacity to 60 GW in 2030 and 300 GW in 2050 (European Commission, 2020). According to the Dutch Climate Agreement, offshore wind energy even has the potential to become the most significant green power source for the Netherlands (Dutch Government, 2019). To realize these goals, the number of windmills, as well as the capacity of individual windmills, is increased. Increasing the capacity and thus the size of wind turbines requires larger monopiles (TNO, n.d.). These larger monopiles also need to be sea fastened which results in geometrical challenges.

Monopiles are the most used foundations for offshore wind turbines (Kaynia, 2019). The main task of these tubular steel structures, as windmill foundations, is to support the wind turbine and transfer the loads to the subsoil (TNO, n.d.). Vessels are used to transport the monopiles to the offshore windfarm location. During transport, waves and current cause vessel motions, which impact the structures transported. Monopile sea fastening installations are necessary to ensure monopile stability under accelerations caused by the vessel motions. Constraining the monopile on both ends is traditionally applied as sea fastening. These traditional sea fastening structures are present on the depicted vessel in Figure 1.1. In Figure 1.2 the monopiles have been placed in the sea fastening.

Figure 1.1. Vessel with traditional sea fastening for monopiles (adjusted Windenergie Nieuws, n.d.)

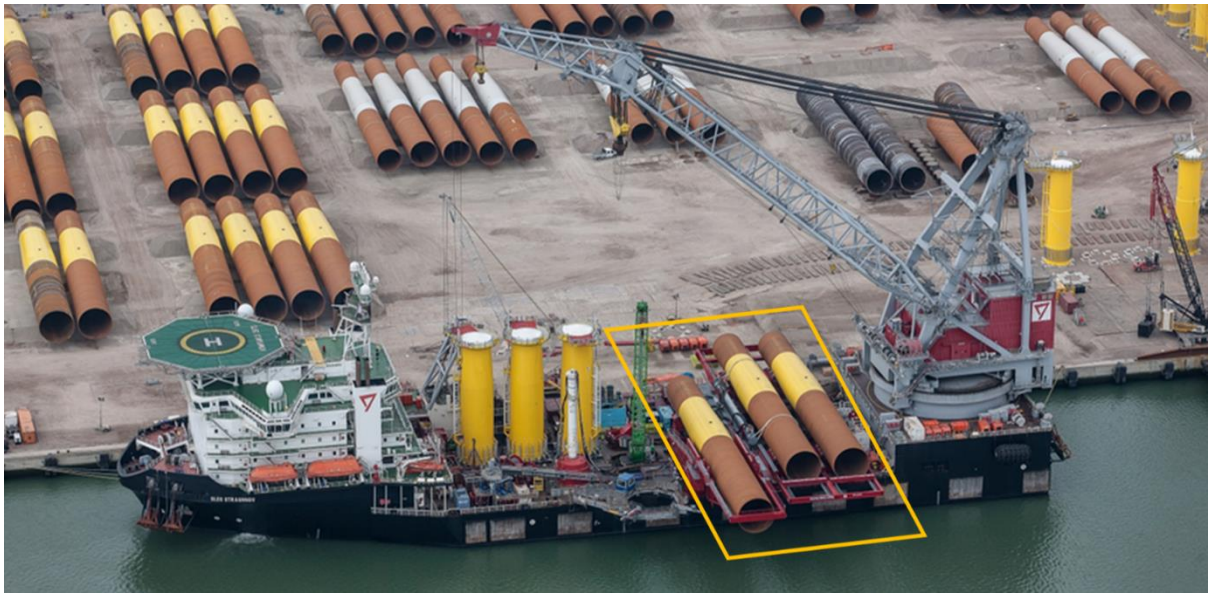

Figure 1.2. Monopiles in traditional sea fastening (adjusted DT Hydraulics, n.d.)

The size of the vessels on which the monopiles are transported cannot grow at the same rate as the size of the monopiles. In most cases, sea fastening with fixed constraints is only possible by means of a different orientation or using large outboard structures, as in Figure 1.1 and Figure 1.2. The different orientation of the monopiles is not desirable since cranes used for the monopile installation do not always have sufficient capacity to lift. Large outboard structures are not desirable since these structures become complicated and expensive, considering the larger cantilever. Friction-based sea fastening without fixed constraints would thus be a good alternative (Figure 1.3). In this way, the monopile is supported by cradles only. On these cradles, rubber, polyurethane (PU), or wooden supports are often used as friction interfaces (Figure 1.4). These contact areas must resist the inertial loads induced on the monopile by vessel motions.

Figure 1.3. Friction-based monopile sea fastening (DEME, 2018)

(a) *(b)*

Figure 1.4. Support interface of monopile sea fastening: (a) sea fastening structure (DEME, 2016)*, (b) support pad (made on 28-4-2022)*

1.2 Problem description

A design standard developed by DNV is used to determine friction coefficients for offshore applications, which includes friction-based monopile sea fastening. This design standard describes two methods for determining a friction coefficient. The first method is to use prescribed friction coefficients by DNV. In the second method the friction coefficients are determined with tests, according to a DNV test standard.

1.2.1 Prescribed friction coefficients

DNV lists friction coefficients for limited sets of materials (DNVGL-ST-N001 11.9.2, 2020). Both wet and dry conditions are considered. For all friction coefficients prescribed, it is required that no oil or other lubricating fluids are present at the interface. There are also upper bound friction coefficients mentioned when the cargo is supported by cribbing only (DNVGL-ST-N001 11.9.2, 2020). The upper bound values depend on the cargo weight and the cargo overhang. From scientific literature, it is known that other factors affect the friction coefficient as well (hardness, roughness, temperature, viscoelastic properties, consolidation time, coating, rate of loading) (Archard, 1974; Bowden & Tabor, 1966; Briscoe & Tabor, 1978; Capanidis & Sokolska, 2020; Dillavou & Rubinstein, 2019; Ivkovic et al., 2000; Laber, 2012; Myshkin et al., 2005; Richardson & Nolle, 1976). These factors are not incorporated in the prescribed values. This makes the prescribed friction coefficients either unsafe or too conservative.

1.2.2 Testing friction

No test setup or procedure is mentioned in the test standard of DNV. This is a problem since not every test setup or procedure is suitable of representing relevant monopile sea fastening friction behavior.

The DNV standard on testing friction is not clear on the factors which should be considered during tests (see standard below). The testing conditions should represent the expected friction surface and load intensity as close as possible (DNVGL-ST-N001 5.4.4, 2020). The expected surface might refer to the materials that are used with a certain hardness and roughness, but these factors are not specifically mentioned. The load intensity is a clear referral to the pressure which is present at the friction interface. One other factor is specifically mentioned, namely wet and dry surfaces (lubrication). Consolidation time, temperature, and geometry are not mentioned in the standard.

The standard mentions that at least five samples need to be tested twice. There are no rules that state how these tests should be performed. Determining the coefficient of friction from tests is another essential part that is not mentioned. There are guidelines on how to use the obtained coefficient of friction in design. In case of monopile sea fastening the characteristic coefficient of friction should be based on the 5th percentile, since lower friction is conservative. To obtain the design value of the coefficient of friction, the characteristic value should be divided by a material factor. Based on the number of tests performed, this material factor can increase or decrease. Specific values and the amount of tests required for an increase or decrease are not provided. It is unknown what the material factor covers and whether these safety measures are sufficient.

Current standard for monopile sea fastening friction tests (DNVGL-ST-N001 5.4.4, 2020)

1. Testing may be carried out in order to establish applicable friction coefficients. The testing conditions should represent the expected friction surfaces and load intensity as close as possible.
2. Where testing is carried out, a detailed test procedure shall be documented.

   Guidance note:

   The test procedure should consider the following

   a) Possible variations in applicable conditions (e.g. wet and dry conditions). See [1].

   b) The characteristic friction coefficient should be defined based on the 5th percentile confidence level of the test results.

   c) At least 5 test pieces should be made, and each tested at least twice for each actual condition.

   d) The design friction coefficient is calculated using the characteristic friction coefficient and an appropriate material factor. See [3].

   e) Where fewer tests are performed e.g. because of the scale, more conservative material factors should be used.

   f) Where a greater number of tests are performed, less conservative material factors may be justified and used.

3. A material factor of minimum $\gamma_m = 1.4$ should normally be used to calculate the lower bound design friction coefficient for load bearing friction effects

Guidance note 1:

In each case, the design friction coefficient should be obtained by dividing the characteristic friction coefficient by the material factor.

Guidance note 2:

Where less conservative material factors have been justified, the factor used to calculate the lower bound design coefficient should not be reduced below 1.25.

1.2.3 Friction behavior

Often only the coefficient of friction is mentioned when friction is considered. However, the behavior to reach that amount of friction is also important. Some pre-sliding displacements are present before the interface has reached its highest friction. These pre-sliding displacements can affect the load distribution over the cradles. The load distribution is currently calculated based on the normal force on the cradle and the determined friction coefficient. This may be correct in the case of maximal friction, but the distribution can be different when the friction is not completely build up yet.

1.2.4 Problem statement

The problem is summarized in a problem statement. The problem statement is *the friction testing standard to validate monopile stability is incomplete, unsafe and not economical*.

1.3 Objective

This research investigates *how the current friction design standard should be improved to validate monopile stability during sea fastening*. The following sub questions contribute to the main research question:

1. Factors that affect friction

What factors influence sea fastening friction tests?
What is the effect of the factors on friction?
Why are specific effects of the factors on friction observed?

2. Testing friction

What are existing test methods?
What test method is best for sea fastening friction tests?
What test setup is best for sea fastening friction tests?

3. Modelling

What models can be used to describe static friction?
What are correlations between model parameters and factors that affect friction?

4. Safety

What uncertainties are present in monopile sea fastening?
In what way do safety factors relate to factors that affect friction?
What are possible improvements for safety in design?

Scope

This research will focus on friction measurements done for friction-based monopile sea fastening. Therefore, only the factors (and the ranges) applicable to this situation are studied in this research. Materials used in this study are steel (blank, coated, corroded) and polymers (different material properties). Polymers are studied since this material is most common in current practice, as it does not damage the coating on the monopile and it is flexible and strong.

Wear is not included in the scope of this research. Wear is affected by conditions similar to friction, but measurements do not yet show a correlation between the amount of friction and the amount of wear (Bartenev et al., 1981; Briscoe & Tabor, 1978; Popov, 2010).

1.4 Research structure

In Chapter 2, friction definitions and developments are introduced that follow from a literature study.

1. Factors that affect friction

The factors that affect friction are investigated one by one in Chapter 3. Correlations between the factors and the coefficients of friction are investigated, based on literature and previous test data. The observed effects are explained with theories from Chapter 2. The factors that affect friction are related to monopile sea fastening by boundary conditions relevant to monopile sea fastening. For several factors the effect on friction is indicated in literature and previous test data, but additional research is necessary to prove correlation. A dedicated test campaign will be performed to prove these effects for several factors.

2. Friction testing

Friction test methods are explained, based on existing standards and literature. A set of criteria which a test method for monopile sea fastening friction test should meet is defined. Once the set of criteria is known, the tests are compared. This results in the best method to test monopile sea fastening friction. The test method and the test procedure used in this research are highlighted.

3. Modelling

Chapter 6 focusses on the relevance of friction modelling and how these models can be used in practice. A comparison between several models is made, based on the ability to model pre-sliding displacements and the complexity of the model. The effect of the model parameters on the force-displacement graph is explained. A strategy to fit the model to the test data is set and carried out. Correlations are investigated between model parameters and factors that affect friction

4. Safety

This part investigates why material factors are required and if the material factors are sufficient. Therefore, the uncertainties and the variability in the tests is analyzed. The existing determination of the characteristic value for the friction coefficient (5^{th} percentile) prescribed in DNVGL-ST-N001 5.4.4 (2020) is applied on an example. An alternative for determining the characteristic value is studied.

2 Theory & definitions

This Chapter focusses on establishing a general understanding of friction. It provides definitions that will be used in the remainder of this study. Theories from previous research are highlighted and are used in Chapter 3 to explain relevant effects that factors have on friction.

2.1 Friction fundamentals

Friction is defined as the reaction force between two surfaces in contact (Briscoe & Tabor, 1978; Myshkin et al., 2005; Olsson et al., 1997). The two surfaces are subjected to a normal force. A tangential force, perpendicular to the normal force, is applied to initiate relative motion of the surfaces. This motion is resisted by the friction force (Figure 2.1).

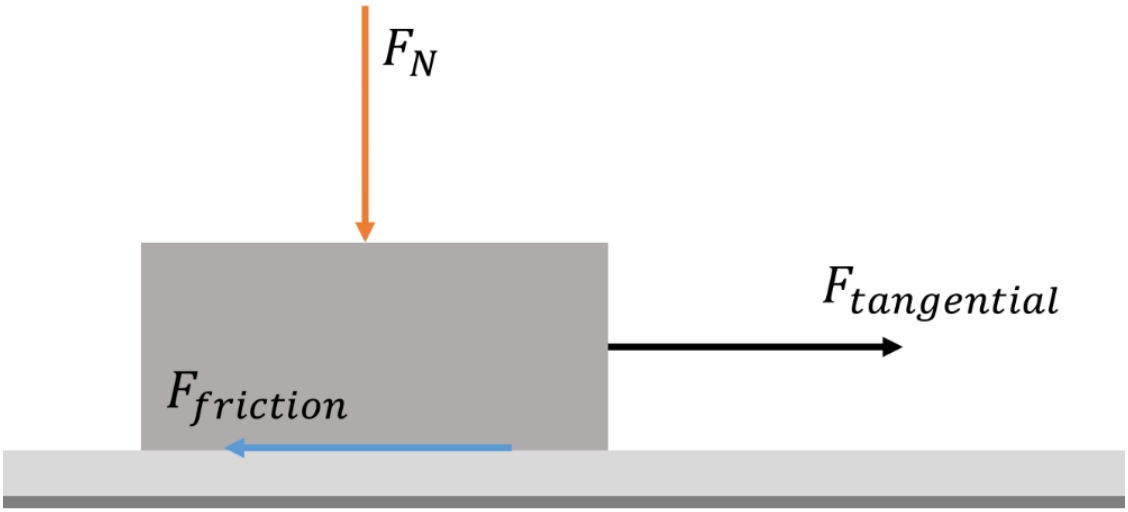

Figure 2.1. Forces acting on a friction interface

2.1.1 Static friction (pre-sliding)

Friction can be divided in static and kinetic friction. Static friction is present when two surfaces in contact are not moving relative to each on macro-scale. In the static regime, pre-sliding displacements are present. Asperity junctions break and deform which result in pre-sliding displacements. By an increasing force, more and more junctions will break and deform resulting in more displacement and eventually in break-away (Balci, 2021; Swevers et al., 2000). The force which is required to start global relative movement of the surfaces is called static friction force.

2.1.2 Kinetic friction

When two surfaces are moving relative to each other, kinetic friction is considered (Berman et al., 1996; Briscoe & Tabor, 1978; Yoshizawa et al., 1993). Kinetic friction can be divided into sliding and dynamic friction. Sliding friction is the friction when a constant force is present for the displacement of the object, without large fluctuations in the applied force (Tonazzi et al., 2015). In other cases, the sudden tangential force-drops large are followed by periods of tangential force increase, this is called dynamic or stick-slip friction (Tonazzi et al., 2015). Several studies relate pressure, velocity, lubrication and temperature to the appearance of stick-slip over continuous sliding. At higher pressures stick-slip will occur more often (Tonazzi et al., 2015; Viswanathan et al., 2016; Zuleeg, 2015). Stick-slip will also occur more often for lower velocities (Lundgren, 2016; Tonazzi et al., 2015; Viswanathan et al., 2016). Under the presence of lubrication, stick-slip will occur less often (Dong et al., 2017; Zuleeg, 2015). The effect of temperature is only mentioned, but not elaborated (Zuleeg, 2015). Sliding friction and dynamic (stick-slip) friction are shown in Figure 2.2. The friction force in the kinetic regime is, in most cases, smaller than the static friction force (Briscoe & Tabor, 1978; Rabinowicz, 1951).

Friction measurements are often presented in a force-displacement graph. In these graphs, the transition from the static to the kinetic regime is clearly visible in some cases. In Figure 2.2 this is the case. The tangential force is increasing until it drops at a certain displacement. This is called the point of transition from static to kinetic friction. In other cases, this transition is less clear and the transition could be pinned to a transition region.

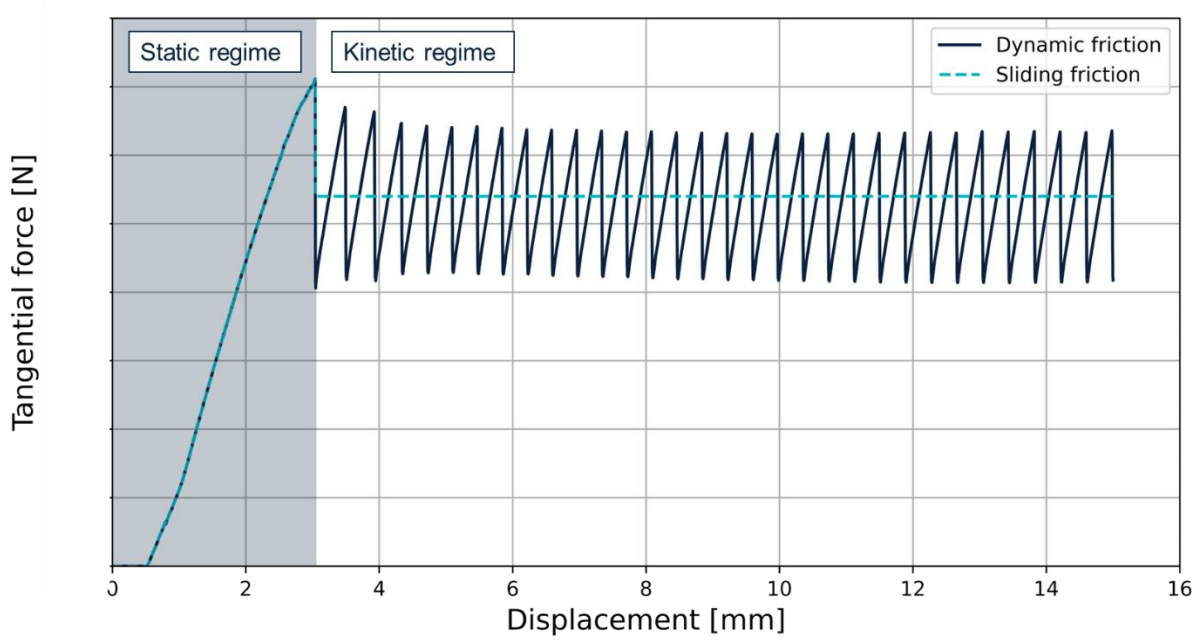

Figure 2.2. The static and kinetic regime in friction graph (dynamic friction curve based on test with polyurethane and steel, see Appendix A)

2.2 Literature study

2.2.1 Da Vinci

The first recorded systematic studies regarding friction were performed by Leonardo Da Vinci (Gao et al., 2004). In Figure 2.3a the simple test setup is displayed. Da Vinci connected weights to a block on a horizontal plane to determine the friction force that was required to move the block (Hutchings, 2016). According to Hutchings (2016), it can be assumed that Da Vinci used wood as material for his experiments. Da Vinci made two important observations (Gao et al., 2004; Hutchings, 2016):

1. When the mass of the block is doubled, the friction force is doubled as well, so the friction depends on the load pressing the two surfaces together.
2. The friction force is independent of the area. He made this conclusion by comparing the friction of the same block in different positions on the horizontal plane (Figure 2.3b).

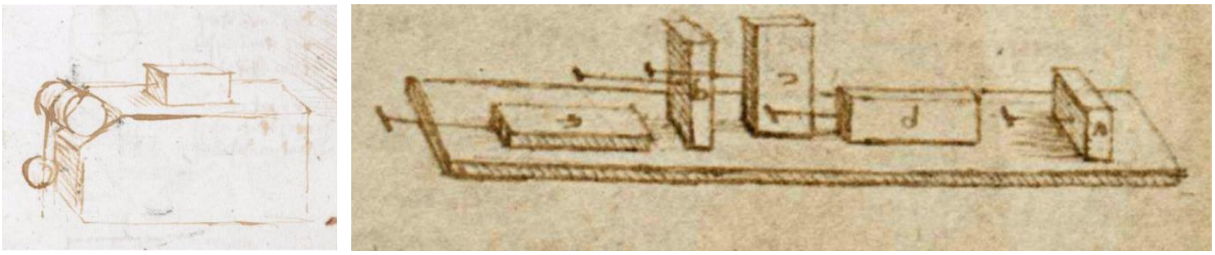

(a) *(b)*

Figure 2.3. Da Vinci friction tests: (a) test setup, (b) same test block in different positions (Hutchings, 2016)

2.2.2 Amontons and Coulomb

Amontons rediscovered these observations made by Da Vinci. When Coulomb studied the friction of wood, he made the same observations and added that friction is independent of velocity (Gao et al., 2004; Popova & Popov, 2015). The following observations were made:

- Friction is dependent on the applied load
- Friction is independent of the contact area
- Friction is independent of the sliding velocity

Formula 2.1 can be obtained based on the observations of Coulomb. In this Formula, $F_{friction}$ is the force that is applied to initiate movement between two surfaces. The normal force which presses both surfaces together, is F_N. The ratio between these forces is the coefficient of friction μ.

$$\mu = F_{friction}/F_N = constant\ (independent\ on\ area\ and\ velocity) \qquad 2.1$$

The main idea, supporting these observations, is that the asperities of one surface must slide over the asperities of the other surface to establish or maintain sliding (Bowden & Tabor, 1966; Gao et al., 2004).

For each asperity, an individual force is required to lift over the asperity. This force is equal to the applied normal load ($F_{N,i}$) multiplied by $tan(\theta_i)$, where the maximum slope of the asperity is θ. The sum of these individual forces is the friction force, see Formula 2.2 (Gao et al., 2004). This results in the same equation as in Formula 2.1.

$$F_{friction} = \sum F_i = \sum F_{N,i} \cdot tan(\theta_i) = \mu \cdot F_N \qquad 2.2$$

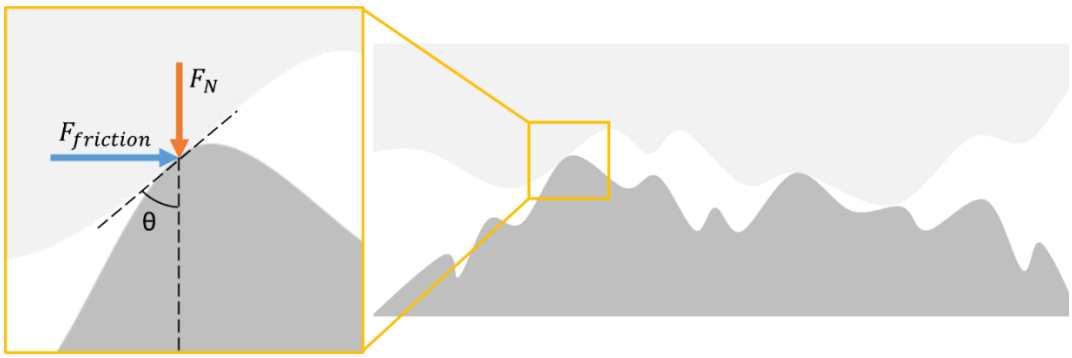

Figure 2.4. Schematic representation Formula 2.2

2.2.3 Bowden, Briscoe and Tabor

Bowden and Tabor made the distinction between two friction components in steel-polymer friction, namely adhesion and deformation. This deformation component consists of ploughing, grooving and cracking (Bowden & Tabor, 1966; Briscoe & Tabor, 1978). Both components have different energy dissipation regions (Figure 2.5a). In these regions, friction can be build up by energy dissipation. The interfacial region, the thin region near the surface, is related to adhesion. The friction resistance is here established by plastic shear or fracture. Adhesion does not cause films of polymer to be transported (Briscoe & Tabor, 1978). Ploughing is related to the bulk region, which is larger than the interfacial region. In this region, friction is caused by gross plastic flow losses or viscoelastic losses (Figure 2.5b). Gross plastic flow can cause the transfer of polymer films and is dominant in rolling friction and properly lubricated sliding friction (Briscoe & Tabor, 1978).

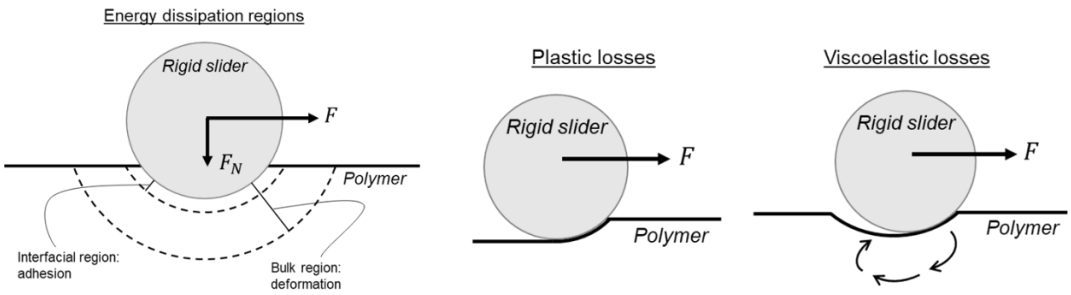

(a) *(b)*

Figure 2.5. Friction components. (a) Energy dissipation regions, (b) Deformation processes (Briscoe & Tabor, 1978)

According to Bowden & Tabor (1966) and Briscoe & Tabor (1978), the interaction between adhesion and deformation can be neglected, thus they can be treated separately. They formulate that friction caused by adhesion is dependent on the real contact area (A_R) and the shear strength (τ). The real contact area is the area of two surfaces that is in actual contact, caused by asperities that are touching on a micro-scale level. This is different from the apparent contact area (A_A), which is the contact on macro-scale. Friction caused by deformation is covered by a component P. Plastic and viscoelastic losses contribute to this deformation component. Formula 2.3 presents these dependencies and can be applied both in the static and the sliding regime (Briscoe & Tabor, 1978).

$$F_{friction} = F_{adhesion} + F_{deformation} = \tau \cdot A_R + P \qquad 2.3$$

2.3 Definitions

List of definitions used in this research

- Friction force – the reaction force between two surfaces in contact
- Normal force – the force that brings two surfaces in contact, perpendicular to sliding plane
- Tangential force – the force applied to initiate relative motion of the surfaces in contact
- Static friction – friction that is present without relative motion of the surfaces in contact
- Kinetic friction – friction that is present with relative motion of the surfaces in contact
- Transition point – the point where relative motion of the surfaces in contact starts
- Dynamic friction – kinetic friction with large fluctuations in the force-displacement graph in which memory effects and hysteresis influences friction
- Sliding friction – kinetic friction without fluctuations in the force-displacement graph
- Stick-slip friction – kinetic friction with sudden tangential force-drops followed by periods of tangential force increase
- Pre-sliding displacement – friction displacements that occur in the static regime
- Real contact area – the area of two surfaces that is in actual contact, caused by asperities that are touching on a micro-scale level
- Apparent contact area – the area of two surfaces that are in contact on macro-scale

3 Factors that affect friction

In the current test standard only a few factors are considered. This Chapter investigates the factors related to monopile sea fastening friction. These factors are visualized in Figure 3.1 and will be treated independently in this Chapter. They can be split in three categories:

1. Support pad factors: material properties and roughness of the support pad (treated in Section 3.1 and Subsection 3.2.2 respectively)
2. Counter material factors: monopile roughness, coating type and coating thickness (treated in Subsection 3.2.1 and Section 3.3)
3. Environmental, operational and loading factors: applied pressure, lubrication, rate of loading, temperature, consolidation time (treated in Sections 3.4 to 3.8)

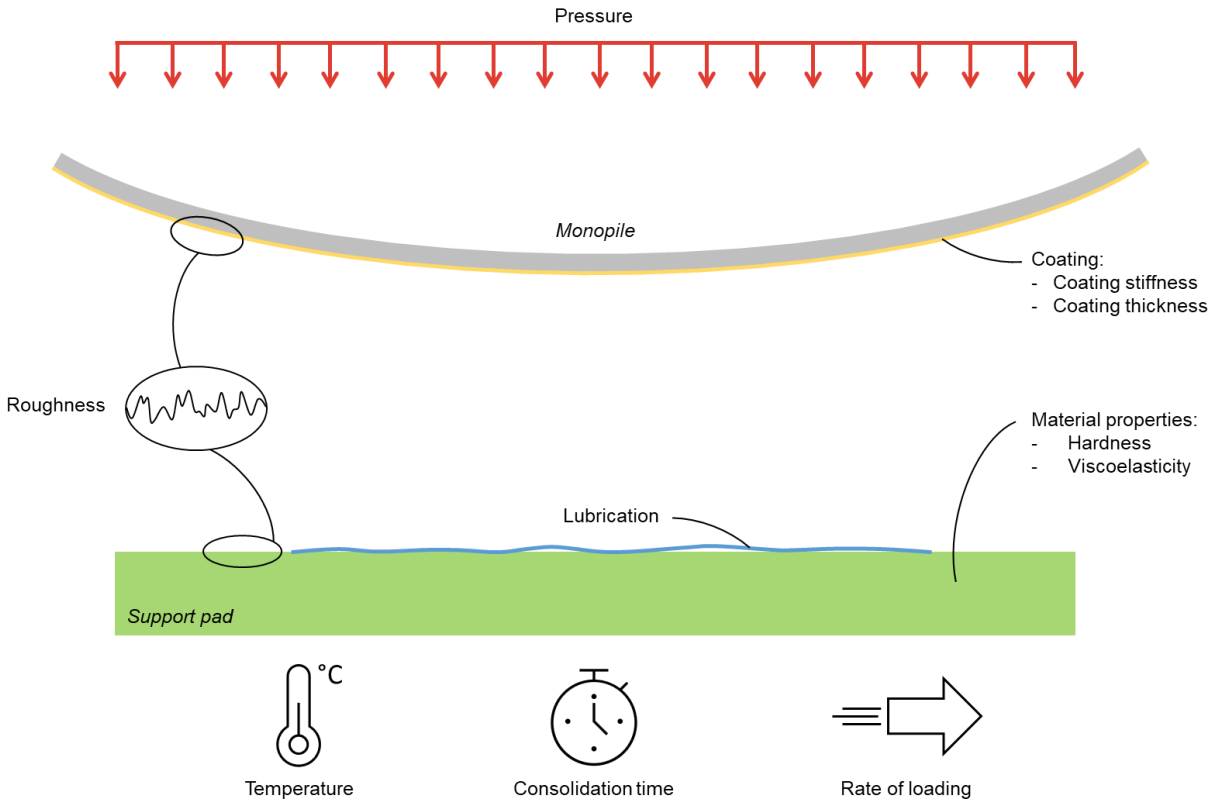

Figure 3.1. Overview of factors that affect friction in monopile sea fastening (Figure made on 18-4-2022)

3.1 Material properties of support pads

Polymers are often used as supporting material in monopile sea fastening structures (Section 1.1). The material properties of these polymers affect their frictional behavior (Bowden & Tabor, 1966; Briscoe & Tabor, 1978). The most mentioned material properties in the studies of Bowden & Tabor (1966) and Briscoe & Tabor (1978) are hardness and viscoelasticity.

3.1.1 Hardness

Hardness is the resistance that a solid shows to local (plastic) deformation (Sakaguchi et al., 2019; Tabor, 1970). Hardness can be expressed in different quantities: Vickers, Knoop, Barcol, Brinel, Rockwell and Shore hardness (Sakaguchi et al., 2019; Tabor, 1970). The hardness of polymers is often expressed in °Shore A and °Shore D. Shore hardness measurements can be performed with measurement devices comparable to the device depicted in Figure 3.2. The device has a pin on the bottom that is placed on the material. Based on the displacement of the pin, the hardness is obtained and can be read from the device (ASTM D2240, 2000; DIN 53505, 2000; NEN-EN-ISO 868, 2003).

Figure 3.2. Shore hardness measurement of a polyurethane (pictures made on 19-4-2022)

In a study of Briscoe & Tabor (1978) hardness is related to the real area of contact of a friction interface. They suggest that the total load F_N (in N) divided by the hardness (in N/mm^2) is equal to the real contact area (Formula 3.1). This indicates that the real contact area would decrease for materials with a higher hardness. If the other components, the shear stiffness and the deformation component, remain constant, the friction resistance would decrease for materials with a higher hardness, according to the Formula 3.1 (Briscoe & Tabor, 1978).

$$A_R = \frac{F_N}{hardness} \qquad 3.1$$

The effect of hardness on friction has been tested by Capandis & Sokolska (2020). The study tested friction for polyurethane and the counter material steel. The friction resistance decreased for increasing hardness, when tested in dry conditions (Figure 3.3). Tests performed in wet conditions resulted in a different effect (Capanidis & Sokolska, 2020). The two hardness extremes (75 and 93 °Shore A) had less friction resistance than the middle hardness samples (80 and 83 °Shore A) (Figure 3.4).

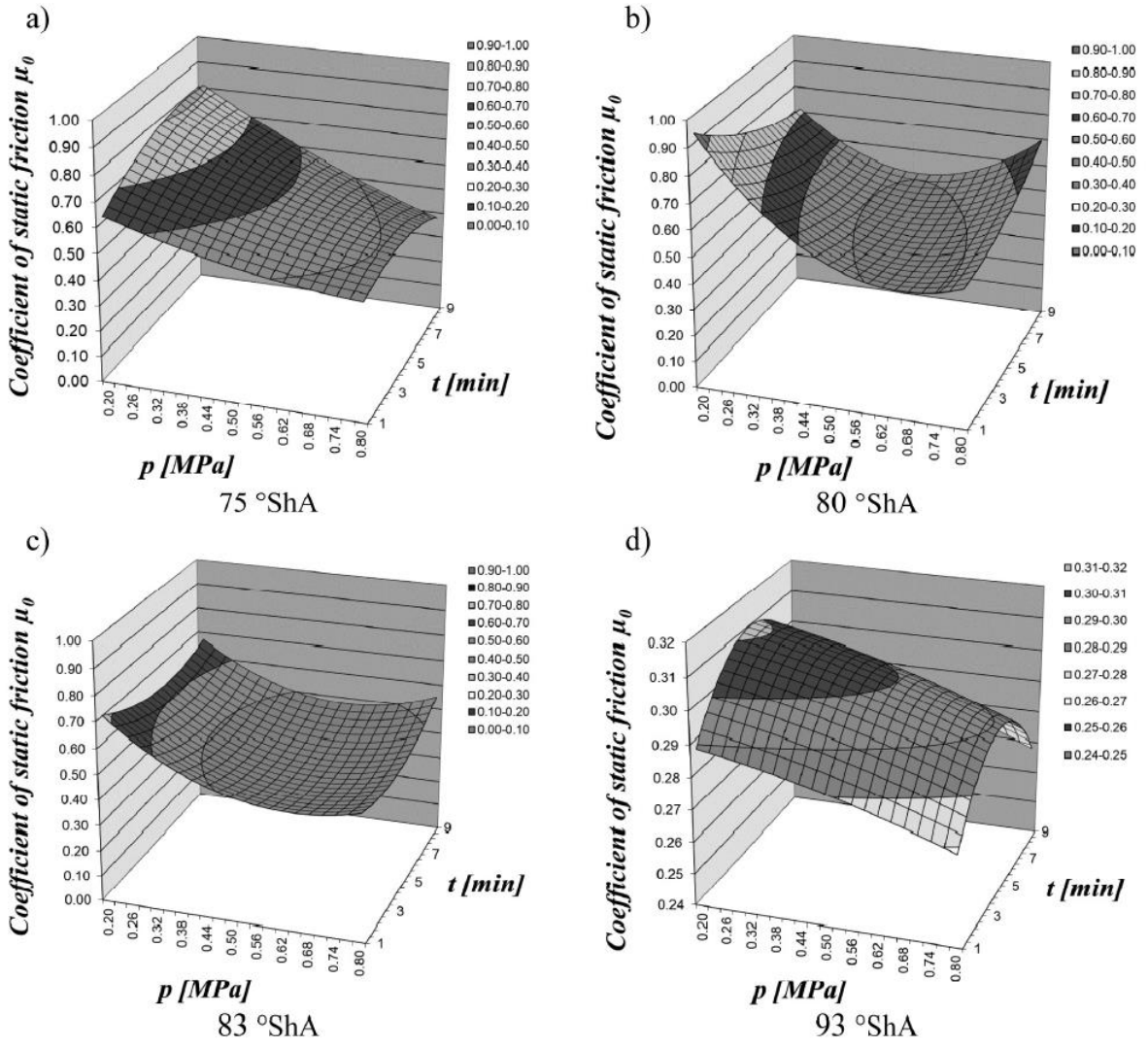

Figure 3.3. Static friction coefficients for different hardnesses, pressures and consolidation times under dry conditions (Capanidis & Sokolska, 2020)

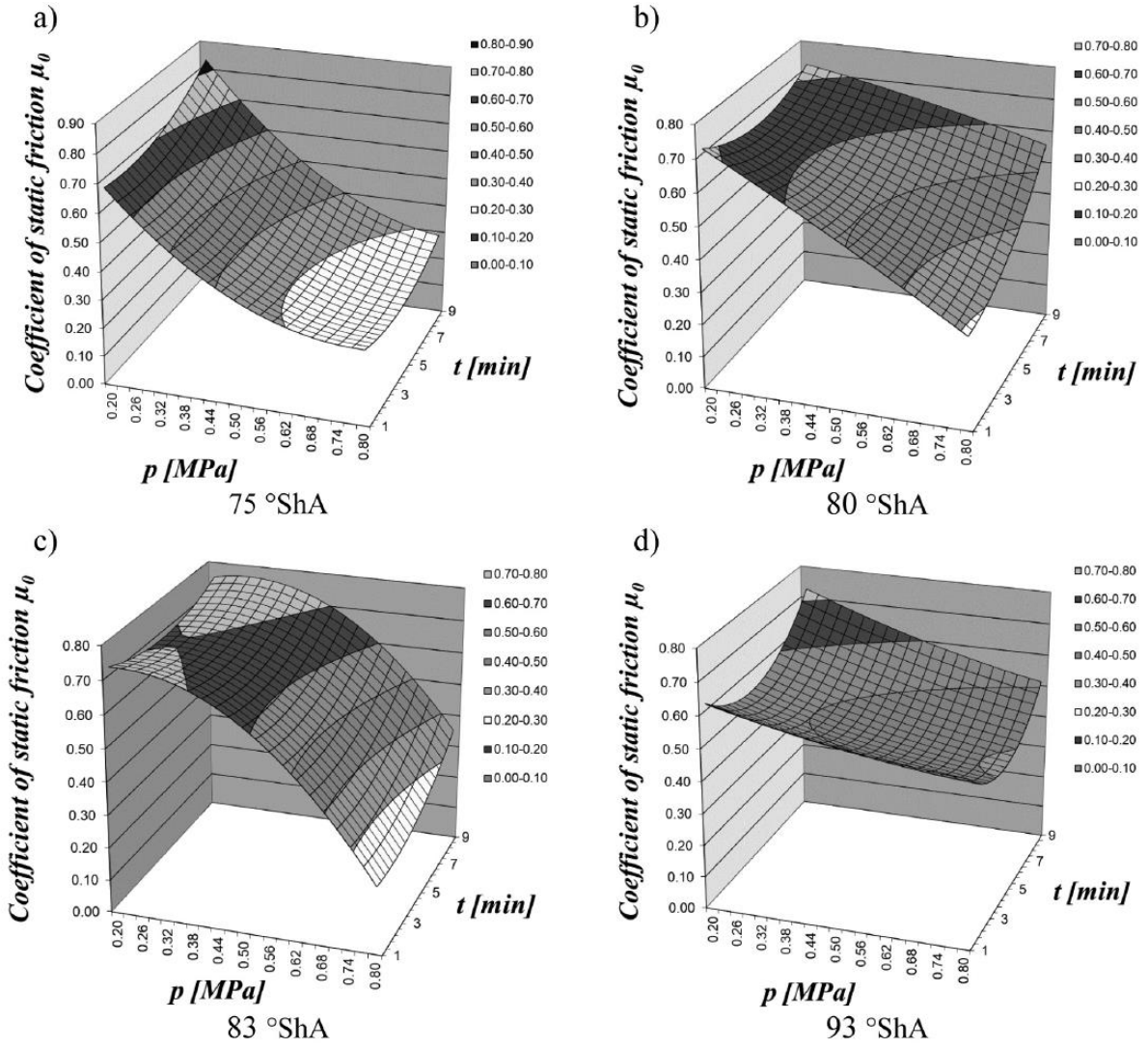

Figure 3.4. Static friction coefficients for different hardnesses, pressures and consolidation times under wet conditions (Capanidis & Sokolska, 2020)

In measurements performed by TWD (2020a) previously to this research, the effect of hardness on friction was investigated. Two polyurethane samples with different hardness were tested with corroded steel as counter sample. The interface was lubricated with seawater. For an increase in hardness, a small increase in friction resistance was observed (Figure 3.5). In Figure 3.6 the effect of hardness on friction graphs is shown. The difference between the tests with the same hardness are caused by the counter sample. The same corroded counter sample is used for the samples with the same hardness. The sample loses some of its corrosion during testing. It is also observed that the friction curves with hardness 87 °Shore A have a steeper slope than those with a hardness of 70 °Shore A. This is caused by a difference in the shear stiffness of the pads (Subsection 6.4.2). The kinetic friction forces of the higher hardness material is also slightly higher.

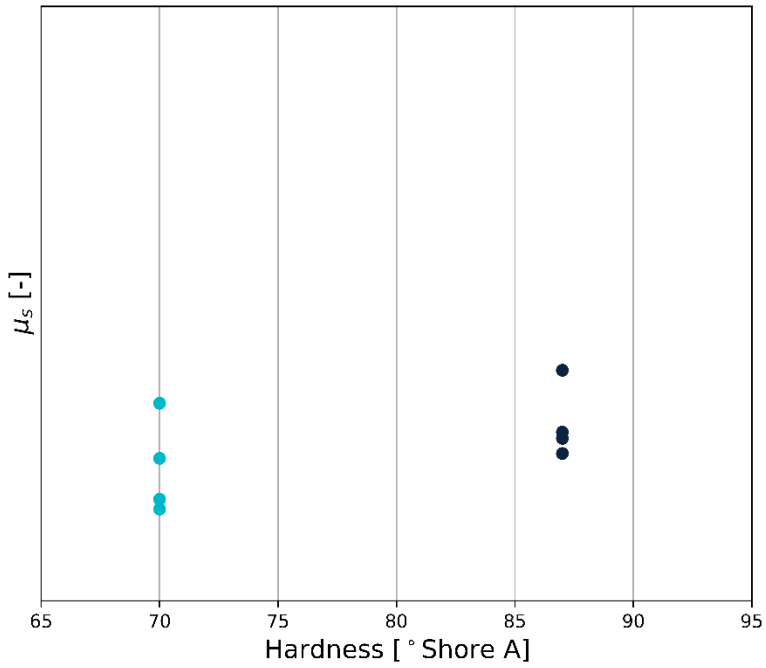

Figure 3.5. Hardness impact on friction, measurement (TWD, 2020a)

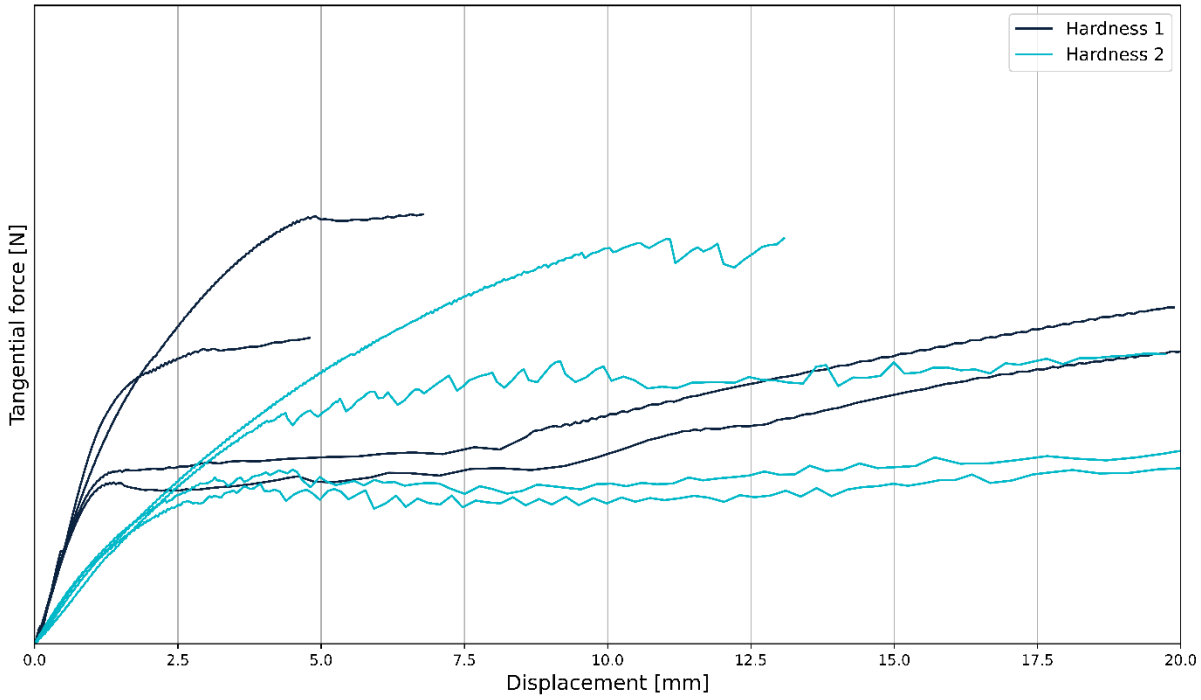

Figure 3.6. Friction graphs hardness (TWD, 2020a)

The difference in observed effects between both studies might be caused by the pressure that is used for testing. In the study of Capandis & Sokolska the pressure is between 0.2 and 0.712 MPa, in TWD (2020a) the pressure is 3 MPa. It is also possible that the differences are caused by the different hardness ranges that were investigated. In TWD (2020a) polyurethane with hardness 70 and 87 °Shore A tested. Between these values a decrease in friction resistance was observed in Capandis & Sokolska (2020). The used testing method differs, which could also affect the friction measured (Chapter 4).

Table 3.1. Factors and testing methods hardness effect study

	Capandis & Sokolska (2020)	TWD (2020a)	Unit
Testing method	Inclined plane	Vertical plane	
Support material	Polyurethane	PU	
Steel type	Steel	Corroded steel	
Roughness steel (R_a)	-	1.381 [b]	µm
Lubrication	Dry, water, lubrication	Water	
Rate of loading	Slow [a]	kgf/min	
Consolidation time	1 – 9	7	min
Load	-	3768	N
Pressure	0.2 – 0.712	3.0	MPa
Temperature	-	17	°C
Hardness range	75, 80, 83, 93	70, 87	°Shore A
Increase hardness effect	**Decrease μ_s (dry)** **Lowest μ_s for 80 and 83 °Shore A (water)**	**Increase μ_s**	

Note. Factors and test methods from (Capandis & Sokolska, 2020; TWD, 2020b).

[a] Research does not mention a specific rate of loading, but mentions that the movement is slow.

[b] Measured value, see Appendix A.

The hardness of the polymer materials for monopile sea fastening applications ranges from 60 °Shore A to 50 °Shore D. There is not a fixed value for the hardness of a material, different mixtures for polyurethane or rubber can influence the hardness. It is also important that the polymer support material has enough stiffness to remain intact under the loads due to vessel motions and monopile weight.

Previous studies indicate a hardness effect on friction resistance (Capanidis & Sokolska, 2020; TWD, 2020a). A clear effect has not been observed. Additional research must be performed to investigate the effect of hardness on friction.

3.1.2 Viscoelasticity

Viscoelastic materials react partially in an elastic and partially in a viscous way to applied stress (Malvern Instruments Limited, 2016; Sakaguchi et al., 2019). The complex modulus (G*) represents the resistance to deformation of the material. The phase angle δ indicates how elastic or how viscous a material behaves (Brinson & Brinson, 2015; Malvern Instruments Limited, 2016; Sakaguchi et al., 2019). For a material which behaves purely elastic, δ is 0° (Malvern Instruments Limited, 2016). For a purely viscous material, δ is 90° (Malvern Instruments Limited, 2016). For viscoelastic materials, δ is always between 0 and 90°. With these parameters, the storage modulus (G') and the loss modulus (G") can be determined. The storage and loss modulus respectively represent the elastic contribution and the viscous contribution to the resistance to deformation (Brinson & Brinson, 2015; Malvern Instruments Limited, 2016). All parameters are summarized in Figure 3.7. The formulas to calculate the viscoelastic parameters are presented in Formula 3.2 and Formula 3.3.

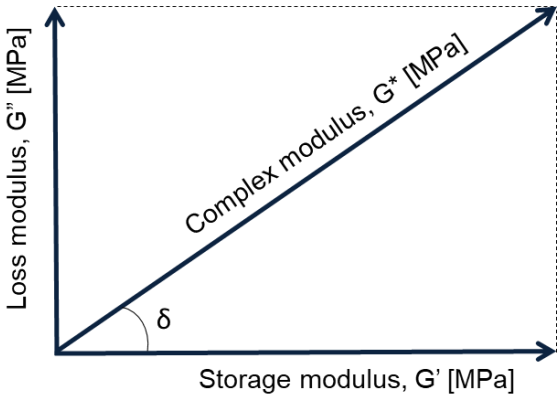

Figure 3.7. Viscoelastic properties (made on 20-4-2022, based on Brinson & Brinson (2015) and Malvern Instruments Limited (2016))

$$tan(\delta) = \frac{G''}{G'} \quad 3.2$$

$$G^* = \sqrt{(G'')^2 + (G')^2} \quad 3.3$$

Viscoelastic properties are temperature dependent. The temperature that corresponds with the largest tan(δ) is the glass transition temperature (T_G) (in Figure 3.8, T_G = - 45 °C). In Ludema & Tabor (1966) frictional properties were linked to viscoelastic properties of polymers. The study focused on sliding and rolling friction. For sliding friction, no correlation between friction and viscoelastic properties was observed for temperatures below the glass transition temperature. For rolling friction a correlation between friction resistance and viscoelastic properties is observed (Figure 3.9). These correlations could indicate a correlation between viscoelastic properties and static friction as well.

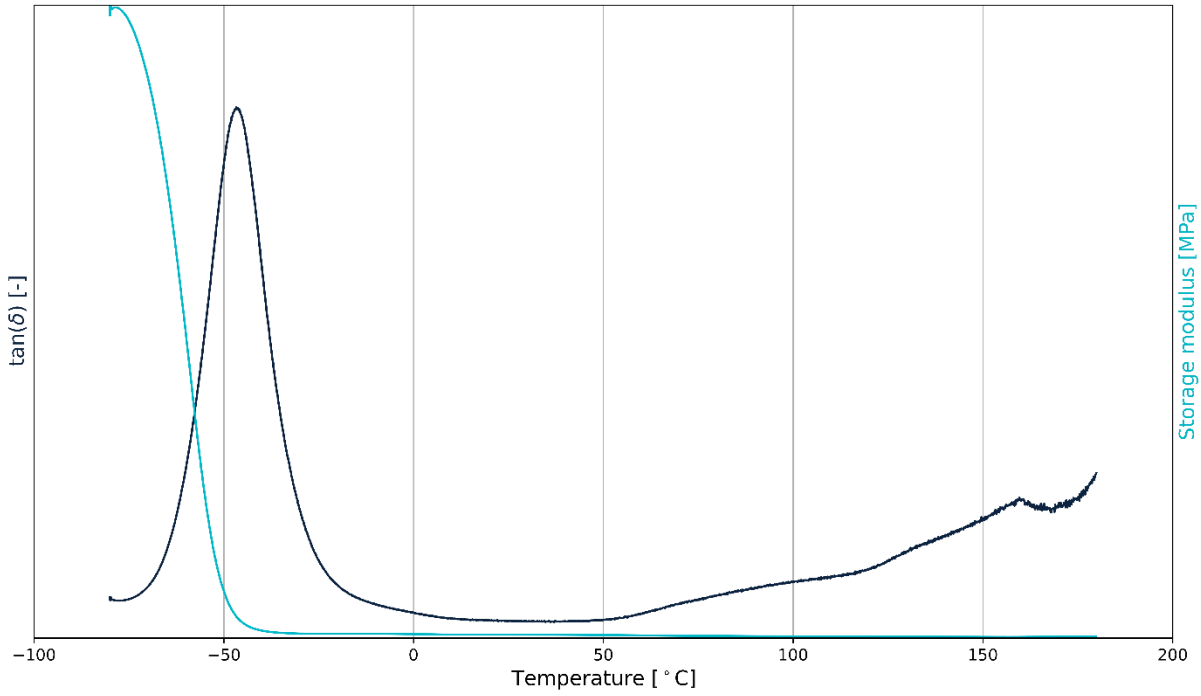

Figure 3.8. DMA curve with T_G = - 45 °C, PU sample with hardness °Shore A

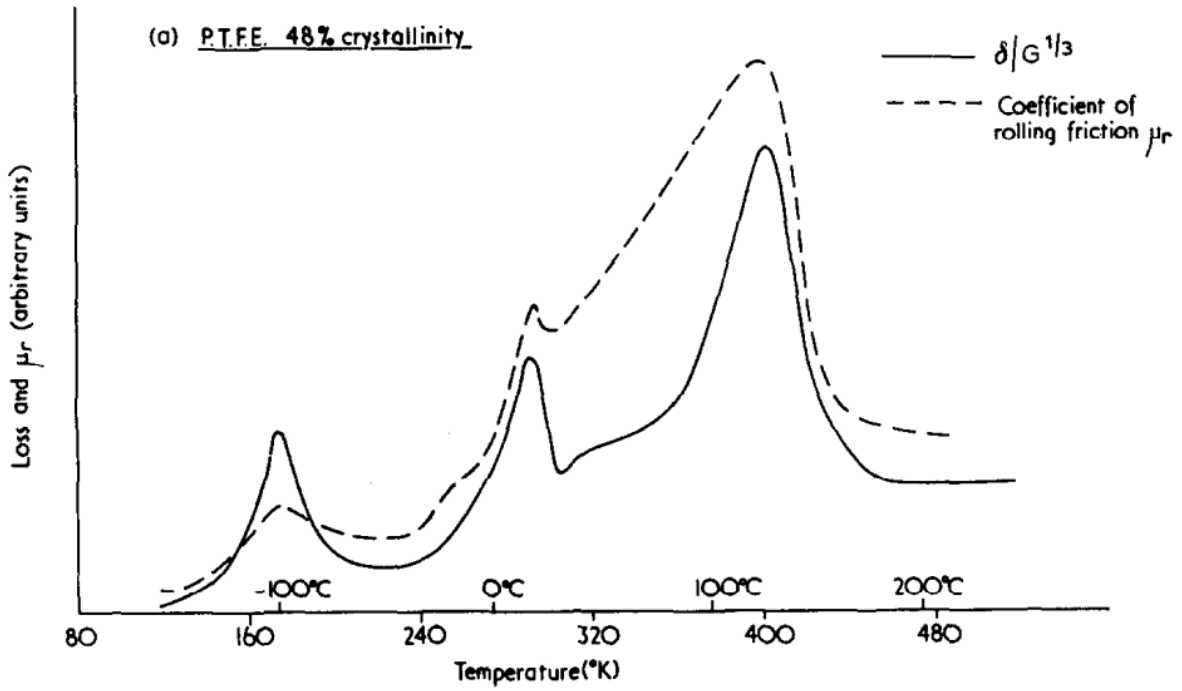

Figure 3.9. Viscoelastic properties and coefficient of rolling friction compared over temperature (Ludema & Tabor, 1966)

Previous studies only indicate a relation of viscoelastic properties and friction. A coherent answer on the effect of viscoelastic properties is lacking. The temperature dependency of viscoelastic properties might explain the effect of temperature on friction (Subsection 3.7). Additional research is required to investigate the effect of viscoelastic properties on static friction resistance.

3.2 Roughness

The impact of the roughness of solids on static friction was investigated by Ivkovic et al. (2000). In this study the solids used for the testing are not mentioned. This study concluded that the static friction resistance increases with increasing roughness. Other studies mention, but do not prove a roughness effect (Archard, 1974; Bowden & Tabor, 1966).

Roughness can be measured in the arithmetic mean height parameter, R_a, and the maximum height R_z. For the measurement device used in this research, the roughness parameters are defined like those in Figure 3.10 (Amaral et al., 2009; ANSI B46.1, 1985; JIS B 0601, 1994; NEN-EN-ISO 21920-2, 2022). Measurements show very good correlation between parameters R_a and R_z (R^2 = 1.0) in the measurements performed on steel samples used in Section 5.2 (Appendix B). To reduce the number of variables to describe the roughness, only R_a is used. Higher values for the roughness parameter indicate a rougher surface with more deviation. In this thesis a distinction is made between monopile roughness and support pad roughness to eliminate the effect of material properties in the comparison.

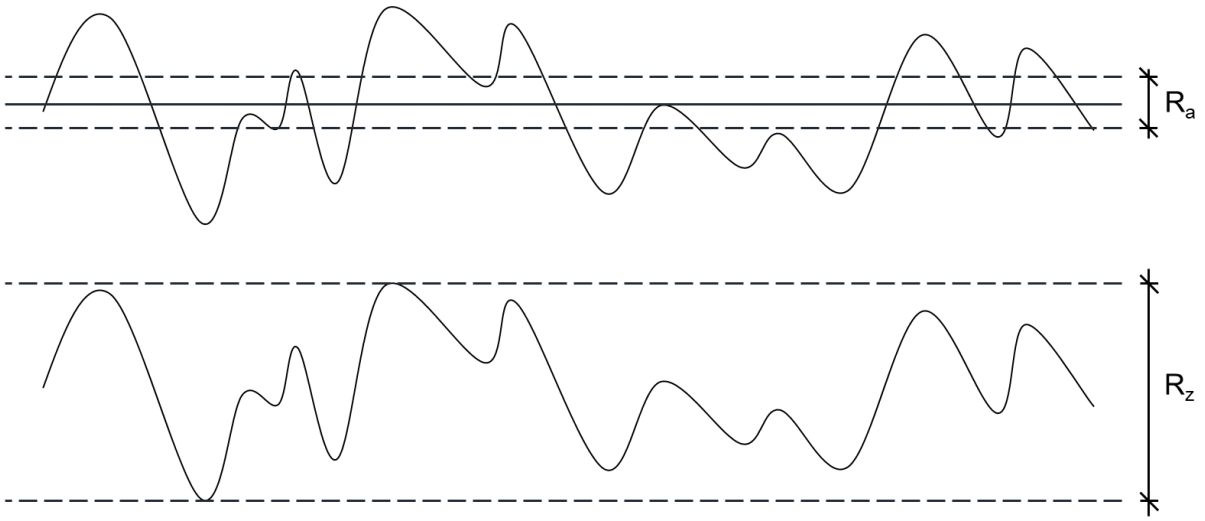

Figure 3.10. Roughness parameters R_a and R_z in TWD measurements (made on 18-4-2022)

3.2.1 Monopile roughness

A study on the impact of corrosion has been performed by TWD (2021b). Corroded monopiles are rougher than monopiles that are not corroded (and where the surface is blank steel) (Figure 3.14). In the test campaign, 30 tests were performed with corroded steel and 30 tests were performed with blank steel. These tests showed that the static friction resistance was higher for the corroded steel samples and that the measurement variability was lower (Figure 3.11). This variability is also observed in the force-displacement graphs is different (Figure 3.12).

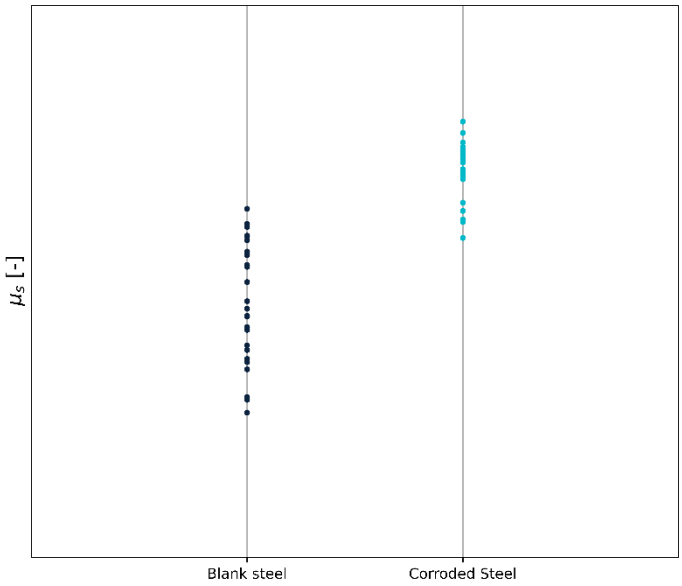

Figure 3.11. Roughness impact on friction, measurement (TWD, 2021b)

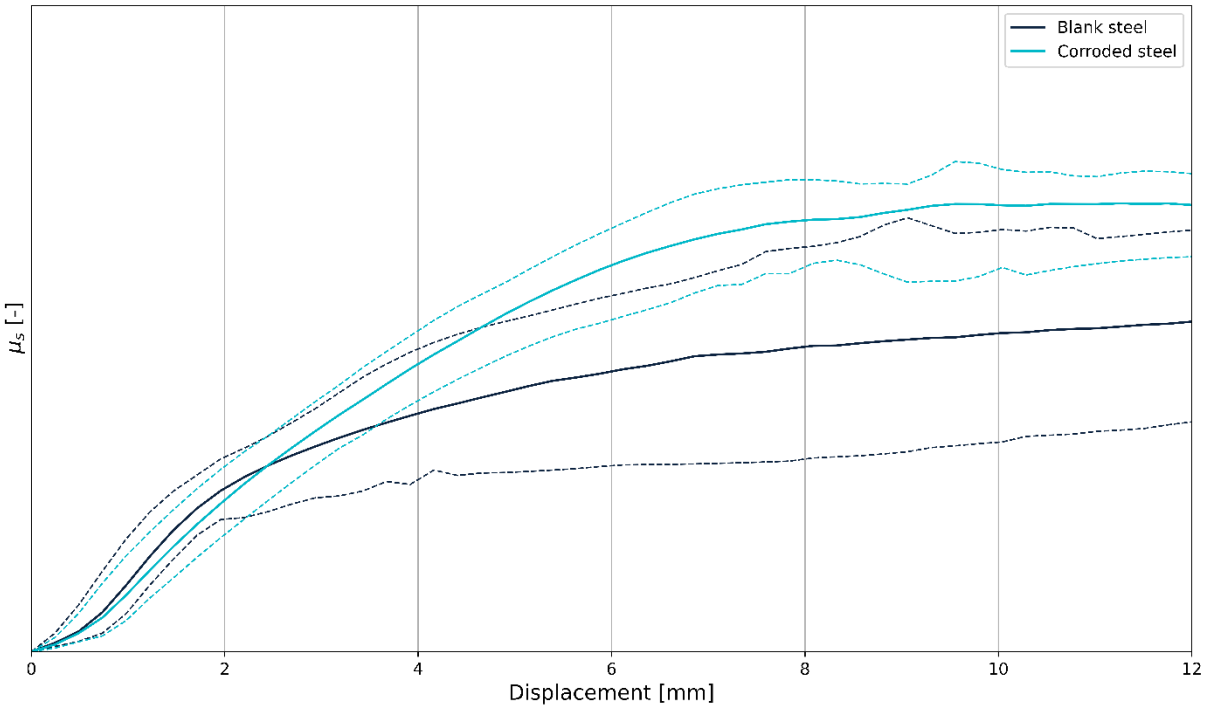

Figure 3.12. Mean force-displacement graphs with 5th percentile boundaries for blank and corroded steel friction measurements

The monopile surface and thus the roughness varies for different locations on the monopile. The bottom side of the monopile which is below the waterline after installation, will not be coated. Before transportation, the surface of this part can be blank steel or the steel corroded in different degrees of corrosion (Figure 3.13). The difference in roughness of both surfaces is depicted in Figure 3.14. The part of the monopile above the waterline is coated. For this coated part different types and thicknesses of coating (Subsection 3.3) are used. In Figure 3.14 a microscopic picture of a coated sample is depicted next to the other surface types. It is important to note that these differences in friction can also be caused by a change in the material properties of the surface of the corroded sample.

Figure 3.13. Partially corroded monopile (Duerst, 2016)

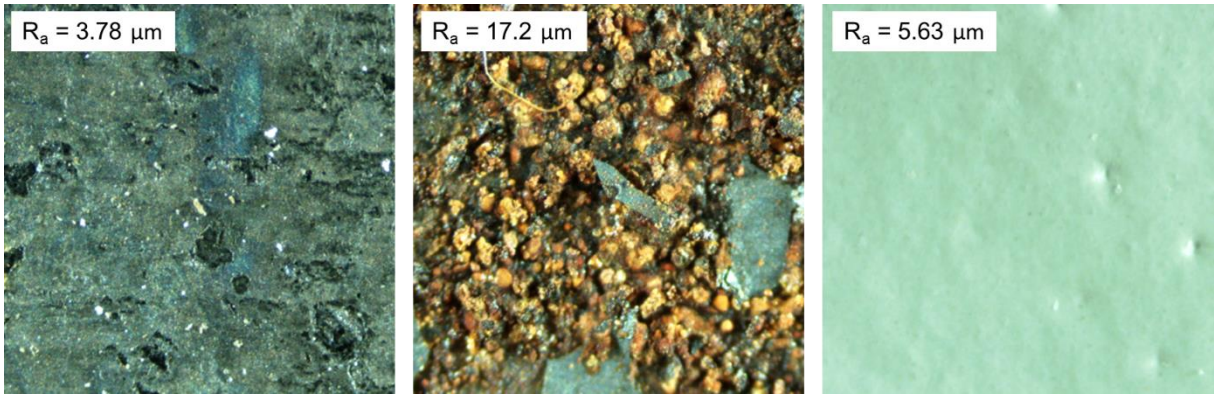

(a) *(b)* *(c)*

Figure 3.14. The microscopic structure and roughness of monopile surfaces. (a) Blank steel, (b) Corroded steel, (c) Coated steel with low roughness (pictures made on 21-4-2022)

Current research is insufficient to show an effect of roughness only on friction. The increase in roughness can cause an increase in real contact area. An increase in real contact are results in an increase of static friction, if the shear strength of the polymer and the ploughing component remain the same (Subsection 2.2.3). Additional research is required to investigate the effect of roughness independently from corrosion on friction.

3.2.2 Roughness of support pads

The roughness of the support pads can vary as well. In general, smooth polyurethane has a roughness (R_a) of approximately 1.0 µm (Appendix A). Polyurethane can also be post-treated. This process can increase the roughness to approximately 14 µm (Appendix A). The effect of support pad roughness on friction is analyzed from previous test data (TWD, 2021c). The tested PU samples differ in hardness (87 and 90 Shore A for the smooth and the rough PU respectively) and are made by different manufacturers. The tests were performed in contact with coated steel samples both in wet and dry conditions. The applied pressure was 3 MPa and the tests were performed at room temperature. The consolidation time was 7 minutes and the rate of loading was kgf/min. The friction increases with increasing roughness of the PU when in contact with the steel sample with the thin coating. This effect is not visible for the PU in contact with the thick coating. The effect observed can also be caused by the difference in hardness.

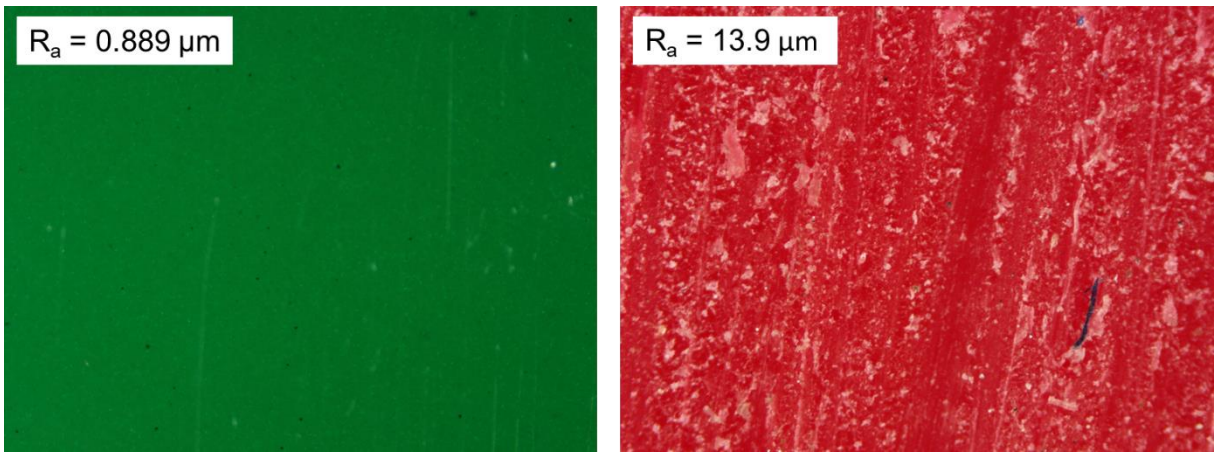

(a) *(b)*

Figure 3.15. The microscopic structure and roughness of support pad surfaces. (a) Polyurethane, (b) Post-treated polyurethane (pictures made on 21-4-2022)

The support pads in a friction-based monopile sea fastening can become rougher due to wear caused by the interaction with the monopile. Test exercises indicate a relation between friction and PU roughness. However, in these tests other factors differed as well, which could trouble the results. Additional research is required to investigate the effect of the roughness of the support material.

3.3 Monopile coating

The study of Ren et al. (2021) studied the tribological behavior of polymer composite coatings. This study showed some relation between shear strength and friction. A higher coefficient of friction was observed for higher shear strength coatings. Two of the coatings used for monopiles are studied by Ren et al. (2021). An epoxy coating showed high friction together with a low wear rate. Lower friction and more wear was observed for PU coatings. The study states that the performance of the coatings also depends on the factors: temperature, load and velocity.

The effect of coating thickness on friction can be investigated by analyzing data of previous performed test exercises (TWD, 2021a). To quantify the coating thickness, the dry film thickness (DFT) is measured (ISO 19840, 2012). In the test exercises, two coating thicknesses (same coating type) were tested with two polymers (PU1 and PU2). It is important to note that the polymers differ in roughness and hardness and are made by different manufacturers. Test details are to be found in Table 3.2.

The effect of coating thickness differs for the different support materials. The effect of different coating thicknesses is minimal for the rougher support material PU1 (Figure 3.16). For support material PU2, an increase in coating thickness leads to an increase in friction resistance (Figure 3.16). The difference in effect between PU1 and PU2 are caused by either the different hardness, different roughness or different manufacturing processes. This study shows that coating thickness has an effect on friction, but other factors might nullify this effect.

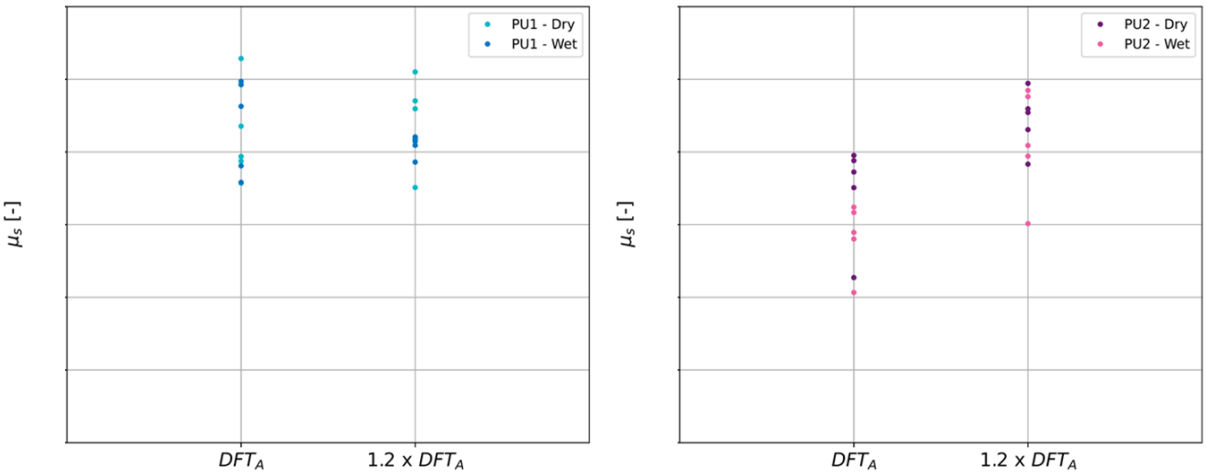

Figure 3.16. Coating thickness impact on friction for PU1 and PU2, measurement (TWD, 2021a)

Table 3.2. Factors and testing method coating thickness effect study

	TWD (2021a)	TWD (2021a)	Unit
Testing method	Vertical plane	Vertical plane	
Lubrication	Dry, water	Dry, water	
Rate of loading			kgf/min
Consolidation time	7	7	Min
Pressure	3.0	3.0	MPa
Temperature	17	17	°C
Support material	Polyurethane (PU1)	Polyurethane (PU2)	
Steel type	Polyurethane coating [a]	Polyurethane coating [a]	
Steel roughness (R_a)	1.90, 1.08	1.90, 1.08	
Coating thickness	DFT_A, 1.2 x DFT_A [b]	DFT_A, 1.2 x DFT_A	
Increase coating thickness effect	**Constant μ_s**	**Increase μ_s**	

Note. Factors and test methods from (TWD, 2021a)

[a] For both steel samples the same coating type was used, only the thickness differs.

[b] The coating thickness is not revealed in this thesis, because it is client specific.

Coating is applied on monopiles to prevent degradation due to environmental conditions. ISO prescribes different coating thicknesses for different locations on the monopile (NEN-EN-ISO 12944, 2018). The part which is in the splash zone needs the most protection since this part is periodically exposed to salt water and oxygen. This often results in a thicker coating layer. Along the monopile the coating thickness, coating type and coating roughness can differ. In Figure 3.17 a monopile is shown which is coated on the top part (yellow and grey coating) and uncoated at the bottom part (corrosion).

Figure 3.17. Coated monopile (Sif Group, 2021)

Coating is one of the factors that affects monopile sea fastening friction. Literature shows a relation of coating properties and friction. Previously performed test exercises relate coating thickness to friction. Additional research is required to prove the effects of coating on friction.

The coating of monopiles is often a given parameter in monopile sea fastening. Therefore, coating types are out of scope of this thesis. Tests should always be performed with steel that is coated with the same coating type and the same coating thickness, as in their intended application.

3.4 Applied pressure

The applied pressure is the applied load divided by the apparent contact area (F_N/A_A). This is the reason that the effect of applied load and applied pressure can be compared. This Subsection will not consider the real contact area pressure in which the area is the real contact area (F_N/A_R).

Da Vinci, Amontons and Coulomb already observed that friction is load dependent (Section 2.2). Several studies show an effect of applied pressure on friction as well (Bowden & Tabor, 1966; Briscoe & Tabor, 1978; Myshkin & Kovalev, 2009; Zhou et al., 2017). However, the consequence of pressure on the coefficient of friction deviates in studies. In the study of Capandis & Sokolska (2020) a decrease in friction as a result of increasing pressure was observed.

The effect of pressure on friction has been studied by TWD (2020b). This study was performed with rubber as support material. Blank steel and two different coating types were used as counter material. In all cases, the same effect was observed. The measurements showed a decrease in the coefficient of friction for an increase in pressure (Figure 3.18).

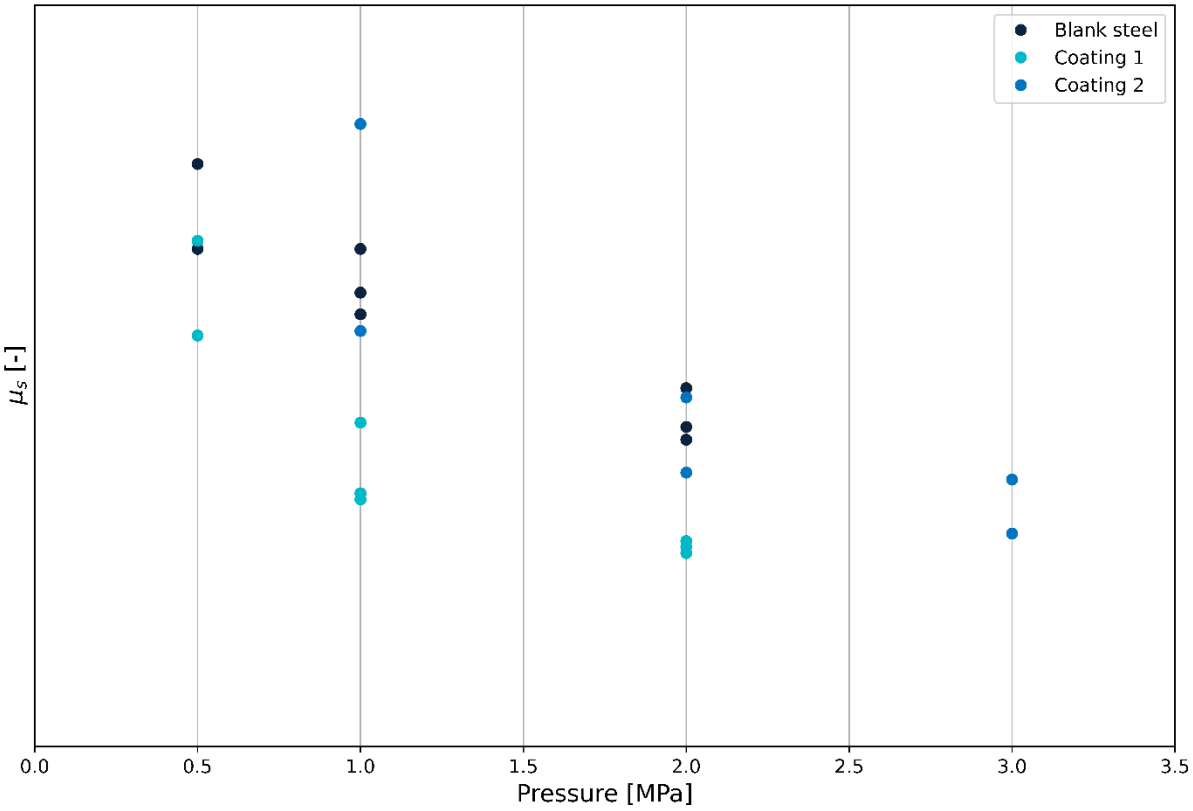

Figure 3.18. Pressure impact on friction, measurement (TWD, 2020b)

In Table 3.3 the factors and test methods of both studies (Capandis & Sokolska, TWD) are listed. Both studies are comparable, since most conditions are similar. The testing methods are not the same, but both methods are focused on testing static friction. The support material is also different, but comparable based on the hardness. The viscoelastic properties of the used materials are unknown. The effect of pressure on friction is in both studies the same.

Table 3.3. Factors and testing methods pressure effect studies

	Capandis & Sokolska (2020)	TWD (2020b)	Unit
Testing method	Inclined plane	Vertical plane	
Support material	Polyurethane	Rubber	
Hardness	75, 80, 83, 93	80 [b]	°Shore A
Steel type	Steel	Blank steel, coated	
Roughness steel	-	1.381 [b]	µm
Lubrication	Dry, water, lubrication	Water	
Rate of loading	Slow [a]	kgf/min	
Consolidation time	1 – 9	7	min
Load range	-	628 – 3768	N
Pressure range	0.2 – 0.712	0.5 – 3.0	MPa
Temperature	-	17	°C
Increase pressure effect	**Decrease μ_s**	**Decrease μ_s**	

Note. Factors and test methods from (Capanidis & Sokolska, 2020; TWD, 2020b).

[a] Research does not mention a specific rate of loading, but mentions that the movement is slow.

[b] Measured value, see Appendix A.

Pressure is a factor that is relevant for monopile sea fastening. The pressure on the friction interface is caused by the weight of the monopile, the area of the supports, and vessel motions. Currently, the pressure at monopile sea fastening interfaces is a maximum of approximately 5 MPa. When monopiles become larger, the pressure is likely to increase as well. Due to vessel motions the pressure on the interface can increase or decrease. The vessel motions should thus be considered when determining the pressure.

Pressure must be considered in the friction standard. It is important to test for the pressure which corresponds with the pressure present during operational conditions. If a pressure assumption must be made, a higher pressure would be conservative.

3.5 Lubrication

Lubrication has an explicit effect on friction. Compared to dry situations, the friction resistance decreases when lubrication is applied (Bowden & Tabor, 1966; Capanidis & Sokolska, 2018; Zhou et al., 2017). The asperities of both surfaces can be separated with a liquid layer when lubrication is applied. In rougher surfaces the lubrication might be in deeper cavities. This will not lead to the separation of the asperities of both surfaces. The friction resistance depends in that case more on the viscous resistance of the fluid, than on the material properties (Bowden & Tabor, 1966). The same effect of lubrication is also seen in a measurement campaign of TWD (2019), see Figure 3.19. In this campaign polyurethane and steel were tested for both dry and wet (seawater applied) conditions. The seawater was sprayed on the pad samples and the steel sample before placing the samples in the test bench. The tests were performed with polyurethane as support material and blank steel as counter material.

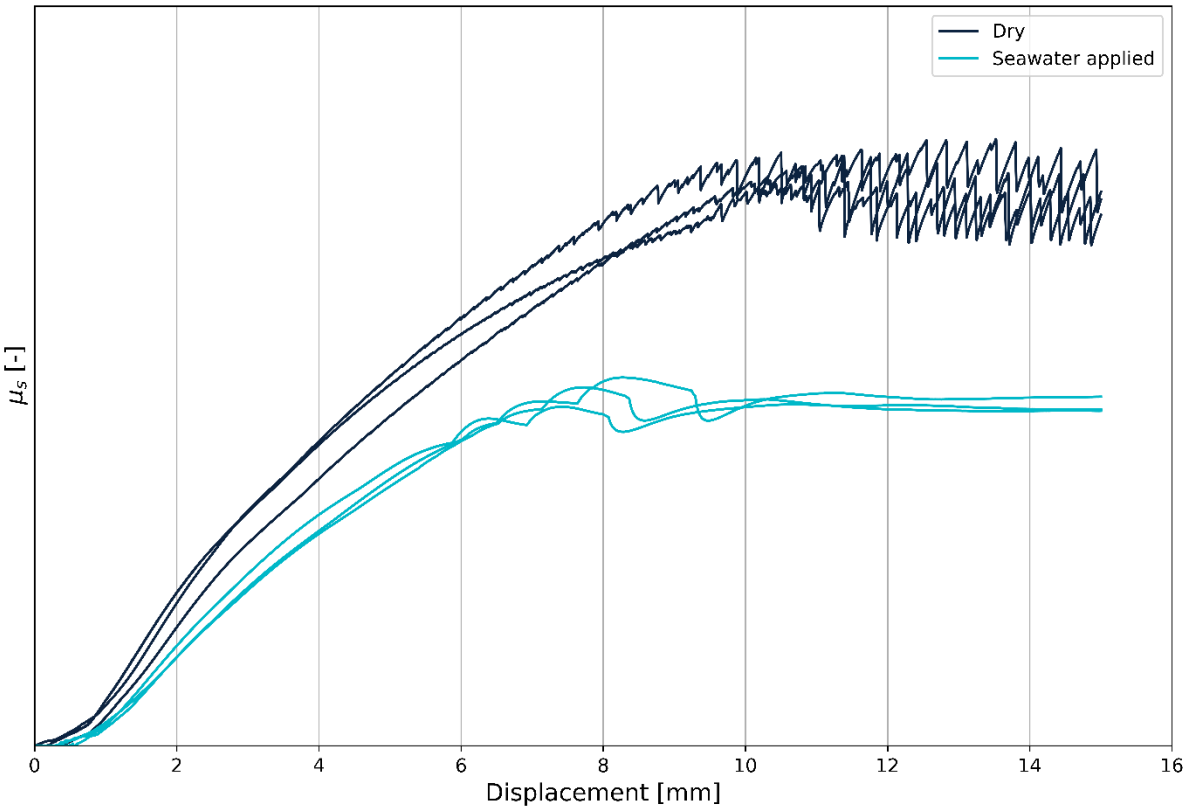

Figure 3.19. Impact of lubrication on friction resistance (TWD, 2019)

The lower tangential force and thus the lower friction resistance is not the only observation that can be made from Figure 3.19. The graphs also show a difference in behavior. The dry friction graphs are steeper in the beginning than the lubricated friction graphs. In the dry friction tests, the friction resistance is caused by the elastic deformation of the polyurethane samples in this region. In the lubricated tests, the curve is less steep. For the kinetic part, there are also differences between the curves. Stick-slip behavior is observed for the dry friction tests and more continuous sliding behavior is observed for the lubricated tests. This difference due to lubrication corresponds with the findings of Zuleeg (2015).

In monopile sea fastening, lubricants are not applied on purpose since this would decrease the friction resistance. However, seawater and rain are potential fluids that might be present between both surfaces. This can be caused by the environmental conditions before loading the monopile on the sea fastening (due to rain) or by environmental conditions during operations (splashing). The amount of water between the surfaces is hard to quantify in reality, so the only distinction made is between dry and wet.

Lubrication has an unambiguously negative effect on friction resistance. It is thus important to consider lubrication in the friction standard. In tests lubrication must be applied if this will be present at the surface during operations.

3.6 Rate of loading

The rate of loading is the speed in which the tangential force is applied. Several studies mention the effect of the rate of loading on friction (Dillavou & Rubinstein, 2019; Richardson & Nolle, 1976). In the study of Johannes et al. (1973), the impact of the rate of loading on the friction resistance of lubricated steel samples was investigated. For increasing loads the friction resistance decreases until it converges to a constant value.

In a measurement campaign of TWD (2022) the impact of the rate of loading on friction was investigated. In these tests, the friction resistance between polyurethane samples and a steel sample was measured in dry conditions. For each rate of loading two tests were performed. The rate of loading is quantified in kgf/min (1 kgf/min ≈ 0,164 N/s). It can be observed that the test at 30 kgf/min has a constant displacement slope over time (Figure 3.20). For the load cell used in these tests a minimum velocity during the friction tests is set. In the case of a loading rate of 30 kgf/min, the displacement caused by the tangential force is lower than the minimum velocity of the machine. For this reason, the test is not representative for static friction tests, since there is no clear difference between static and kinetic friction. For tests with higher loading rates, this is not the case (Figure 3.21). For these tests increasing friction resistance is observed for increasing loading rates (Figure 3.22). This is different from what Johannes et al. (1973) found, which can be caused by different support materials and lubrication. Both studies show convergence to a constant static friction coefficient for higher rates of loading.

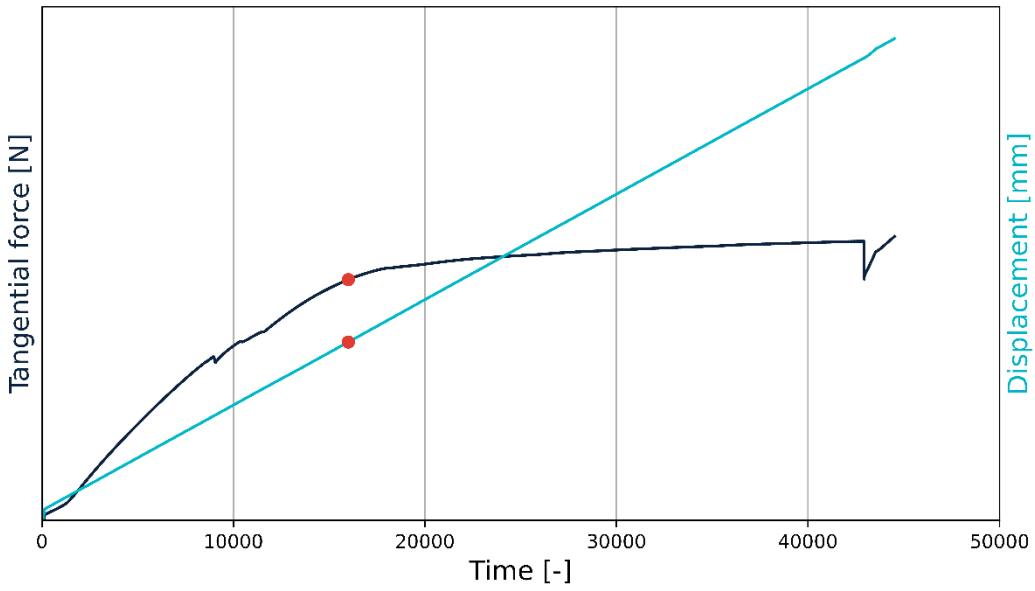

Figure 3.20. Force-displacement graph, rate of loading) kgf/min (TWD, 2022)

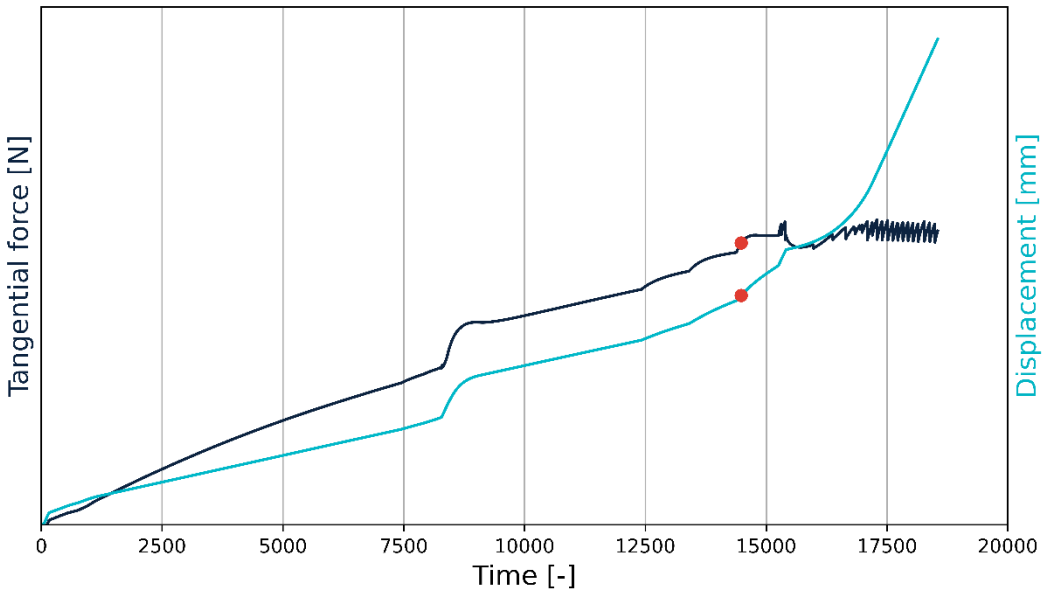

Figure 3.21. Force-displacement graph, rate of loading kgf/min (TWD, 2022)

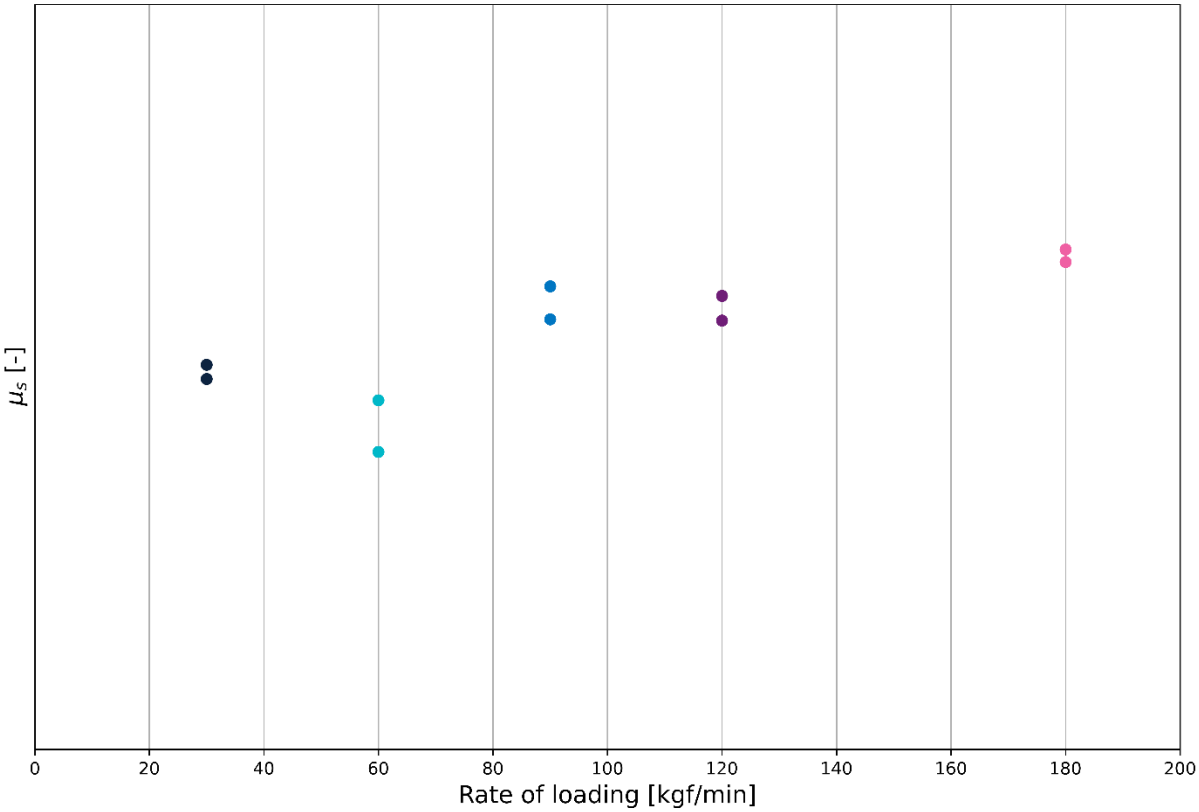

Figure 3.22. Rate of loading impact on friction, measurement (TWD, 2022)

In Figure 3.23 the different friction graphs for the tests are compared. The first part of the curve is similar for all rates of loading. This is the part where the polyurethane samples deform elastically (Subsection 6.4.2). After this deformation the graphs of the different loading rates differ. Another observation was that the higher the loading rate, the larger the total measured displacement.

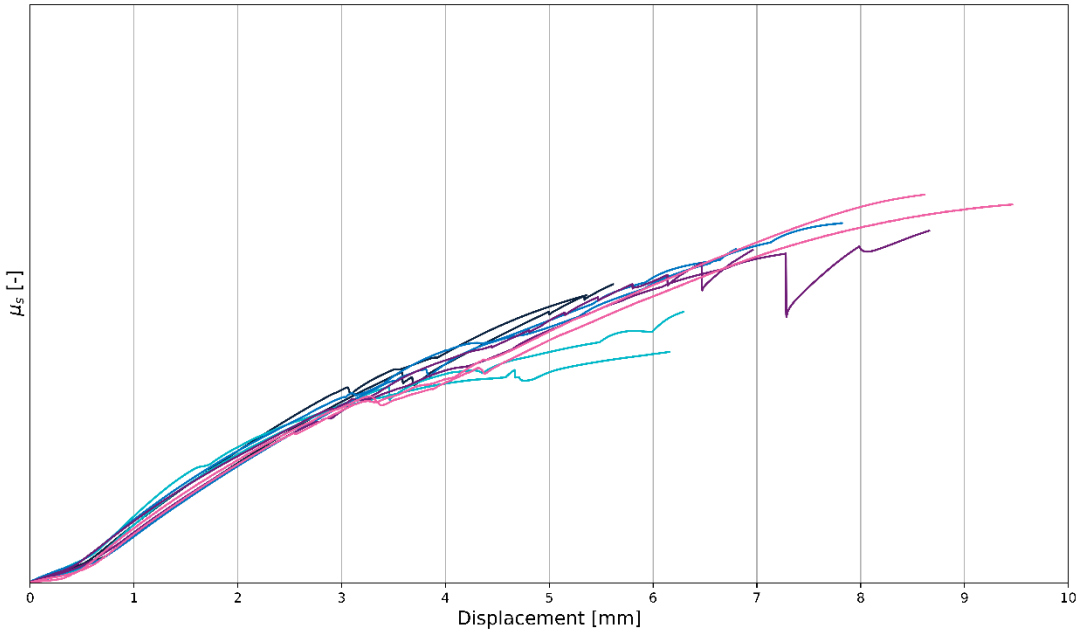

Figure 3.23. Force-displacement graphs different rates of loading, measurement (TWD, 2022)

In monopile sea fastening, vessel motions are responsible for the time in which the tangential force builds up on the interface. In Figure 3.24 the six possible vessel motions are defined. These motions can be divided in translational (sway, heave and surge) and rotational motions (pitch, yaw and roll). Depending on the orientation of the monopile, a combination of pitch and surge or a combination of sway and roll motions are the important vessel motions for the rate of loading. The tangential force depends both on vessel motions and the monopile weight. The vessel motions induce accelerations on the monopile that determine the tangential force in combination with the monopile weight. There is a large variation in these vessel motions and thus in the rate of loading.

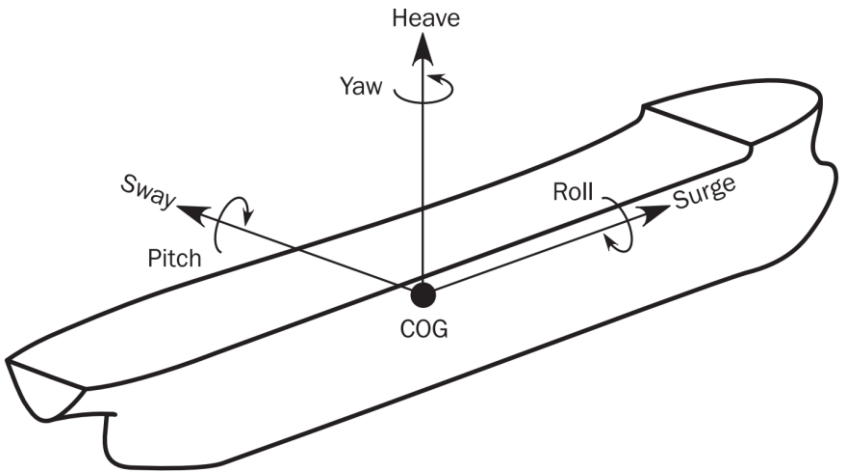

Figure 3.24. Vessel motions (DNVGL-RU-SHIP-Pt3Ch4, 2018)

The rate of loading has an effect on friction resistance and should thus be considered in the design standard. The rate of loading is to be determined based on vessel motions and the monopile weight. It is advised to perform some initial tests to indicate a conservative rate of loading.

3.7 Temperature

Friction resistance is affected by temperature (Bowden & Tabor, 1966; Briscoe & Tabor, 1978; Ludema & Tabor, 1966; Myshkin & Kovalev, 2009). The change in friction resistance might for example be caused by changes in the viscoelastic properties of the materials (Section 3.1).

The effect of temperature was investigated by TWD (2021). In these tests, the friction resistance was measured between polymers and blank steel samples at 0.5 MPa. It is observed that the temperature affects the friction resistance. In this case an increase in temperature results in an increase in friction resistance (Figure 3.25).

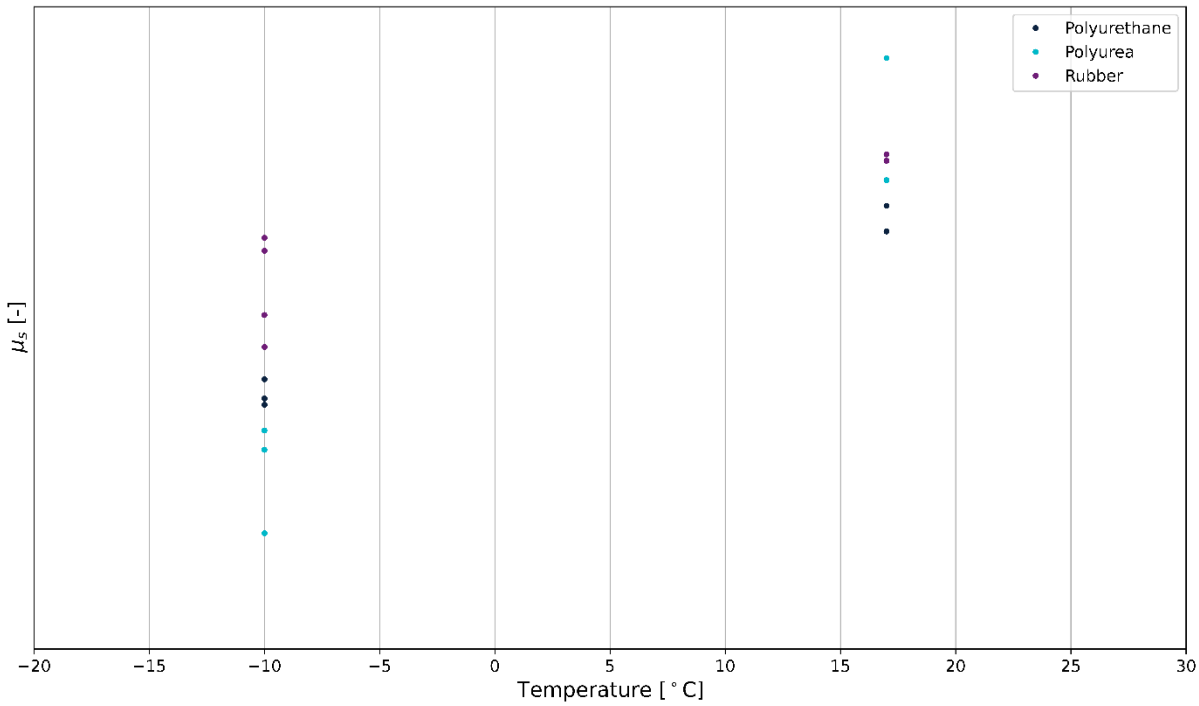

Figure 3.25. Temperature impact on friction, measurement (TWD, 2021d)

Monopiles are transported in different areas with different climates. According to DNV guidelines, marine operations should be designed to withstand the loads that are caused by the most adverse environmental conditions expected (DNVGL-ST-N001 3.1.1, 2020). The wave height, wind speed, and other relevant environmental conditions specified for the design of a particular marine operation are included in the design environmental conditions (DNVGL-ST-N001 3.2.1, 2020). Specific ranges for the temperature are not mentioned in DNVGL-ST-N001. In other offshore standards upper bound temperatures are specified. For gangways (DNVGL-ST-0358 5.2.1, 2021) and offshore and platform lifting appliances (DNVGL-ST-0378 1.1.7, 2019) upper bounds for the temperature are respectively 35 and 45 °C.

The Royal Netherlands Meteorological Institute (KNMI) records meteorological data on thirteen places in the North Sea, Figure 3.26. The minimum and maximum temperature measured at four of the stations is presented in Table 3.4. These stations were chosen because of the spread of their locations. Between 2011 and 2020, the temperature of these stations varied between -6,7 and 31,6 °C.

Table 3.4. Temperatures measuring stations (KNMI, 2020a, 2020b, 2020c, 2020d)

Measuring station	Minimum temperature [°C]	Maximum temperature [°C]
Euro Platform	-5,6	31,6
Hoorn-A	-6,7	30,5
F16-A	-5,0	27,8
A12-CPP	-5,0	26,5

Figure 3.26. KNMI measuring stations in the North Sea (KNMI, n.d.)

It is important to test the friction resistance at different temperatures, since literature and test exercises link temperature to friction. The effect of temperature on friction is not known yet. Additional tests could also be performed in an attempt to link the change in viscoelastic properties to the change in friction resistance. A temperature range between -10 and 40 °C is considered in this thesis, since this is relevant for most monopile sea fastening operations.

3.8 Consolidation time

Consolidation time is the moment that two surfaces first come in contact and the moment that the tangential force is introduced. In various studies the impact of consolidation time on friction is investigated. These studies show an increase in friction for longer consolidation times (Berthoud et al., 1999; Capanidis & Sokolska, 2020; Dillavou & Rubinstein, 2019). According to Dillavou & Rubinstein (2019) the static friction coefficient grows logarithmically over time under a constant normal load. In the study of Dillavou & Rubinstein this phenomenon is called ageing. They state three underlying reasons for this increase in friction resistance are (Dillavou & Rubinstein, 2019):

- The real contact area grows over time
- Chemical bonding, formation of bonds between atoms into molecules, crystals and other stable species (Atkins, 2021)
- The formation of capillary bridges, minimized surfaces of liquid or membrane between two rigid solids (Petkov & Radoev, 2014)

A short test campaign is performed to confirm the effects seen in literature. In this measurement campaign, the impact of consolidation times is limited, see Figure 3.27. This effect aligns with the effect of the previously mentioned studies (Berthoud et al., 1999; Capanidis & Sokolska, 2020; Dillavou & Rubinstein, 2019), even though some factors are different. The factors of the studies are compared in Table 3.5. The applied pressure in the short test campaign is 3 MPa, a lot higher than in the other studies. The high pressure may reduce the increase in real contact area over time, because it is initially relatively large. Another difference between the studies is the counter material. In the studies of Berthoud et al. (1999) and Dillavou & Rubinstein (2019) the counter material is not steel, but the same polymer.

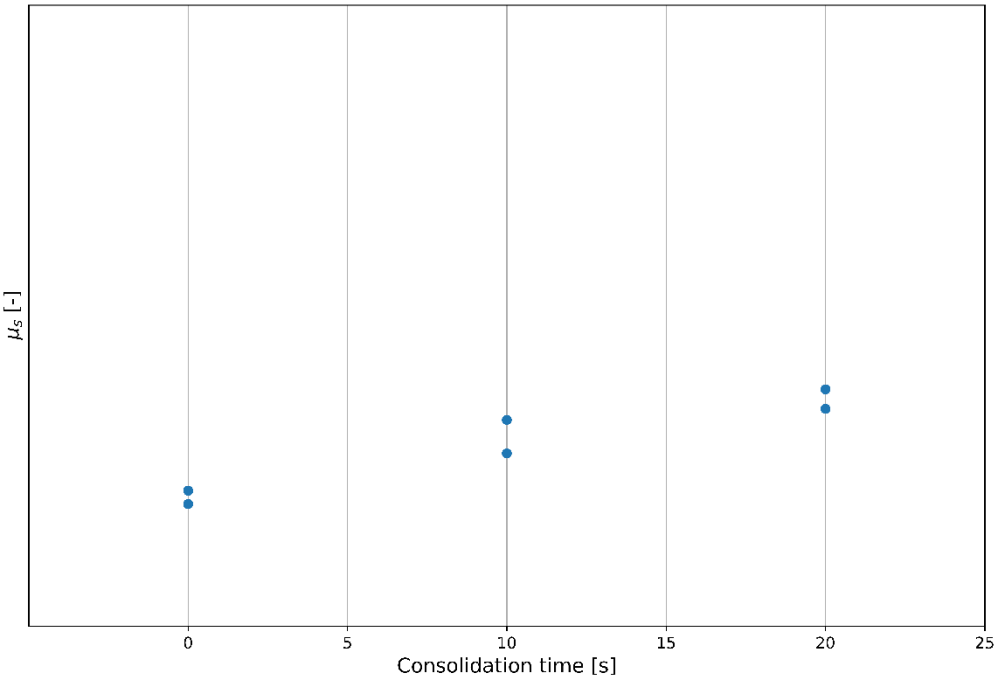

Figure 3.27. Consolidation time impact on friction (measurements performed on 22-6-2022)

Table 3.5. Factors and testing methods consolidation time effect studies

	(Capanidis & Sokolska, 2020)	(Dillavou & Rubinstein, 2019)	(Berthoud et al., 1999)	Consolidation time impact study (22-62022)	Unit
Testing method	Inclined plane	Horizontal plane	Horizontal plane	Vertical plane	
Support material	Polyurethane	PMMA	PMMA	Polyurethane	
Hardness	75, 80, 83, 93	-	-	87	°Shore A
Counter material	Steel	PMMA	PMMA	Blank steel	
Lubrication	Dry, wet	Dry	Dry	Dry	
Rate of loading	Slow [a]	-	-	kgf/min	
Load	-	90	4	3768	N
Pressure	0.2 – 0.712	0.36 – 0.6 [b]	0.08 [b]	3	MPa
Temperature	-	-	21, 72, 111	17	°C
Consolidation time	1 – 9	0.16 – 16.7	0.02 – 8.3	0 – 0.33	min
Increase consolidation time effect	**Increase μ_s (not unambiguous)**	**Increase μ_s (logarithmically)**	**Increase μ_s (larger increases for higher temperatures)**	**Increase μ_s**	

Note. Factors and test methods from (Berthoud et al., 1999; Capanidis & Sokolska, 2020; Dillavou & Rubinstein, 2019).

[a] Research does not mention a specific rate of loading, but mentions that the movement is slow.

[b] Pressure range calculated based on load and area mentioned in study.

In monopile sea fastening the consolidation time is the time between the placing of the monopile in the sea fastening and the start of transport. When transport begins, vessel motions start introducing tangential forces. In practice the consolidation time for monopile sea fastening is a time of several hours. Based on Table 3.5, it can be concluded that the coefficient of friction increases with an increase in consolidation time. It is reasonable to take a representative consolidation time into account in the test standard.

3.9 Conclusion

Factors affecting monopile sea fastening friction are obtained from literature and previously performed tests. In Figure 3.28 an overview of these factors in friction-based monopile sea fastening is provided. The effect of pressure, lubrication and consolidation time is extracted from literature and previously performed tests. An increase in pressure results in a decrease of friction. Applying lubrication on the friction interface will reduce the coefficient of friction, which is caused by the reduction in real contact area. Friction increases with increasing consolidation time. This can be explained by an increase in real contact area over time.

Literature and previous test exercises do not provide a coherent answer for the other factors. Additional research is required for the following factors:

- Hardness
- Viscoelasticity
- Monopile roughness
- Temperature
- Rate of loading
- Coatings
- PU roughness

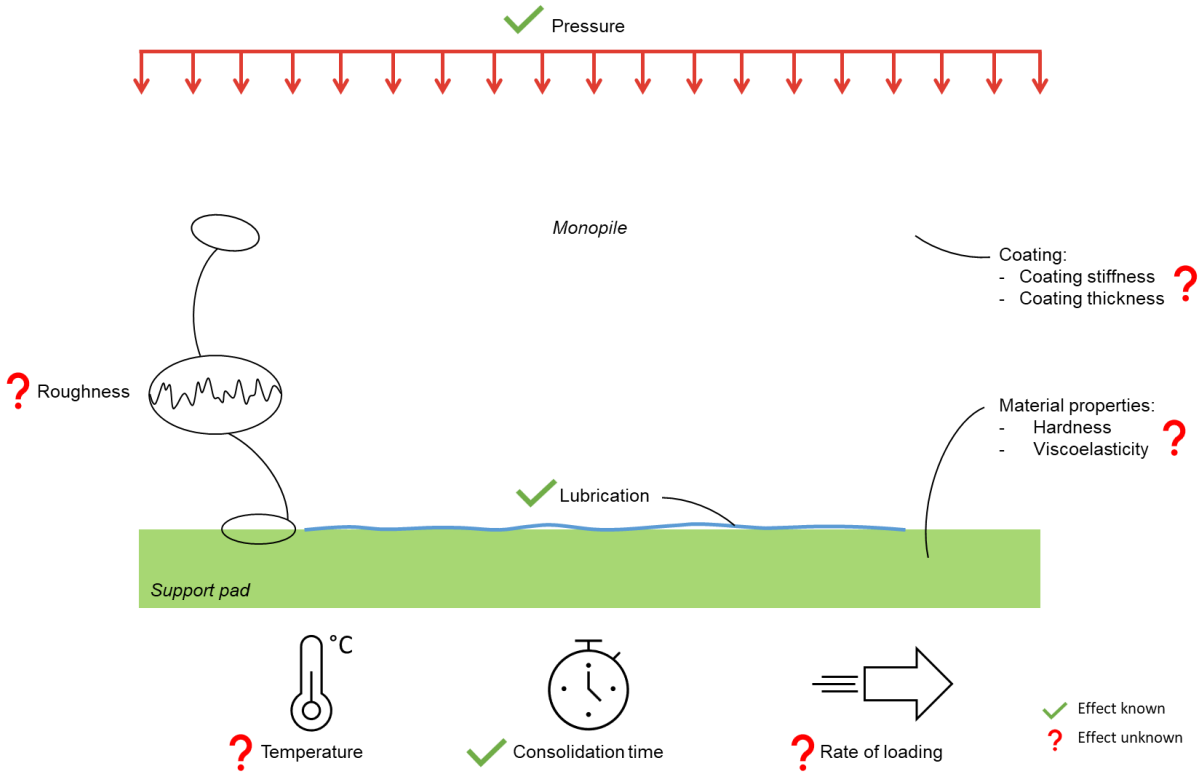

Figure 3.28. Overview of factors that affect friction and the state of the knowledge on the effects the factors have on friction

4 Testing friction

Friction can be tested by using different tests (ASTM G115, 1998). In this Chapter different test methods are compared to indicate which method is most suitable for monopile sea fastening friction tests. Criteria for a friction test method are set and the principles of the test methods are described. The test methods are assessed for the criteria relevant for monopile sea fastening. Finally, a possible test setup is described and the advantages and disadvantages are mentioned.

4.1 Test methods

ASTM G115-98 (1998) is established to act as a guide for selecting a method for measuring frictional properties. 24 test methods are mentioned, with the corresponding standards and measured parameters. The different test methods can be grouped into four main methods.

4.1.1 Horizontal plane method (HP)

One of the methods to measure friction is the horizontal plane (HP) method (Figure 4.1). A HP friction test for plastic films and sheeting is described by an ISO standard (ISO 8295, 1995). The two materials which are the point of interest are brought into contact by placing a block (material 1) on a horizontal surface (material 2). Then, the tangential force is applied parallel to the sliding plane ($F_{tangential}$). The force is increased up to a point where the block starts moving. The can be both force-based, increasing the force constantly over time. The test might also be displacement-based, increasing the force such that the increase of displacement is constant over time. At that point, the static peak is reached ($F_{s,friction} = F_{tangential}$). With this value, the static friction coefficient is calculated ($\mu_s = F_{s,friction}/F_N$).

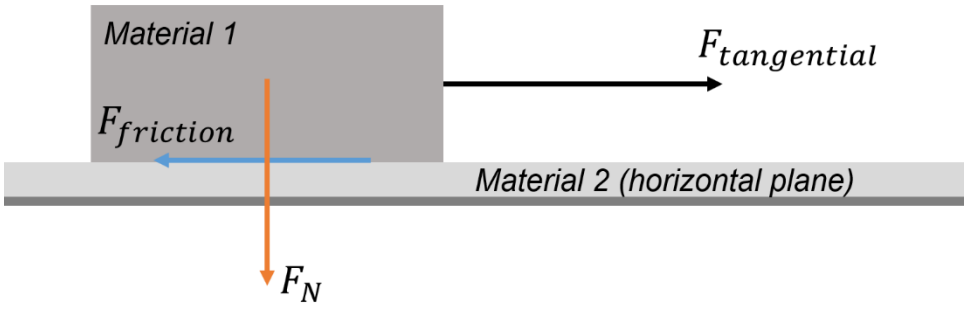

Figure 4.1. Schematic overview of the horizontal plane method

4.1.2 Vertical plane method (VP)

The vertical plane method (VP) is similar to the horizontal plane method, but rotated 90° (Figure 4.2). Normal pressure is introduced by a horizontal force (F_N). One of the materials (middle sample) is compressed between two samples of the other material. Then, the tangential force is introduced and increased to pull out the middle sample. The tangential force and the displacement of the sample are measured. By post-processing the data, the static friction force can be determined and the static friction coefficient can be calculated (in this case $\mu_s = 0.5 \cdot F_{s,friction}/F_N$).

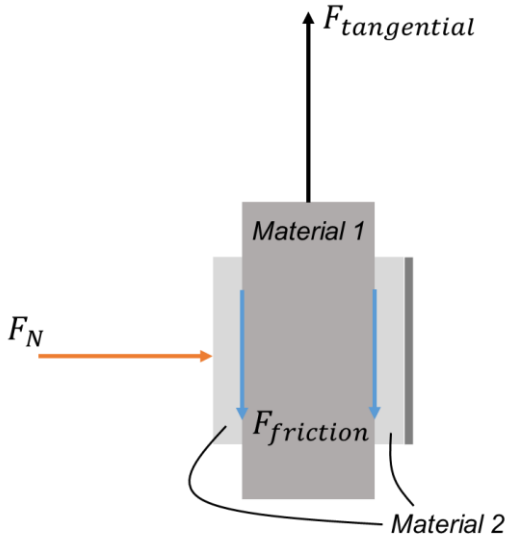

Figure 4.2. Schematic overview of the vertical plane method

4.1.3 Inclined plane method (IP)

In the inclined plane (IP) method, the two materials are brought into contact, by placing a block of one material on a plane of the other material (Figure 4.3). During the test, the angle of the plane is increased until the block starts sliding. The angle at which sliding starts (α) is used to calculate the friction coefficient ($\mu_s = F_{s,friction}/F_N = F_N \cdot tan(\alpha)/F_N = tan(\alpha)$).

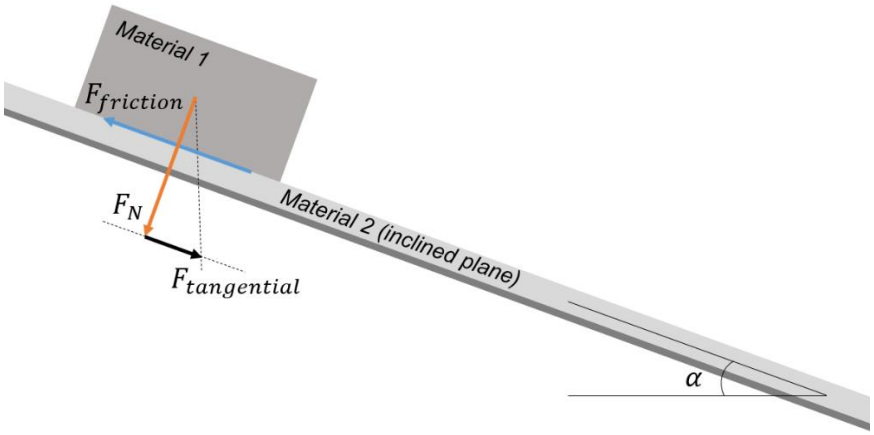

Figure 4.3. Schematic overview of the inclined plane method

4.1.4 Pin-on-disk method (POD)

In the pin-on-disk method (POD), a pin of one material is placed on a disk of the other material (Figure 4.4). The contact pressure is applied by adding dead weight above the pin. It is advised to not directly place the load on the pin, but to add a spring or a hydraulic system to reduce the pressure variation in case of surface variations (Stachowiak et al., 2004b). During the test, the disk is rotated. The tangential force ($F_{tangential}$) at the friction surface is determined based on the deflection of the elastic arm (Kennedy et al., 2015; Shi et al., 2011; Stachowiak et al., 2004a; Wahlström et al., 2017; Ying & Yupeng, 2017). The deflection of the elastic arm is determined with measured strain elongations at both sides of the elastic arm. These elongations are measured by strain gauges or a piezometric gauges (Stachowiak et al., 2004a). The coefficient of friction can be calculated with the tangential force and normal force ($\mu = F_{tangential}/F_N$). A variant of the pin-on-disk method is the ball-on-disk method, in which the pin is replaced by a ball (Wang et al., 2012). The pin-on-disk method is used only for kinetic friction measurements.

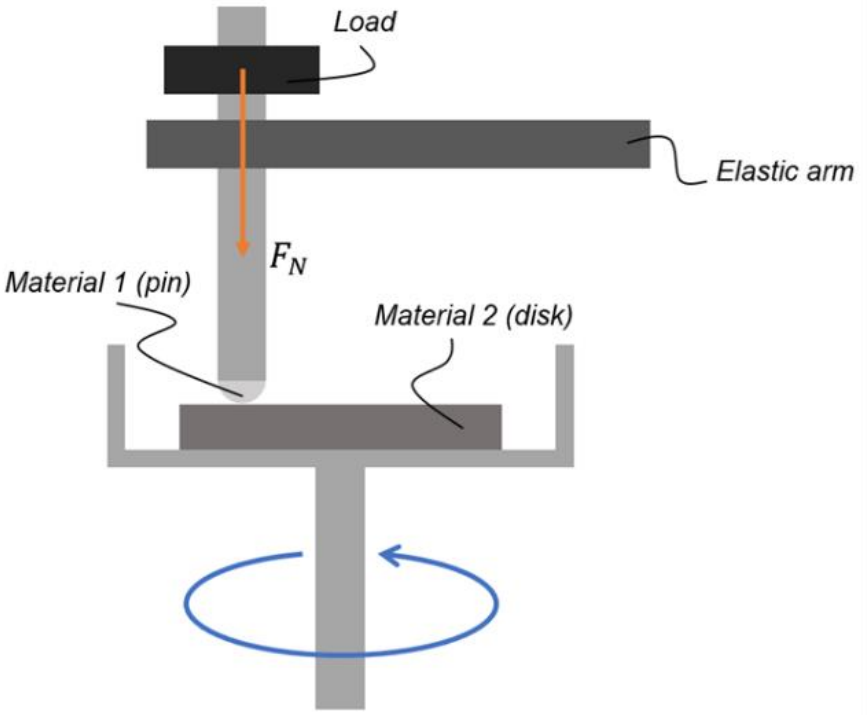

Figure 4.4. Schematic overview of the pin-on-disk method

4.2 Test criteria for monopile sea fastening

The criteria for the test methods are divided into two parts, namely the output and the input. The most important output for monopile sea fastening is the static friction coefficient. A graph including the friction force and the displacement is useful to get more insight into the friction behavior. Kinetic friction is not required output, because the monopile sea fastening should be in the static regime at any times. It is important that the conditions in which tests are performed are comparable to their application because these conditions influence the friction behavior. The effects of these factors are described in Chapter 3. The input criteria are thus based on the factors affecting monopile sea fastening friction. The criteria for the test method, defined in this research, are:

Required output:

1. Static friction (coefficient) can be calculated.
2. It is possible to obtain force-displacement graphs for the static regime.

Factors:

3. Test can be performed at different temperatures. During monopile sea fastening operations, these temperatures are approximately between -10 and 40 °C.
4. A constant pressure can be applied and can be controlled during testing.
5. A consolidation time can be taken into account.
6. It is possible to test in wet and dry conditions.
7. Monopile surfaces and polymer materials can be tested, with different characteristics like roughness, coating thickness, and hardness.
8. The rate of loading can be controlled.

The rate of loading is a factor that can differ significantly between setups in practice. As shown in Section 3.6 the different rates of loading can result in different friction coefficients. It is difficult to determine the rate of loading for a test setup since it is a combination of force and area. For a pin-on-disk test setup, the small area requires a small rate of loading. For an inclined plane setup, the larger area results in a larger rate of loading. It also important to mention that monopile sea fastening can best be described in force-based friction tests. In monopile sea fastening an increase in force results in an increase of displacement, not the other way around.

4.3 Comparison test methods

A decision matrix is composed to compare the different testing methods. Different colors indicate whether criteria are met for a certain test method, see legend (Table 4.1). It can be concluded from the decision matrix, that the best methods for testing monopile sea fastening friction are the horizontal plane method and the vertical plane method.

The pin-on-disk method focusses on kinetic friction by rotating the disk with a set velocity. This makes the method unsuitable for static friction measurements. The pressure cannot be kept constant in the inclined plane method, because of the rotating plane. Lubrication might get lost because of the inclination of the plane.

Table 4.1. Test method decision matrix

	Test method			
Criteria	**HP**	**VP**	**IP**	**POD**
1. Static friction coefficient				
2. Force-displacement graph				
3. Temperature				
4. Pressure				
5. Consolidation time				
6. Lubrication				
7. Tested materials				
8. Rate of loading				

Legend:

Criterium satisfied	
Criterium maybe satisfied	
Criterium not satisfied	

In Figure 4.5 an overview of the factors included in the vertical plane test is provided. This shows that all factors can be considered and in what way these factors are considered.

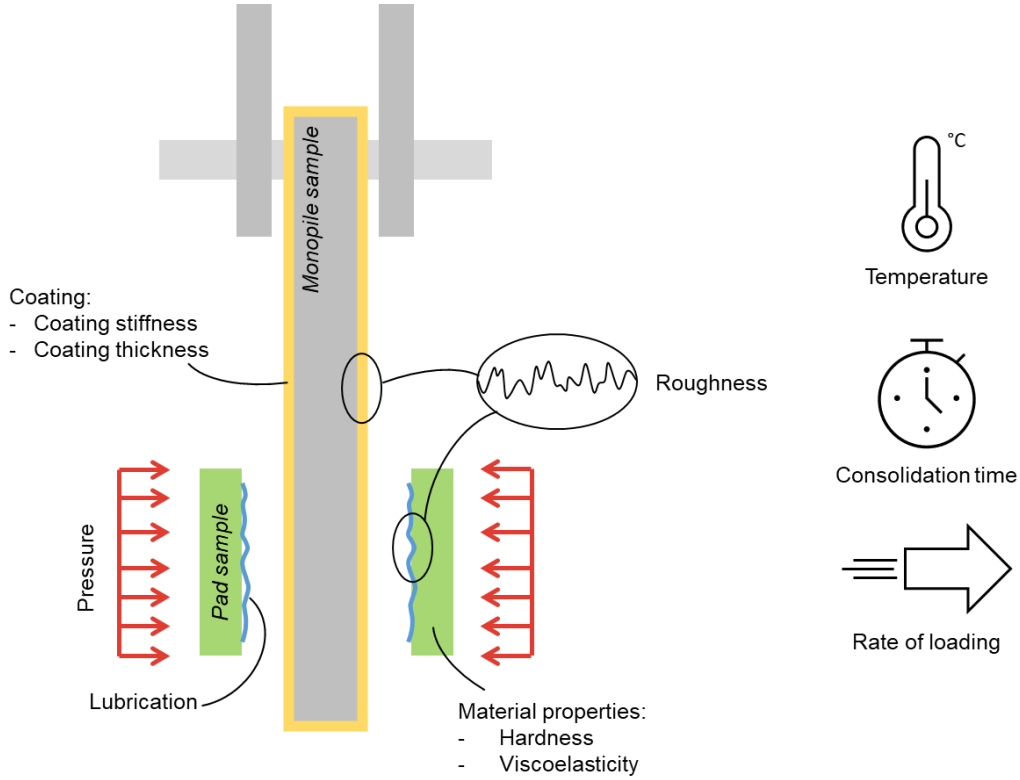

Figure 4.5. Factors affecting friction included in the vertical plane method

4.3.1 Test setups

A common test setup for the horizontal plane method is visualized in Figure 4.6. The pressure is applied by the self-weight of the block. The force to pull out the sample is applied by a string that is connected to the block on one side and the measurement device on the other side. Guidelines for these test setups state that the applied pressure must be around 4.9×10^{-4} MPa (ISO 8295, 1995). For test setups like these, the high pressures that are present in monopile sea fastening structures, cannot be met. There are two possibilities to overcome this issue. The first option is to increase the weight of the pulled object. This would require large and impractical structures. Another option is to use a compressor to push the materials together. A disadvantage of this option is that large moments and stresses are present in the setup (see Figure 4.7).

Figure 4.6. Horizontal plane friction measurement device (IDM instruments, n.d.)

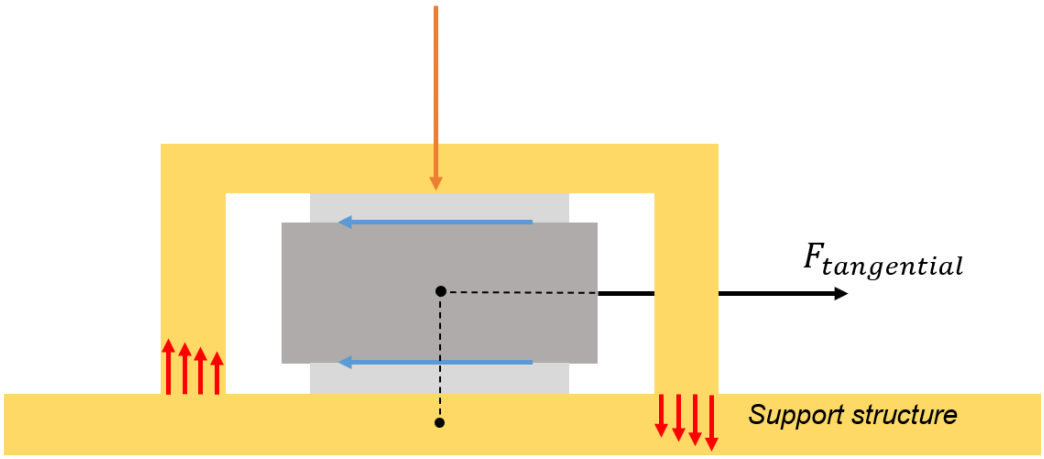

Figure 4.7. Stresses in a horizontal plane test setup with large normal force introduced by compressor

Another option for a test setup for the horizontal plane method is a tribometer with a moving plate. In this case a small specimen can be brought into contact with a counter material which is attached to a base plate. The base plate is displaced with a set velocity. This means that the friction test is displacement controlled, which is not representative to the monopile sea fastening application. The tribometer performs a number of displacement cycles per test. The multiple cycles and thus the continuous movements, probably describe kinetic friction instead of static friction. It is not known if settings in a tribometer can be adjusted such that the test studies static friction. The result of these cycles is often averaged, which results in a coefficient of friction. When performing these tests a more constant value is expected, because the coefficient of friction is determined based on multiple cycles.

The vertical test setup is less common than the horizontal plane method. In Figure 4.8 a test setup for the vertical plane method is visualized. Two samples of the support material are placed in the holders. The steel sample is placed between the two other samples. Since the friction test should resemble the high pressure conditions present in monopile sea fastening, a compressor is used to introduce the pressure on the materials. There are still moments remaining in the setup, but these can be mitigated. The difference in moments in the test setup is a major difference compared with the horizontal plane method. The vertical plane test setup is used for the friction measurements in this research.

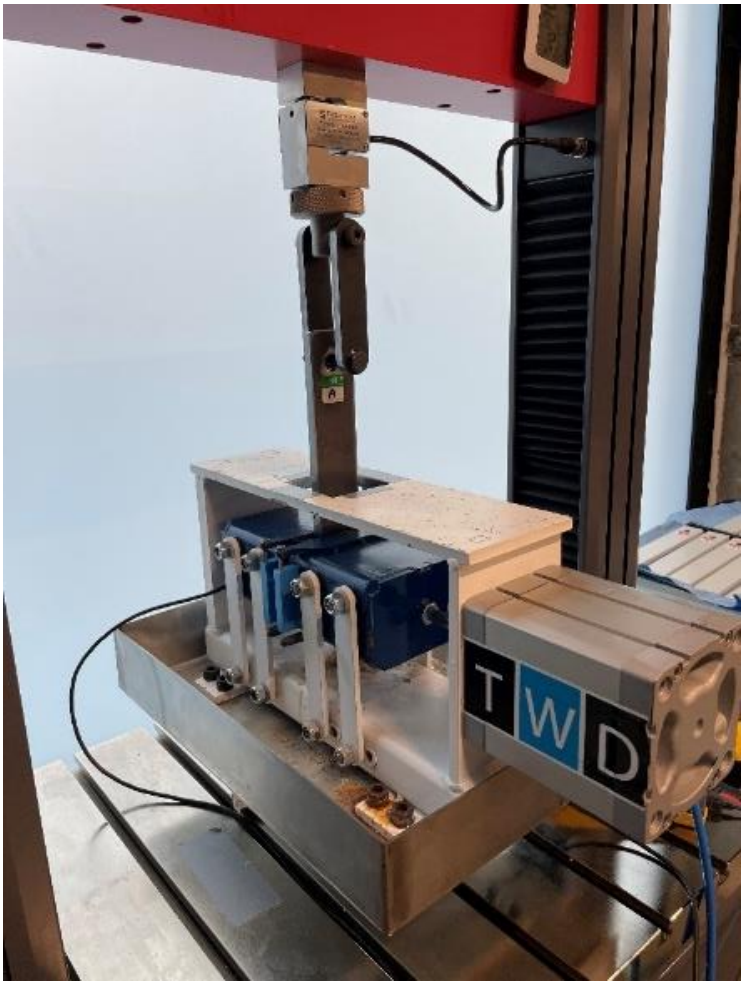

Figure 4.8. Vertical plane friction measurement test setup

An important factor influencing the pressure is the type of contact of the interface. In ASTM G115-98 (1998) eight different types of contact are mentioned. These types of contact can be divided into conforming shapes and Hertzian contacts (Figure 4.9). For conforming shapes, the apparent area of contact can be determined directly by geometrical computations. For Hertzian contacts, the real area of contact must be estimated by formulas that are based on geometry and material properties. The type of contact determines the apparent area of contact and the pressure distribution over this area (Popov, 2010).

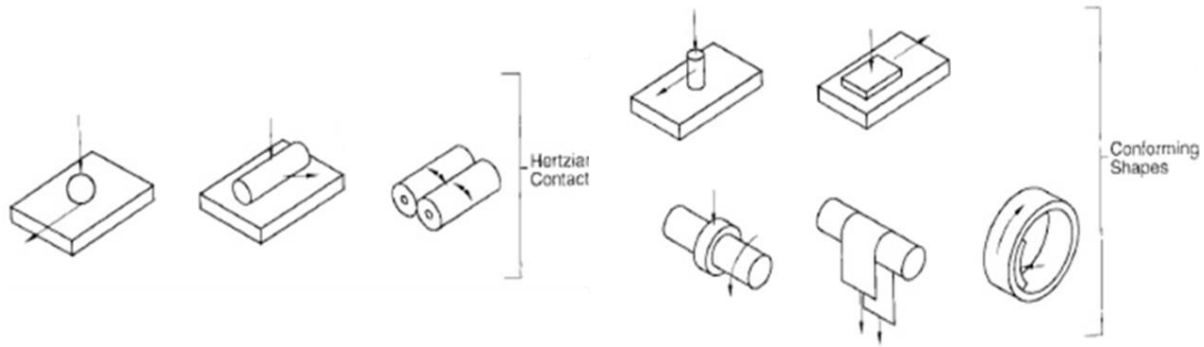

Figure 4.9. Types of contact (adjusted ASTM G115, 1998)

Hertzian type of contact could be present when a monopile encounters a flat support pad. However, a monopile can have a large diameter of 4 up to 7 meters (Negro et al., 2017), which could even increase up to 13 meters. The monopile also deforms together with the support pad. This results in a conforming shape type of contact is present. A conforming shape type of contact is also present when the monopile is supported by a polyurethane with the same rounded shape. The contact type between the monopile and the support can thus be assumed to be conforming shape.

4.4 Test setup used in this research

The testing procedure that is used for the sensitivity tests in Chapter 5 is based on the vertical plane method. To start, the steel sample is placed in the test bench. After that, the support pad samples are placed in the holders and the materials are pressed together by a normal force. After a consolidation time, the steel sample is pulled out by the tangential force which is applied by a load cell. Applying the tangential force is done with a preset rate of loading. The displacement rate has boundaries between 1 and 10 mm/min. During the test the force and the displacement are measured by the test bench.

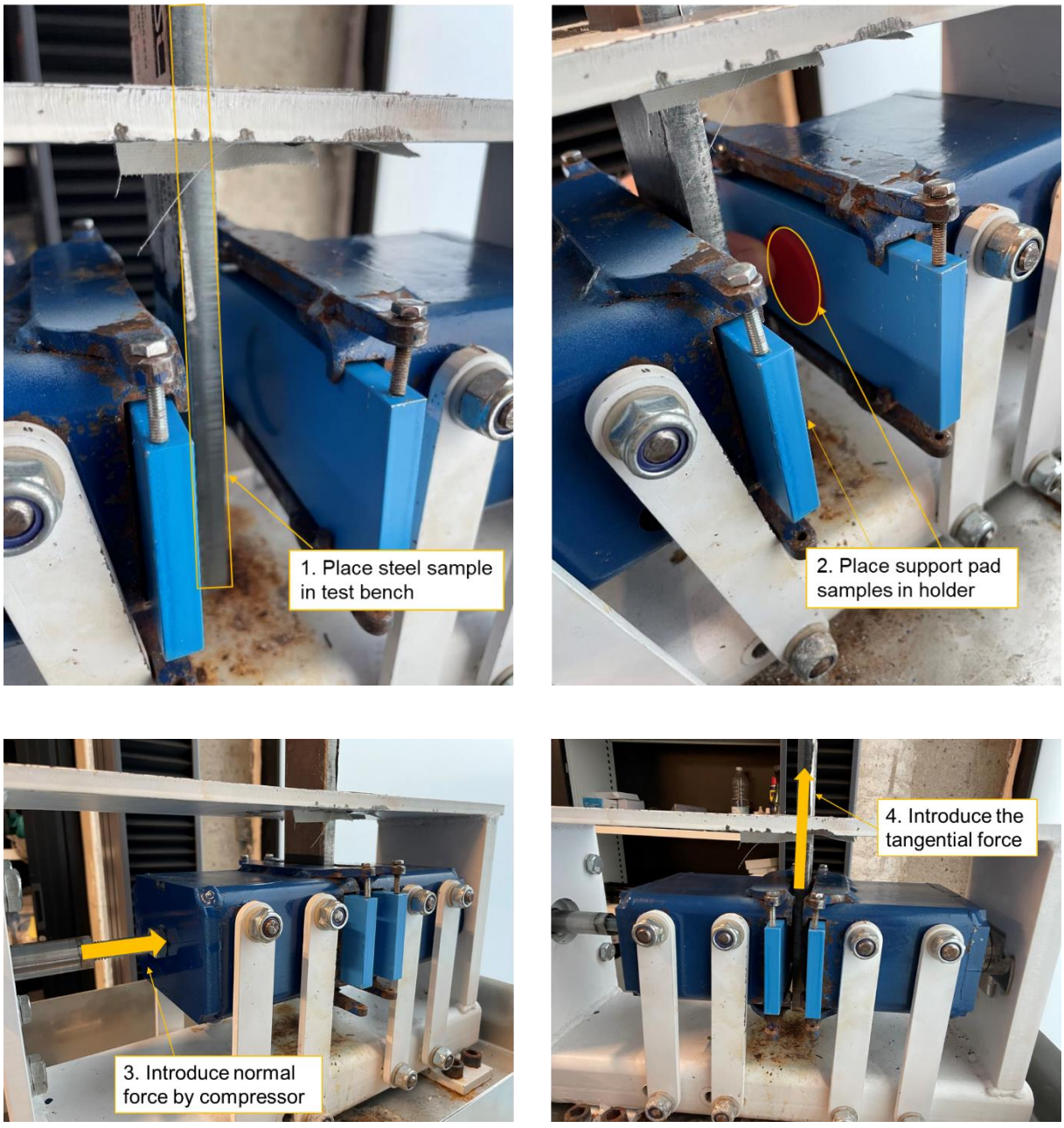

Figure 4.10. Testing procedure vertical plane friction test

4.5 Determining friction coefficient from measurements

Selecting the transition point results in a static coefficient of friction and in a static friction graph. The transition point is the point at which the kinetic regime is reached. This means that relative movement of the surfaces in the friction interface starts from there (Section 2.1). Determining the transition point is thus based on the displacements in friction graphs. A large difference is observed between the static and the kinetic regime when the displacements are plotted over time. The slope of the displacements in the static regime is smaller than the slope of the displacements in the kinetic part (Figure 4.11).

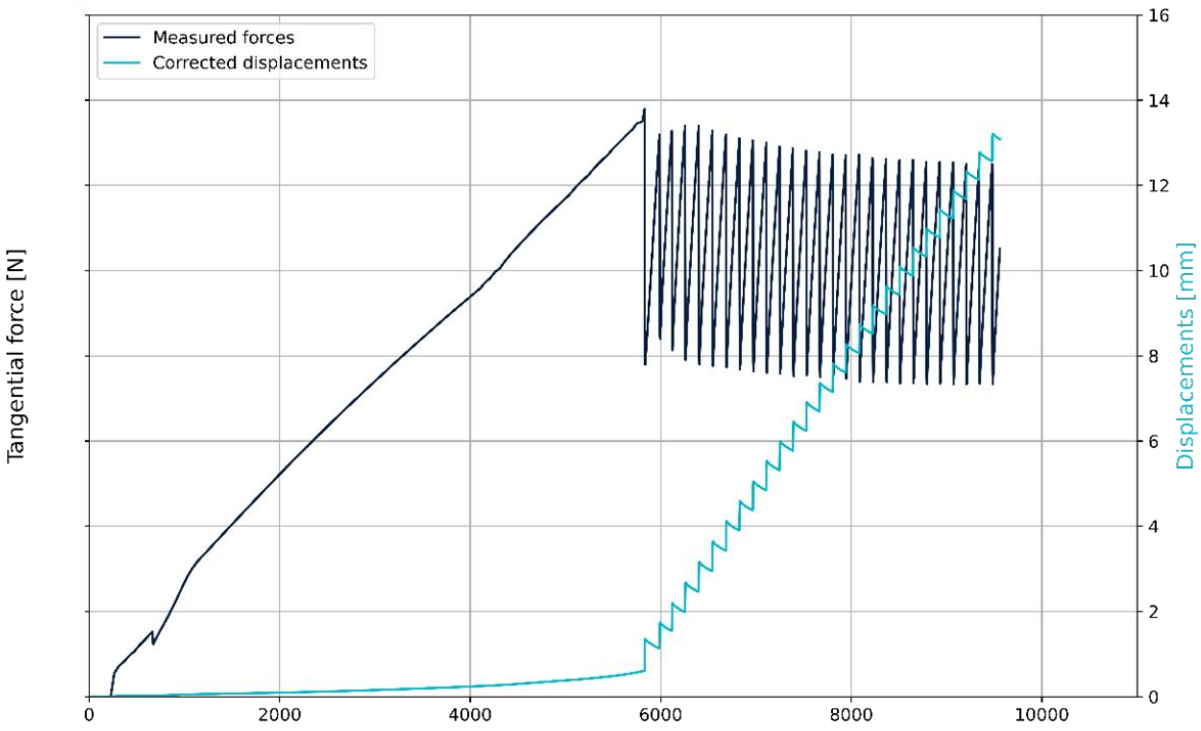

Figure 4.11. Measured forces and displacements
(from temperature-viscoelasticity sensitivity tests, test 15, testing conditions in Section 5.2)

The transition point can be selected manually. An algorithm is introduced to increase the speed and the reproducibility of the selection process. In the algorithm the transition point is the point in which the line approximation of the displacements in the static regime intersects with the line approximation of the displacements in the kinetic regime. The line approximation of the static regime is based on the first part of the measurements and the line approximation of the kinetic regime is based on the last part of the measurements. These outer regions are taken, since it is not yet known where the transition point is. Increasing the range could lead to better approximations, but the risk is present that one of the points is in a different regime.

The number of points for a test series is noted as n in the formulas used. The amount of point in the example used in this section is approximately 9500. The number of points will affect certain set parameters in the algorithm. The two points used for the determining the line approximation through the static displacements are calculated in Formula 4.1 and 4.2. The determination of $d_{static,1}$ is the average displacement of the first 100 points. The average displacement from the 1000th to 1100th point is $d_{static,2}$. The number of points from which the average is determined depends on the total amount of points. Also the values between $d_{static,2}$ is determined also depends on the total number of points. The 1000th point can be decrease for a lower number of points, or increased for a higher number of points. The slope of the line, A_{static}, is calculated in Formula 4.3. B_{static} is calculated in Formula 4.4.

$$d_{static,1} = \frac{1}{100} \cdot \sum_{i=0}^{100} d_i \qquad 4.1$$

$$d_{static,2} = \frac{1}{100} \cdot \sum_{i=1000}^{1100} d_i \qquad 4.2$$

$$A_{static} = \frac{d_{static,2} - d_{static,1}}{1000} \qquad 4.3$$

$$B_{static} = d_{static,1} - A_{static} \cdot 50 \qquad 4.4$$

The same principle is used for the determination of the kinetic points, but instead of using the first points, the last points are used. The points used for approximation the kinetic displacements are calculated with Formula 4.5 and 4.6. The line parameters are calculated with Formula 4.7 and 4.8.

$$d_{kinetic,1} = \frac{1}{100} \cdot \sum_{i=n-1100}^{n-1000} d_i \qquad 4.5$$

$$d_{kinetic,2} = \frac{1}{100} \cdot \sum_{i=n-100}^{n} d_i \qquad 4.6$$

$$A_{kinetic} = \frac{d_{kinetic,2} - d_{kinetic,1}}{1000} \qquad 4.7$$

$$B_{kinetic} = d_{kinetic,1} - A_{kinetic} \cdot (n - 1050) \qquad 4.8$$

With all line parameters present, the index of the transition point can be calculated (Formula 4.9). This is the intersection of the two line approximations. The outcome of this formula should be rounded to an integer, since it is an index.

$$TP_{index} = \frac{B_{kinetic} - B_{static}}{A_{static} - A_{kinetic}} \qquad 4.9$$

The procedure to determine the transition point is visualized in Figure 4.12. A manual check is required since the displacement graphs can differ and result in too high or too low transition point indices.

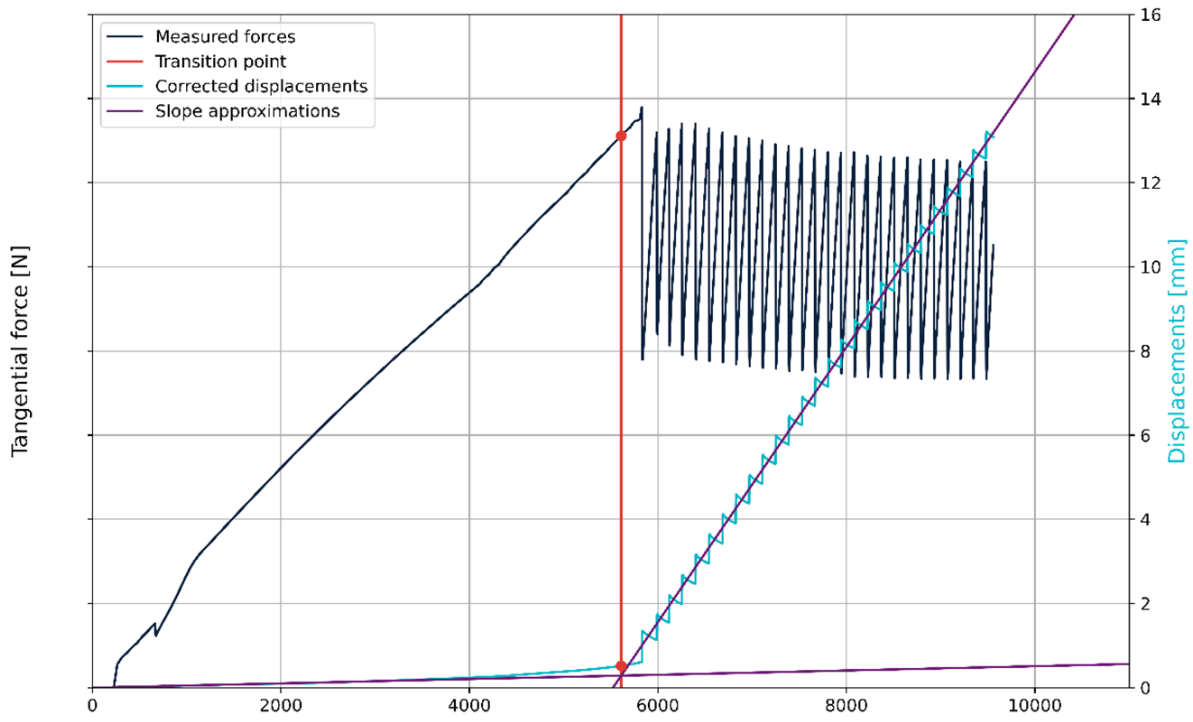

Figure 4.12. Transition point determination

(from temperature-viscoelasticity sensitivity tests, test 15, testing conditions in Section 5.2)

4.6 Conclusion

From a decision matrix it is concluded that the best methods for measuring friction are the horizontal plane method and the vertical plane method. The criteria used in the decision matrix are based on the required output (the coefficient of friction and the force-displacement graph) and required input (friction conditions). It is impractical to reach these high pressures with a test setup based on the horizontal plane method, because of moments occurring in the setup. The comparison between the methods shows that the way of testing friction can affect friction. The testing standard should prescribe a setup that is able to represent the factors that affect friction and should be based on the horizontal plane or vertical plane method to test friction.

5 Sensitivity tests

The purpose of this Chapter is to investigate the effect of factors on friction and to explain these effects. The selected factors and the reason for selecting these factors is highlighted first. This is followed by hypotheses for each factor. Details on the test procedure are mentioned in Section 5.2 and 5.4. The test results are analyzed in Section 5.3 and 5.5.

5.1 Selection of factors & hypotheses

This Section treats the selected factors that affect friction individually. The reason for testing and the hypotheses are explained. Four of factors are selected for a dedicated test series within this research. The selection is based on the amount of knowledge on the effects and the flexibility in the design choices. The selected factors that affect friction are:

- Hardness, since the effect on friction is unknown and the optimal hardness for the support pads can be chosen.
- Monopile roughness, since the effect of roughness only is not known at the specific conditions for monopile sea fastening. Investigating the monopile roughness in combination with the hardness is interesting since both are related to the real contact area.
- Temperature, since the effect of temperature is unknown and design choices can be improved with information of temperature effects.
- Viscoelasticity, since the effect on friction is not known and it can be used in the selection of a support material.

5.1.1 Hardness

It is known that hardness affects friction, but it is not known what that effect is (subsection 3.1.1). Friction is a combination of real contact area and shear strength according to the theory of Briscoe & Tabor (1978). An increase of one the components results in an increase of friction. The real contact area increases and the shear strength decreases for increasing hardness according to the theory from Briscoe & Tabor. This theory is not conclusive on the effect of hardness. The static friction coefficient decreases with increasing hardness according to experimental works of Capanidis & Sokolska (2020). An opposite effect is observed with the data of TWD (2020a), where an increase in hardness resulted in an increase in friction.

The hypothesis for the further research is based on the results from test data of TWD (2020a), because the test conditions are comparable to the test conditions that will be used in these sensitivity tests (Subsection 5.2.1).

Hypothesis 1: Static friction resistance increases with hardness.

Accept if: The static coefficient of friction increases with hardness.
Reject if: The static coefficient does not clearly increase with hardness.

5.1.2 Monopile roughness

The effect of monopile roughness only on friction is not known for the conditions applicable in monopile sea fastening. The increase in roughness can increase the real contact area and thus the friction Briscoe & Tabor (1978). Ivkovic et al. (2000) performed tests on solids in general and found that an increase in roughness resulted in an increase of friction. Corroded samples, with a higher roughness than blank steel, proved to have a higher friction coefficient than blank steel. The corrosion might affect more than just the roughness. It cannot be concluded that the increase in roughness results in an increase of friction. Based on the above mentioned research it is expected that an increase in monopile roughness results in an increase of friction.

Hypothesis 2: Static friction resistance increases with monopile roughness.

Accept if: The static coefficient of friction increases with monopile roughness.
Reject if: The static coefficient of friction does not clearly increase with monopile roughness.

5.1.3 Temperature

The relation of temperature with friction is mentioned in several studies (Bowden & Tabor, 1966; Briscoe & Tabor, 1978; Ludema & Tabor, 1966; Myshkin & Kovalev, 2009). In none of these studies the effect is described. Data from TWD (2021c) shows that friction is temperature dependent. The hypothesis is based on these findings.

Hypothesis 3: Static friction resistance increases with temperature.

Accept if: The static coefficient of friction increases with temperature.
Reject if: The static coefficient of friction does not clearly increase with temperature.

5.1.4 Viscoelasticity

The study of Ludema & Tabor (1966) relates rolling friction to viscoelastic properties. The rolling friction coefficient increases for an increase in viscoelastic properties. Viscoelastic properties change with temperature (Brinson & Brinson, 2015). Viscoelastic properties could affect friction since temperature

affects friction. The hypothesis is based on the temperature effect on friction and the temperature effect on viscoelastic properties (tan(δ), storage modulus and loss modulus). Since the viscoelastic properties are decreasing with increasing temperature, the expected effect on friction is opposite.

Hypothesis 4: Static friction resistance increases with decreasing viscoelastic properties.

Accept if: The static coefficient of friction increases with viscoelastic properties.

Reject if: The static coefficient of friction does not clearly increase with viscoelastic properties.

Hypotheses 1 and 2 are combined in a test series, because both might be related to the real contact area. Since viscoelastic properties are temperature dependent hypotheses 3 and 4 are combined in a test series

To obtain a complete overview of the test results, there are three things added in the review of the results. These things might not directly explain the change in static friction resistance but can increase the understanding of the friction measurements. The following things are considered:

1. The measured force-displacement graphs
2. The static force-displacement graphs without disturbances
3. The pre-sliding displacements (displacement in the static regime due to friction)

5.2 Test procedure: hardness – monopile roughness

The factors hardness and monopile roughness are combined in one test campaign, because possible combined effects can be detected as well. This Section explains the test procedure (hypotheses, test conditions and the test matrix).

5.2.1 Testing conditions

To test the effects of the hardness and monopile roughness, different support pad samples and steel samples are required. Four polyurethane samples are tested with different hardnesses (Figure 5.1). All four samples have the same roughness (R_a = 0.889 µm, Appendix A) and are from the same manufacturer. There are four steel samples as well (Figure 5.2). These originally blank steel samples were treated to achieve different roughness values. For each steel sample 60 roughness measurements were performed (30 for the front and 30 for the back). In Appendix C, the roughness measurements are analysed. The mean value of these 60 measurements is used in this analysis. The mean roughness value for the steel samples are included in Figure 5.2.

Figure 5.1. Tested polyurethane samples with hardness values

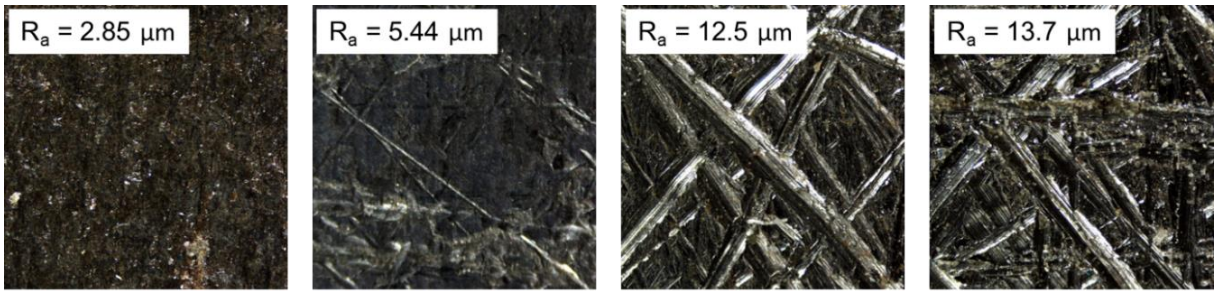

Figure 5.2. Microscopic pictures of tested steel samples with mean roughness values

The tests performed in this campaign focus on the hardness and the monopile roughness. This means that all other conditions need to be constant over all tests. In Table 5.1, these constant conditions are defined.

Table 5.1. Constant conditions roughness - hardness tests

Constant conditions	Value	Unit	Comment
Applied pressure	5	MPa	High pressures are conservative (Subsection 3.4)
Lubrication	Dry	-	Less variance in measurement (due to possible different amounts of lubrication)
Consolidation time	7	min	Little effect on friction (Subsection 3.8)
Rate of loading		kgf/min	-
Temperature	17	°C	Room temperature
Monopile coating	-	-	Blank steel (to eliminate coating effects, Subsection 3.3)
Support pad roughness (R_a)	0.889	µm	Same roughness for all PU samples (Appendix A)

5.2.2 Test matrix

Each combination of hardness and roughness is tested five times with different PU samples on the same steel sample. This results in 80 tests (16 unique combinations tested 5 times each). In Table 5.2, the varying conditions (hardness and monopile roughness) are defined per test.

Table 5.2. Varying conditions hardness – monopile roughness tests

Test	Roughness [µm]	Hardness [°Shore A]
1 – 5	2.85	75
6 – 10		80
11 – 15		90
16 – 20		95
21 – 25	5.44	75
26 – 30		80
31 – 35		90
36 – 40		95
41 – 45	13.7	75
46 – 50		80
51 – 55		90
56 – 60		95
61 – 65	12.5	75
66 – 70		80
71 – 75		90
76 – 80		95

5.3 Test results: hardness – monopile roughness

This section presents the results of the tests performed on the hardness and monopile roughness factors. To obtain the static friction coefficients, the corrected static force-displacement graph and the pre-sliding displacements, the transition points are determined according to Section 4.5. The force-displacement graphs are corrected according to the steps described in Section 6.4. The detailed results per test (static and kinetic regime, displacement graph) are included in Appendix H.

In the tests with steel sample D and PU samples with hardness 75 °Shore A, the PU samples broke loose from the holders (Appendix F). The high friction force in combination with the low resistance to deformation of the PU sample caused the sample to deform enough so that it could break loose. This influences the measurements. Therefore, these tests are not included in the analysis.

5.3.1 Hypothesis 1: Static friction is affected by hardness.

Per roughness a plot is made in which the coefficient of friction is plotted against the hardness (Figure 5.3). An increasing trend of the static friction coefficient for an increase in hardness is observed in this Figure. The same conclusion can be drawn from the mean values of the static friction coefficients. However, the number of measurements is limited (five per hardness) and this is important to consider when drawing conclusions from statistic values (mean and standard deviation).

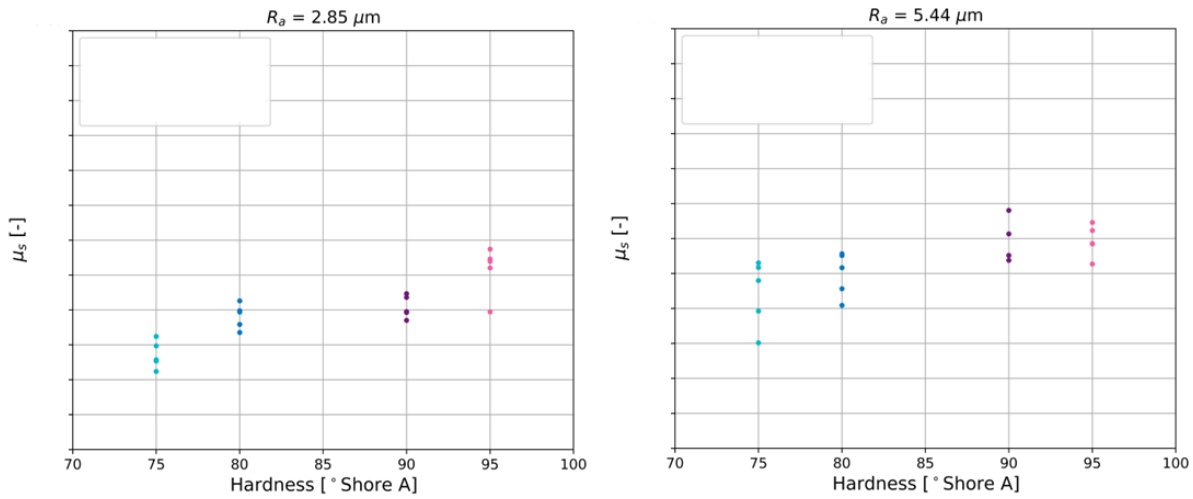

Figure 5.3. Influence of hardness on static friction coefficient (steel sample A and B)

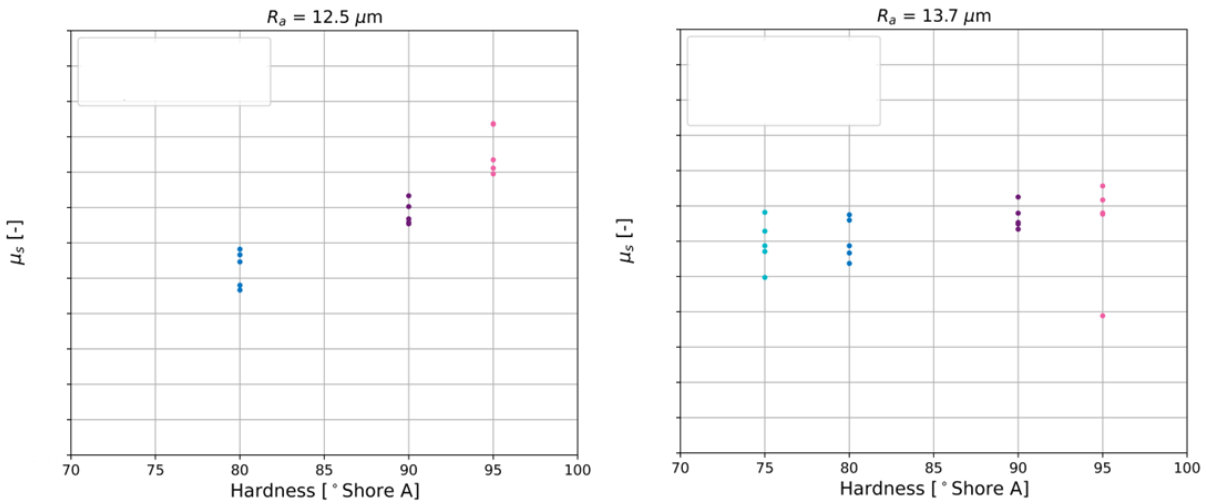

Figure 5.4. Influence of hardness on static friction coefficient (steel sample C and D)

The steel asperities that are in contact with the polymer can break and result in sliding of the surfaces. An increase in hardness results in an increase of polymer resistance. The real contact area reduces for higher hardness polymers. The increase in polymer resistance seems dominant compared to the decrease in real contact area for higher hardness materials (Figure 5.5). A decrease in real contact area would namely result in a decrease in friction resistance (which is not observed).

It is also possible that the polymer deforms such that the steel asperities can slide over it. The observed increase in friction resistance for an increase in hardness can be explained by the higher resistance to deformation of the higher hardness polymers.

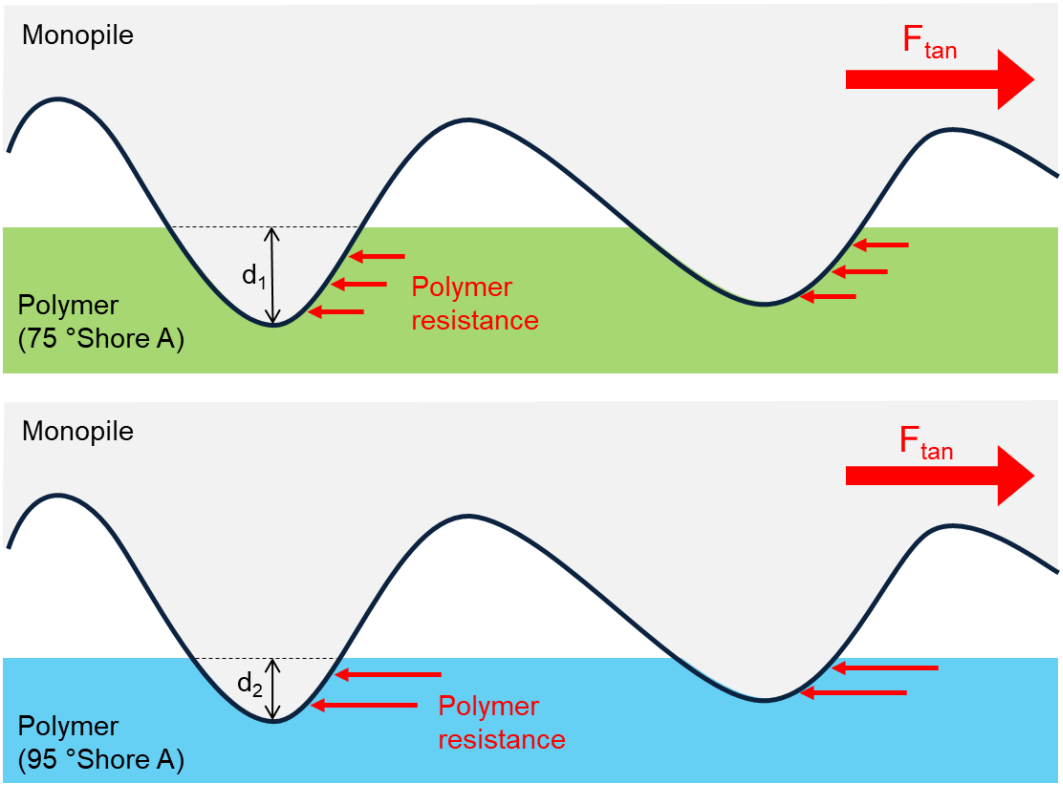

Figure 5.5. Visualization influence of hardness on static friction coefficient

Measured force-displacement graphs

The force-displacement graphs of the measurements performed with steel sample A (lowest roughness) and the four hardnesses are plotted in Figure 5.6. Looking at the static regime, the pad samples with a lower hardness show more variation in the graphs, this can be due to their lower shear stiffness. The pad samples with the highest hardness show the most constant behavior in the static regime. The components that cause the disturbances in the displacement measurements are visible in these graphs. The slope of the static regime of the graph is increasing with hardness. This slope is related to the shear displacement of the pad sample (Subsection 6.4.2). In the graphs a kink is observed in the static regime as well. This kink has to do with the displacement of the pad sample in the pad holder, the clearance of the steel back plate in the friction clamp and the clearance of the pins in the friction clamp (respectively Subsections 6.4.3, 6.4.4 and 6.4.5). The displacements are filtered from the force-displacement graphs and result in the corrected force-displacement graphs.

Although the kinetic regime is not important for the application monopile sea fastening, it can tell something about the variability of measurements. In all graphs stick-slip behavior is visible, except for the graph of test 13 (and partly the graph of test 12). This behavior can be explained by the fact that the tests performed in dry conditions (Section 3.5). The stick-slip behavior of the pad samples with a higher hardness is more constant than that of the pad samples with a lower hardness. This variability might also affect the selection of the transition point and thus the static coefficient of friction.

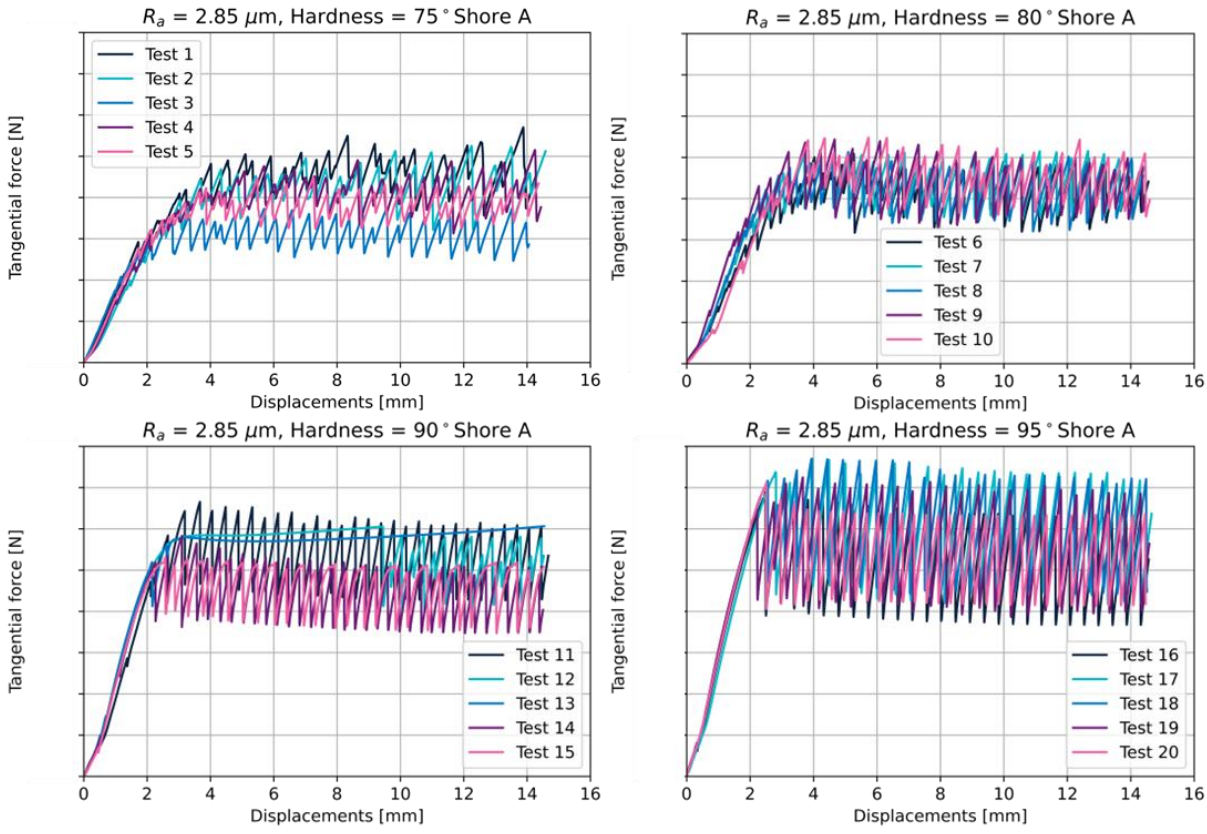

Figure 5.6. Force-displacement graphs for different hardnesses (steel sample A)

Corrected force-displacement graph

Figure 5.7 shows the graphs of the static friction regimes for the tests with steel sample A. In these graphs the displacements not due to friction are eliminated and only the static regime in shown (Section 6.4). Another thing that is noted is that the initial slope of the graphs increases with increasing hardness. The pre-sliding displacement is decreasing with increasing hardness. In Chapter 6 these corrected graphs are used to model friction and to fit model parameters.

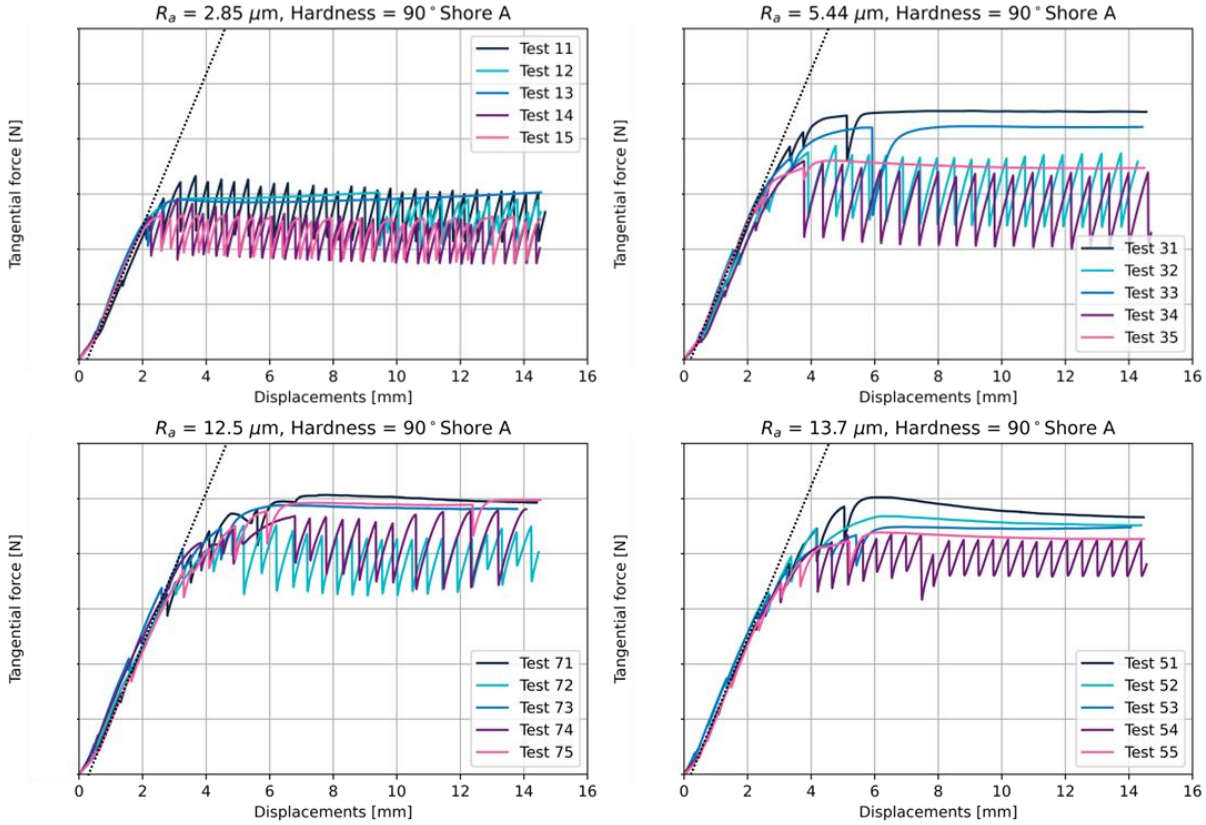

Figure 5.7. Corrected force-displacement graphs for different hardnesses (steel sample A)

Pre-sliding displacements

From Figure 5.7 it could already be observed that the pre-sliding displacements decrease slightly with increasing hardness. For a complete overview, the pre-sliding displacements are plotted against the hardness for the different steel samples in Figure 5.8. From these figures it can be confirmed that the amount of pre-sliding displacement is affected by hardness. In most cases, a higher hardness results in a smaller pre-sliding displacement.

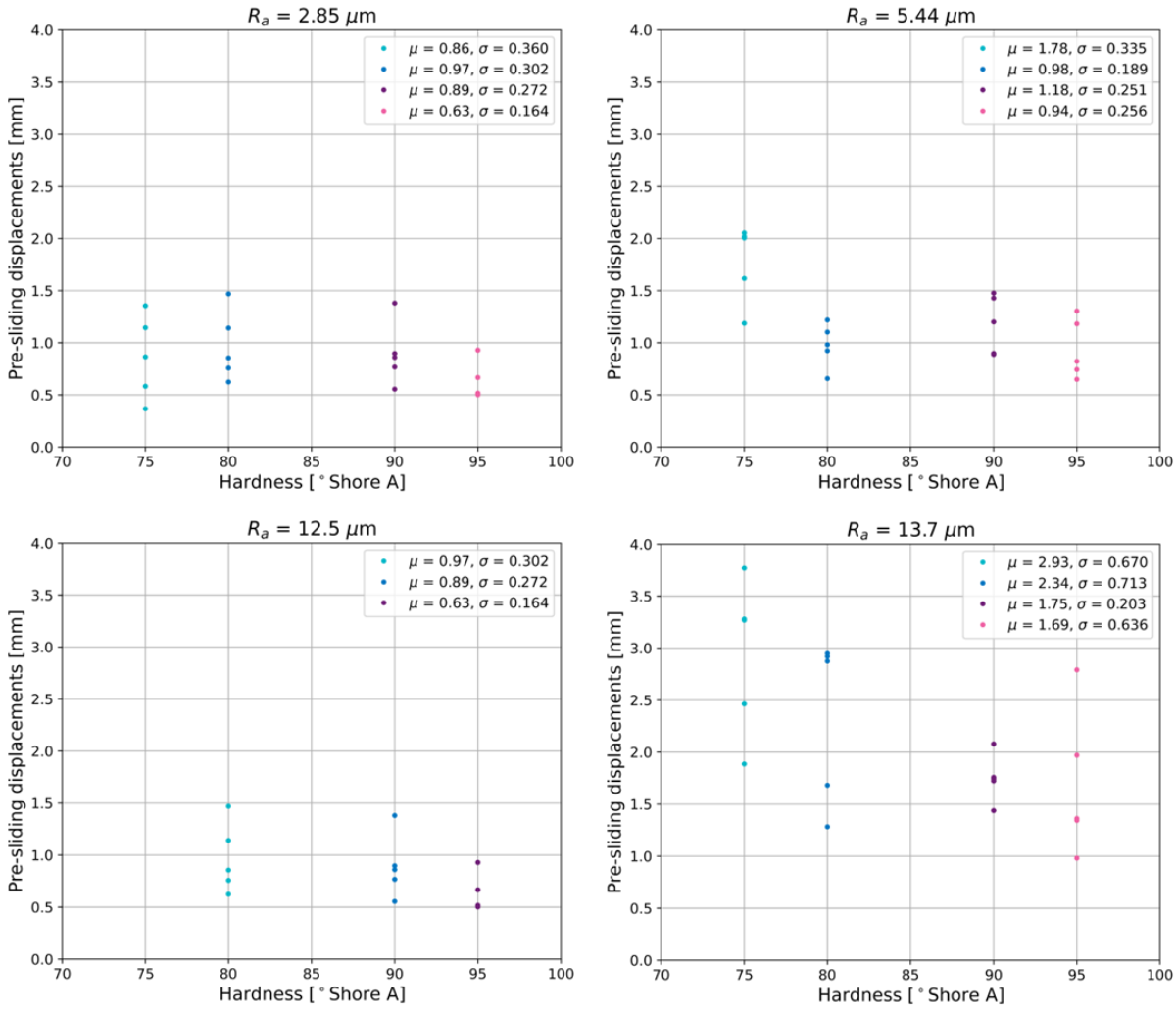

Figure 5.8. Influence of hardness on pre-sliding displacements

5.3.2 Hypotheses 2: Static friction resistance is affected by monopile roughness.

In Figure 5.9, the effect of roughness on the static friction coefficient is depicted. It is shown that a higher roughness results in a higher static friction coefficient. Only for the combination of PU samples with hardness 80 °Shore A and steel samples C and D (R_a is 12.5 and 13.7 µm respectively) this is not the case. The friction coefficient of steel sample D is in this case slightly lower than the friction coefficient of sample C. This might be caused by the limited difference in roughness.

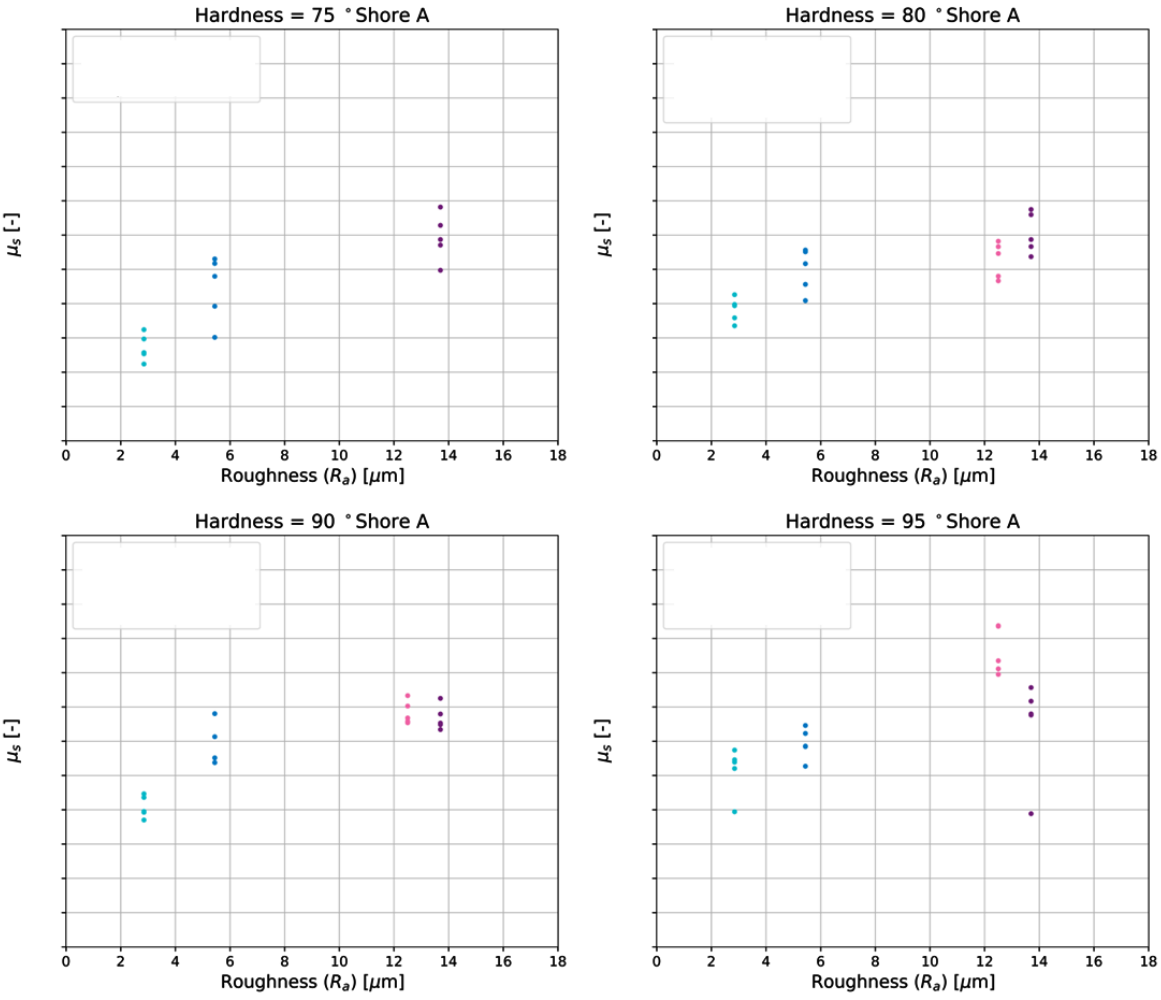

Figure 5.9. Influence of roughness on static friction coefficient

The effect of roughness on friction resistance can be explained by the difference in real contact area. For rougher surfaces the real contact area is larger. The shear strength is not affected by roughness, since this is a property of the PU samples. This means that an increase in roughness results indeed in an increase in friction resistance (Figure 5.10).

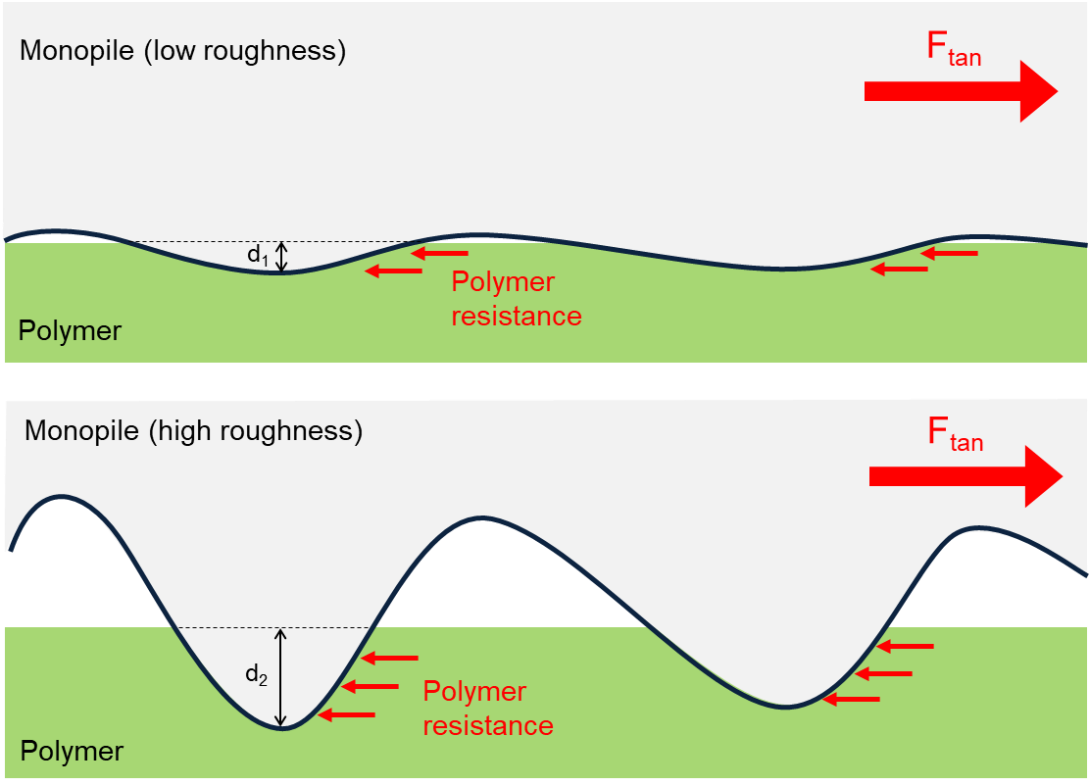

Figure 5.10. Visualization influence of roughness on static friction coefficient

Measured force-displacement graph

In Figure 5.11 and Figure 5.12 the force-displacement graphs of the tests with the 90° Shore A hardness pad samples are shown. The static regime of these force-displacement graphs is constant for the different roughness, because the shear deformation of the pads is similar (section 6.4.2). In all graphs a kink can be observed together with a bit of variation is that is related to the sample in holder clearance (section 6.4.3). In the kinetic regime two things are noticed. The higher the roughness the less often stick-slip occurs. Four out of five tests with the lowest roughness steel sample show stick-slip. For the steel sample with the highest roughness this happens just ones out of five times. This might be caused by the asperities not being able to build-up the contact again. There is no research that confirms this theory.

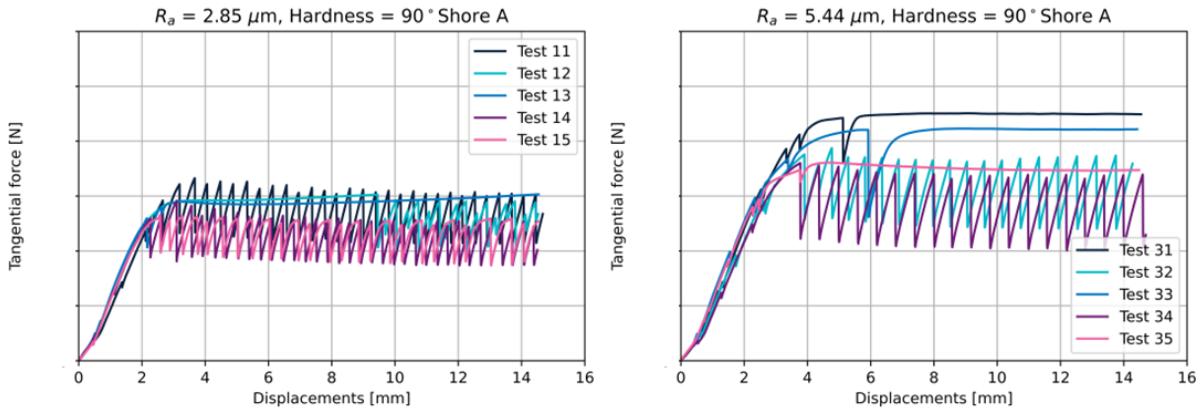

Figure 5.11. Force-displacement graphs for different roughnesses (90° Shore A, steel sample A and B)

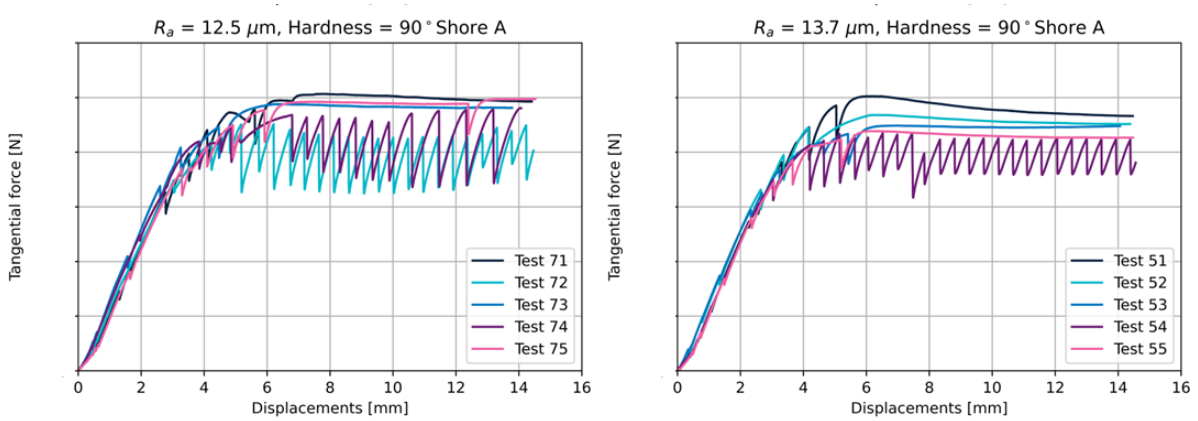

Figure 5.12. Force-displacement graphs for different roughnesses (90° Shore A, steel sample C and D)

Corrected force-displacement graph

Figure 5.13 shows the corrected force-displacement graphs of the static regimes for the tests with the pad samples of hardness 90 °Shore A. It can be observed that amount of variation does not differ significantly between the different roughnesses. The initial slope of the graphs is slightly steeper for the higher roughness materials than for the lower roughness materials. In Chapter 6 the corrected force-displacement graphs are used to model friction and to fit model parameters. The initial slope is one of the parameters that will be estimated.

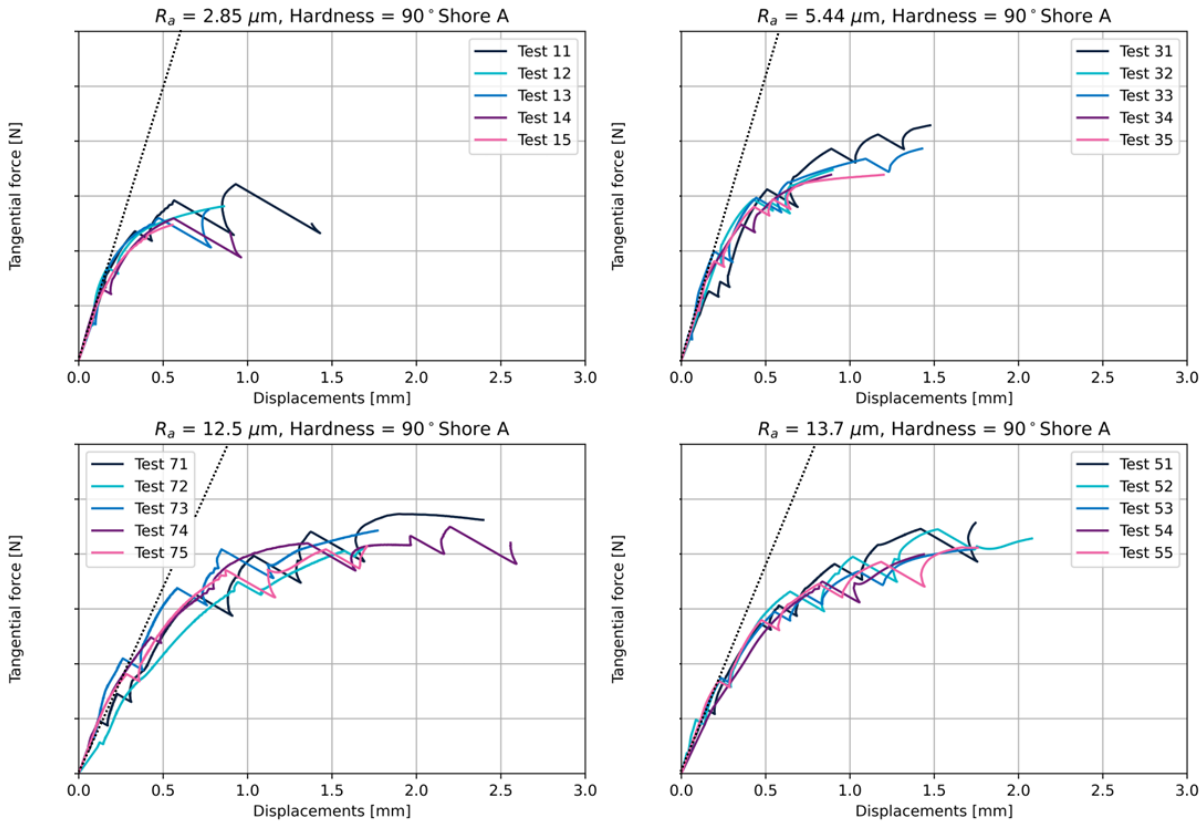

Figure 5.13. Corrected force-displacement graphs for different roughnesses (PU samples of 90° Shore A)

Pre-sliding displacements

The pre-sliding displacement is influenced by the roughness of the steel sample. In Figure 5.14 it is observed that the pre-sliding displacements are larger for samples with a higher roughness. The friction resistance is larger for steel samples with a higher roughness (Figure 5.14). This means that a larger force can be applied, before sliding starts. This larger force will result in more shear displacement of the pad samples.

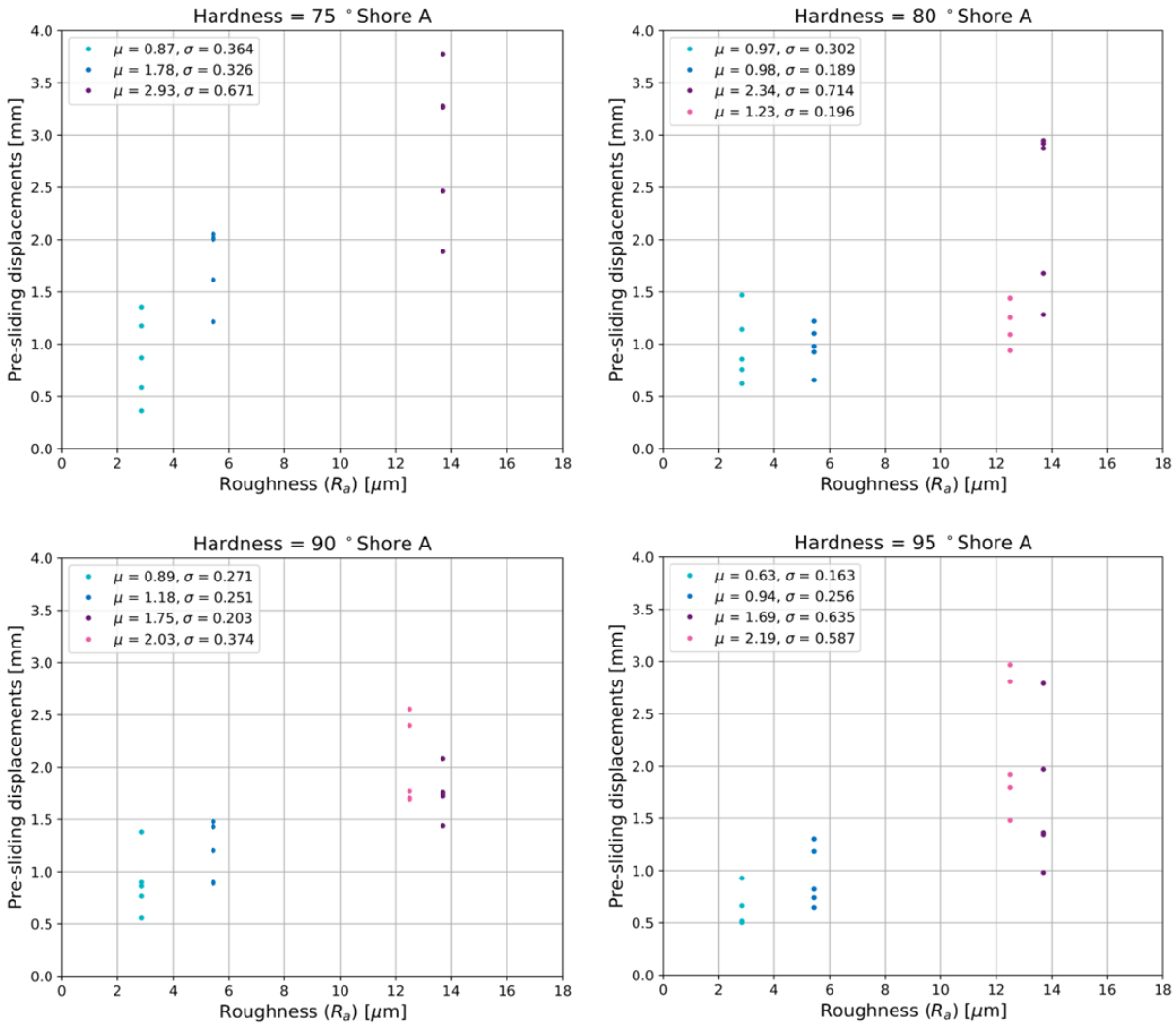

Figure 5.14. Influence of roughness on pre-sliding displacements

5.4 Test procedure: temperature-viscoelasticity

Temperature and viscoelastic properties are the two factors that are combined in this test campaign, this is why viscoelastic properties change with temperature. The test procedure (hypotheses, testing conditions and the testing matrix) is explained in this Section.

5.4.1 Testing conditions

To test the effect of temperature and viscoelastic properties on friction resistance, different polymer samples and temperature conditions are needed. Four PU samples are used, which do have different viscoelastic properties (Figure 5.15 for the materials, Figure 5.16 and Figure 5.17 for the viscoelastic properties). The viscoelastic properties of the PU with hardness 80° Shore A are not known, so the 85° Shore A is added. The tests are performed on room temperature, warm and cold conditions. Since it is difficult to measure the temperature of two surfaces in contact, an indicative value is taken.

Figure 5.15. Tested polyurethane samples with hardness values

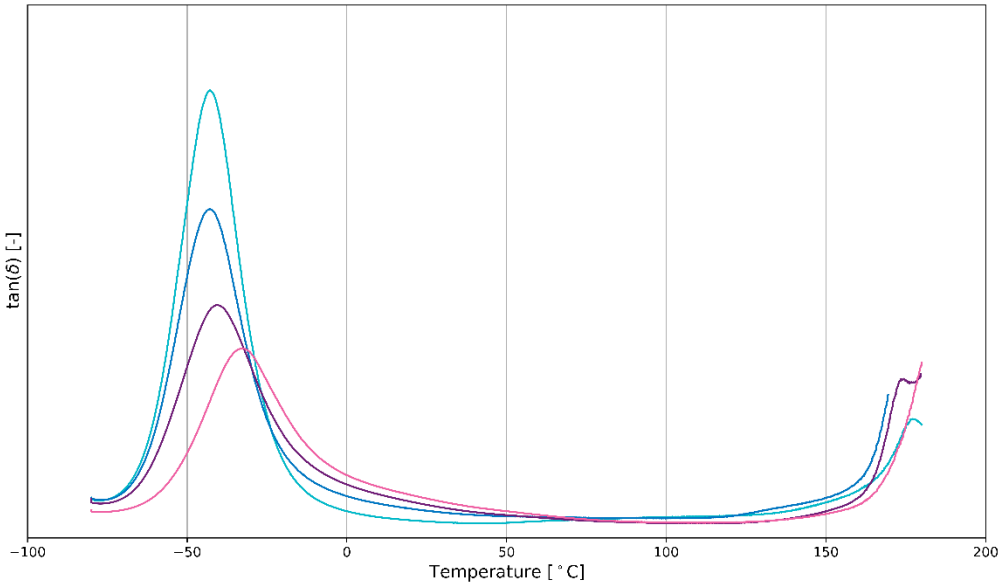

Figure 5.16. Temperature influence on tan(δ) of PU samples

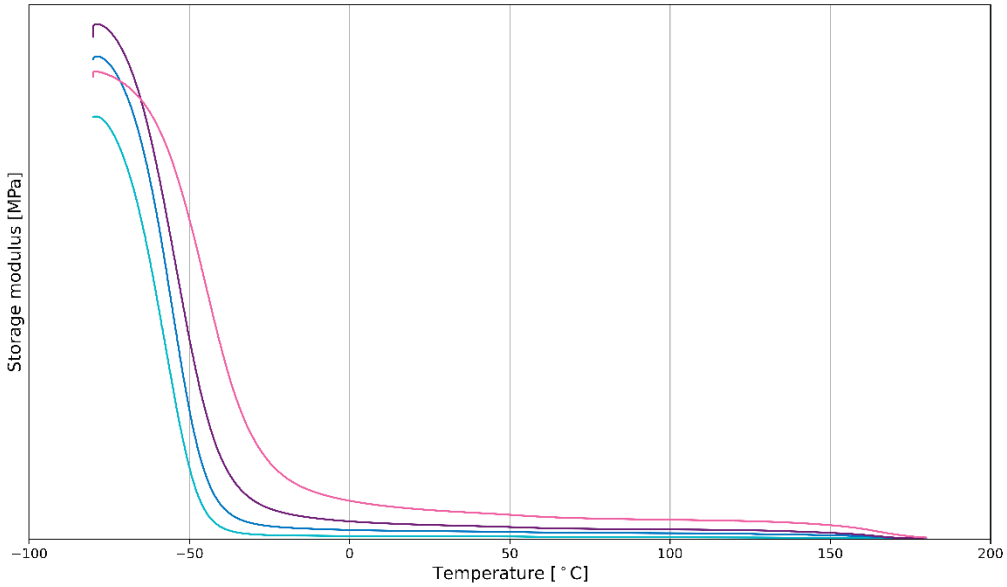

Figure 5.17. Temperature influence on storage modulus of PU samples

The warm tests are performed in a climate control room. The steel sample is placed in the climate control room and heats up to approximately 65 °C. The PU pads are placed in the holders and the pressure is applied. During the consolidation time (seven minutes) the friction interface of the PU samples warms up.

For tests performed in cold conditions, dry ice is used. The steel samples and the PU samples are cooled in a chamber for two minutes. After two minutes, the samples are placed in the test setup. After the consolidation time of seven minutes, the test starts.

To isolate the effect of temperature and viscoelastic properties in this test series, the other conditions must be constant. In Table 5.3 these constant conditions are given.

Table 5.3. Constant conditions temperature – viscoelasticity tests

Constant conditions	**Value**	**Unit**	**Comment**
Applied pressure	5	MPa	High pressures are conservative (Section 3.4)
Lubrication	Dry	-	Less variance in measurement (due to possible different amounts of lubrication)
Consolidation time	7	min	Little effect on friction (Section 3.8)
Rate of loading		kgf/min	-
Steel roughness (R_a)	2.85	µm	Steel sample A from roughness-hardness test campaign
Monopile coating	-	-	Blank steel (to eliminate coating effects, Section 3.3)
Support pad roughness (R_a)	0.889	µm	Same roughness for all PU samples (Appendix A)

5.4.2 Test matrix

Each PU material is tested on three different temperatures. This results in 12 unique combinations. The unique combinations are tested five times each. A total of 60 tests is required in this case. In Table 5.4 the complete overview of the varying test conditions is given.

Table 5.4. Varying conditions temperature – viscoelasticity tests

Test	Temperature	Hardness [°Shore A]
1 – 5	± 17 °C (Room temperature)	75
6 – 10		80
11 – 15		90
16 – 20		95
21 – 25	± -10 °C (Cold)	75
26 – 30		80
31 – 35		90
36 – 40		95
41 – 45	± 65 °C (Warm)	75
46 – 50		80
51 – 55		90
56 – 60		95

5.5 Test results: temperature-viscoelasticity

This section presents the results of the temperature-viscoelasticity tests. The detailed results per test (static and kinetic regime, displacement graph) are included in Appendix I.

5.5.1 Static friction coefficient

For all PU materials, first observations are made on the temperature effect on friction. This is followed by observations on the viscoelastic effects on friction. In Figure 5.18 visualizes the estimated ranges of the temperature in the tests.

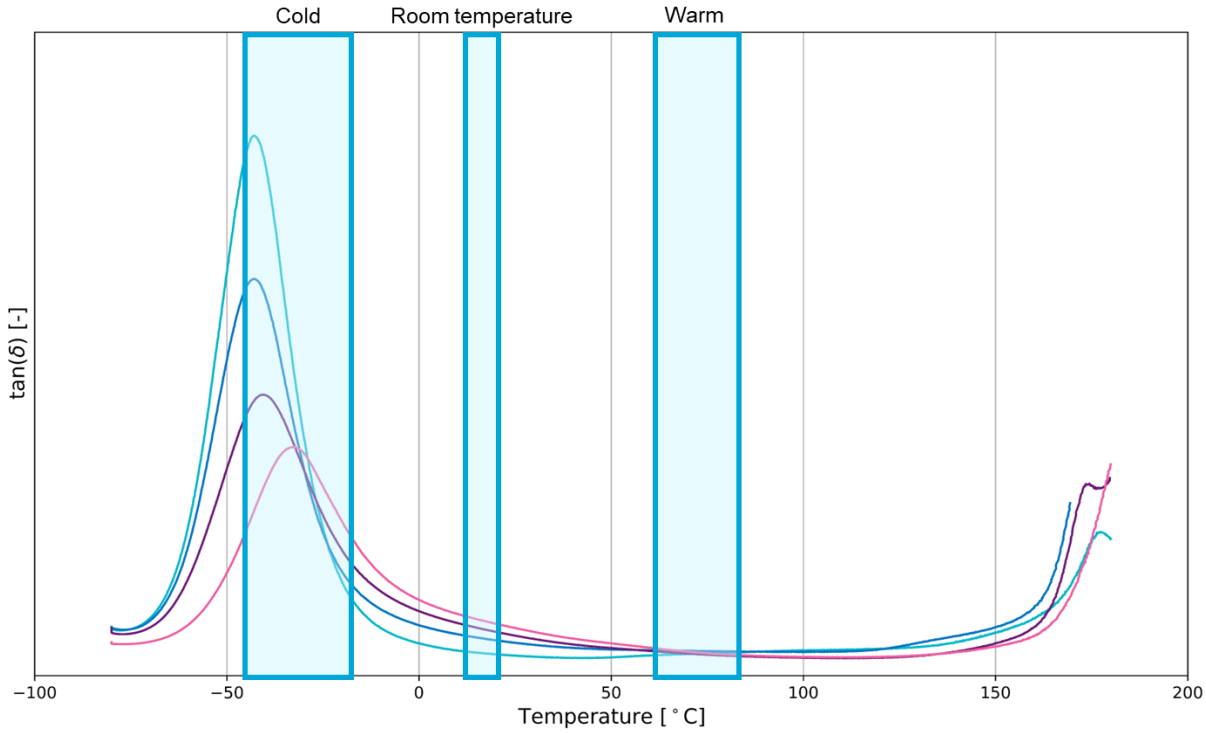

Figure 5.18. Tan(δ) of tested PU samples and indicated temperature ranges

The static friction coefficient decreases with increasing temperatures in the sensitivity tests. This is clearly visible in the friction coefficients of polyurethane materials of hardness 80° and 90° Shore A (Figure 5.19). Tan(δ) also decreases with increasing temperatures for 90° Shore A. No conclusions can be made relating viscoelastic properties to the static friction coefficient for the 80° Shore A PU, since for this material there is no information available on the behavior of tan(δ).

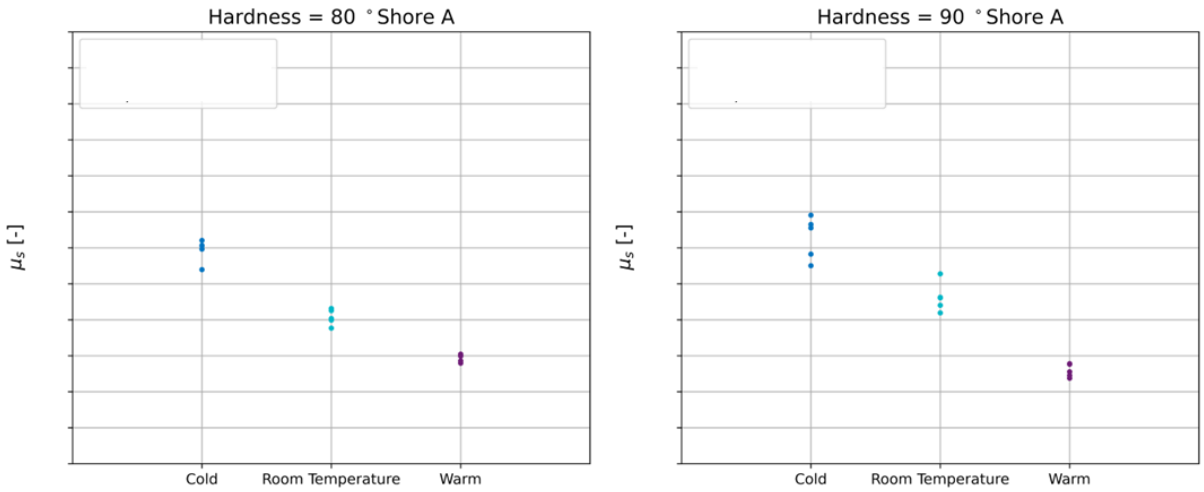

Figure 5.19. Influence of temperature on coefficient of friction (Hardness 80 and 90° Shore A)

For the material with the lowest hardness (75° Shore A) the static coefficient of friction at room temperature is comparable to that in warm conditions (Figure 5.21). For this material the tan(δ) at room temperature and in warm conditions is also similar. This could indicate correlation a correlation between viscoelasticity and friction. The behavior of the 75° Shore A pad sample after the cold test shows that viscoelastic behavior is observed. After the tests the pad sample was deformed and it took several minutes for the material to deform back to its original shape (Figure 5.20). The pads with a higher hardness did not show this behavior.

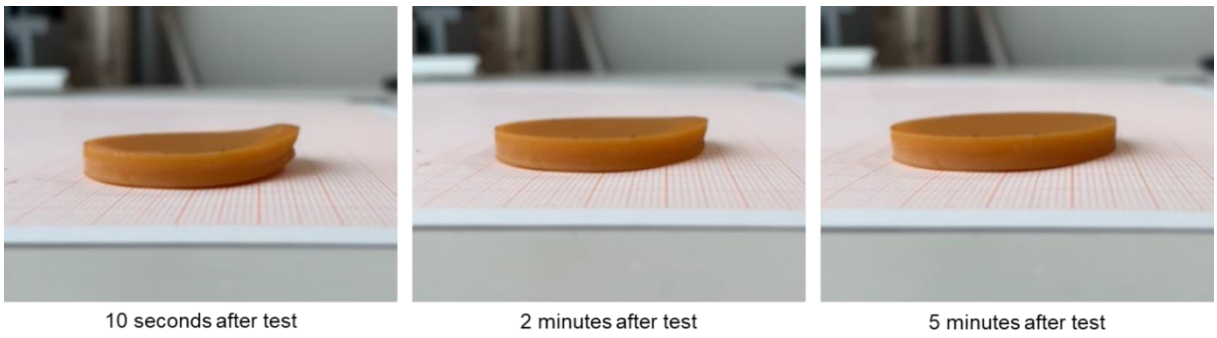

Figure 5.20. 75° Shore A pad sample deformation after cold test (pictures made on 3-5-2022)

The static friction coefficient of the material with the highest hardness (95° Shore A) is similar in cold conditions and at room temperature (Figure 5.21). The tan(δ) of this material differs significantly between room temperature and cold conditions. This would deny correlation of the static friction coefficient and tan(δ).

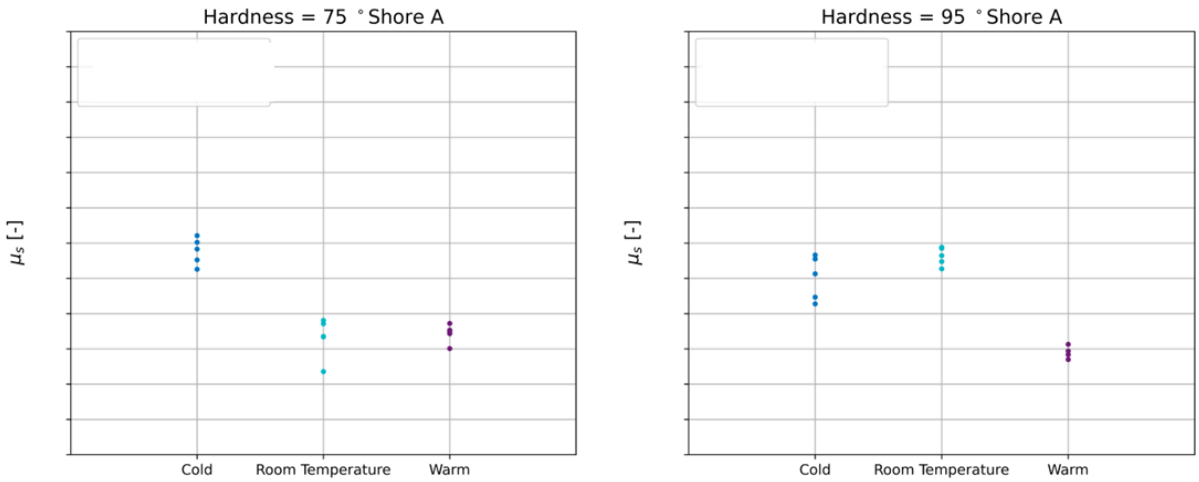

Figure 5.21. Influence of temperature on coefficient of friction (Hardness 75 and 95° Shore A)

5.5.2 Static friction coefficient and hardness at different temperatures

Another perspective in the comparison between friction and viscoelastic properties is added by comparing the variation between PU samples at different temperatures. At room temperature the static friction coefficient increases with increasing hardness. These differences are also visible in the DMA curve (Figure 5.22) at room temperature. The lowest static coefficient mean is for hardness 75 Shore A. The highest mean is for the PU samples with hardness 95 Shore A. The difference between these means is 65%.

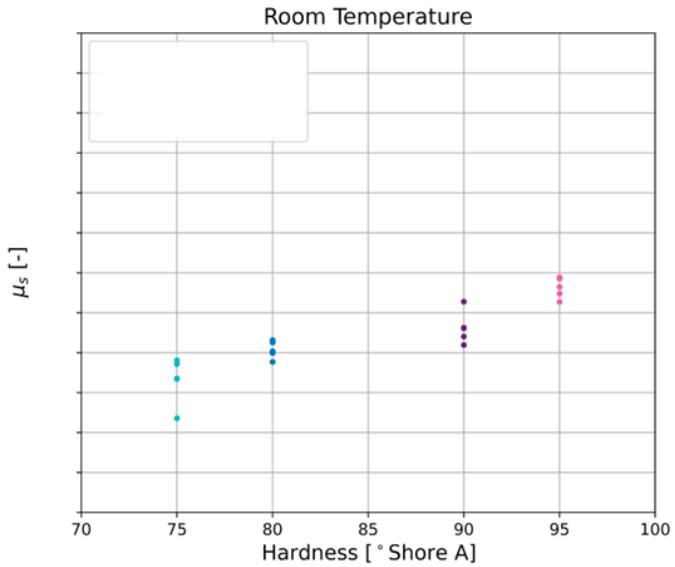

Figure 5.22. Influence of hardness on coefficient of friction at room temperature

At warm temperatures the differences between the different PU hardness samples is corrected. The differences in tan(δ) are also small at warm temperatures (Figure 5.23). The difference between the lowest mean and the highest mean of static friction coefficients in warm conditions is 31%. This difference can also be due to stable sliding in the kinetic regime, which reduces the complexity in determining the transition point.

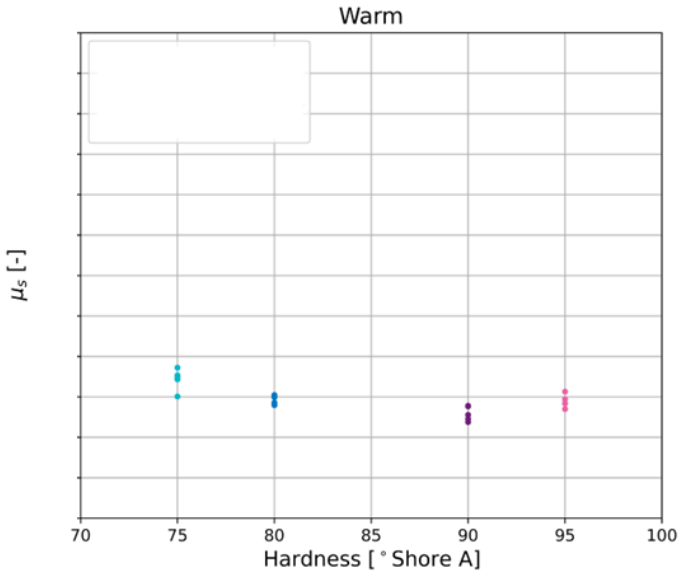

Figure 5.23. Influence of hardness on coefficient of friction in warm conditions

For the cold tests, the static coefficients of friction differ less over hardness (Figure 5.24). The largest difference between the mean values is . In the case of these cold test values, it is hard to relate this reduction in difference to tan(δ). It is difficult to determine whether the difference between the tan(δ) is large or small, since the temperature is not known exactly and since the DMA curves vary a lot within the temperature ranges as provided in Figure 5.18. In case of a small difference, this could be related to the static friction coefficients

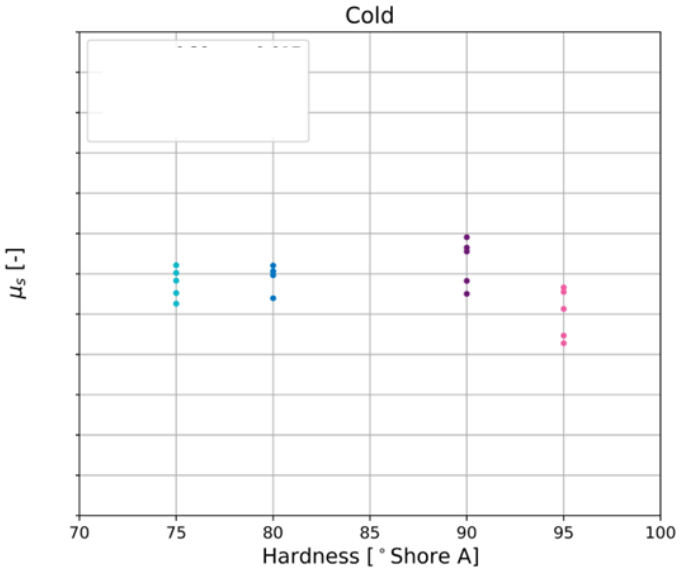

Figure 5.24. Influence of hardness on coefficient of friction in cold conditions

5.5.3 Measured force-displacement graph

In Figure 5.25 force-displacement graphs for the tests performed in cold conditions, warm conditions and room temperature are visualized. It can be observed that all graphs with this hardness have a comparable beginning of the friction test (until approximately 2 mm displacement). A minor difference in this part is the kink that is visible in the graphs for the tests performed at room temperature. After 2 mm displacement, the graphs of tests performed at room temperature enter the kinetic regime and stick-slip behavior starts occurring. In the graphs of the cold tests, there is a decrease of the slope. After this decrease, the slope increases again and stick-slip behavior starts occurring slowly. Zuleeg (2015) indicates a relation between stick-slip and temperature but does not explain how stick-slip behavior is influenced by temperature. The graphs of the tests performed with warm temperatures, show stable sliding behavior after a displacement of 2 mm. These graphs are the most constant, compared to the graphs of tests performed at the other temperatures.

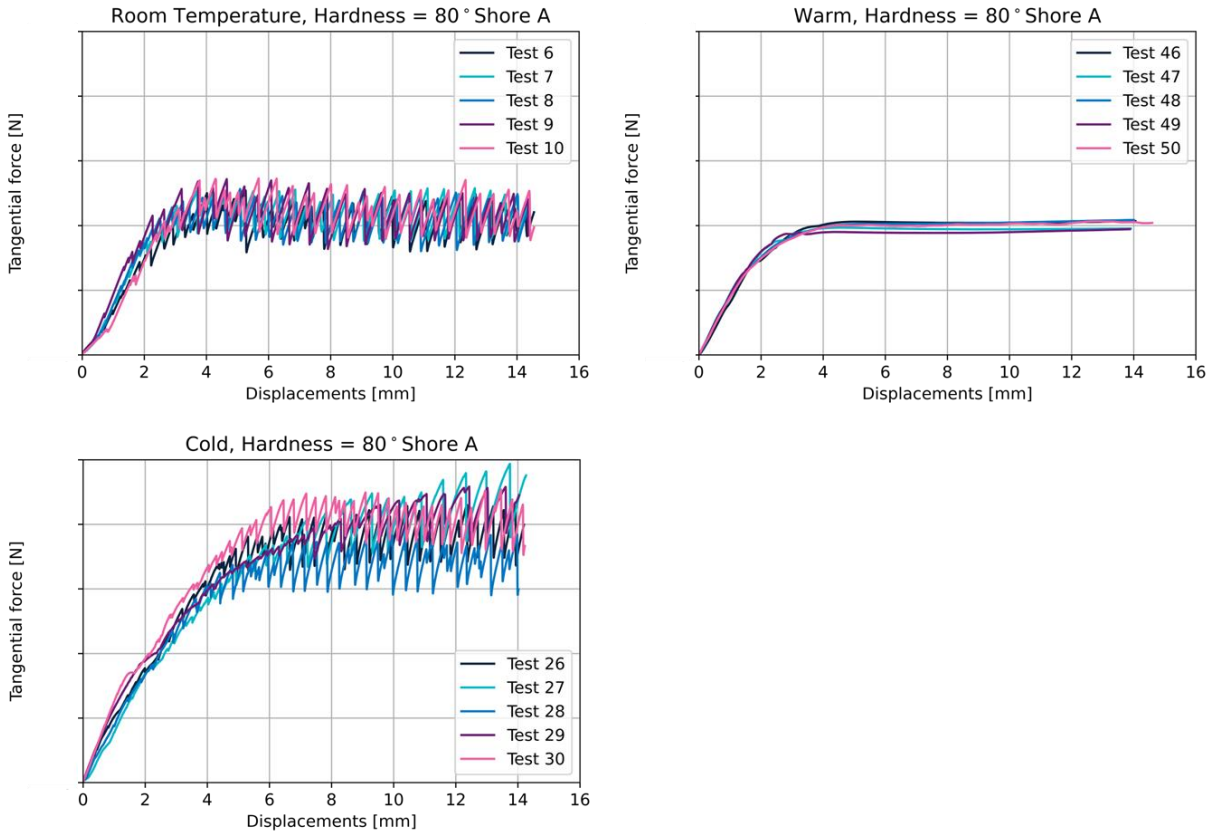

Figure 5.25. Force-displacement graphs for PU with hardness 75° Shore A at the three tested temperatures

5.5.4 Reduced force-displacement graph

The corrected force-displacement graphs of the tests at room temperature and in warm conditions are comparable except for the stick-slip behavior observed at room temperature (Figure 5.26). The corrected force-displacement graph for the tests performed in cold conditions has more pre-sliding displacements and increases towards a larger tangential force. It can be observed that the graphs for cold conditions start below 0 mm displacement. This is caused by the correction for the pad deformation.

This correction is caused by the shear strengths determined by measurements at room temperature. Because of a higher complex modulus (resistance to deformation) at temperatures near the glass transition point, the pad deformation is expected to be less.

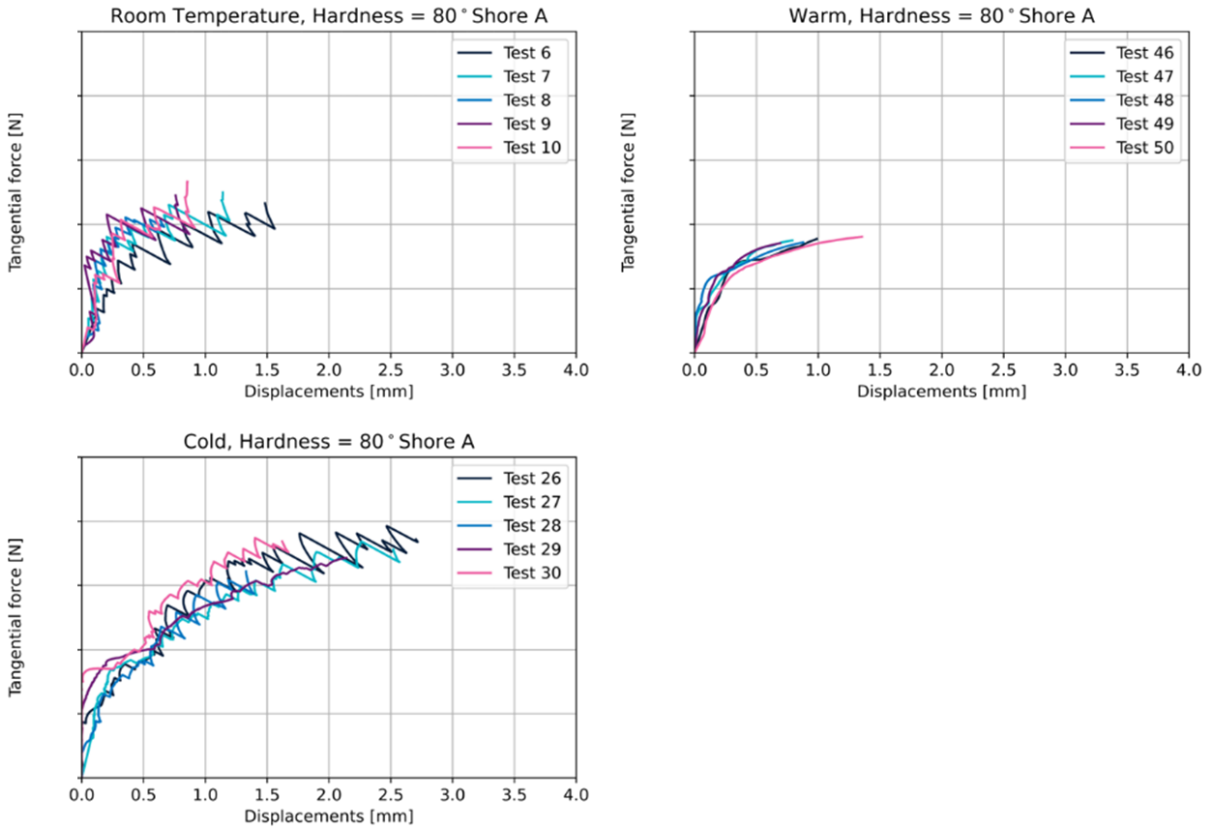

Figure 5.26. Corrected static force-displacement graphs of PU with 80° Shore A

5.5.5 Pre-sliding displacements

The amount of pre-sliding displacement for cold conditions is larger than for warm conditions and room temperature (Figure 5.27 and Figure 5.28). This can be explained by the increase in friction resistance, which results in more displacement. There is also more variation in the pre-sliding displacements at cold temperatures.

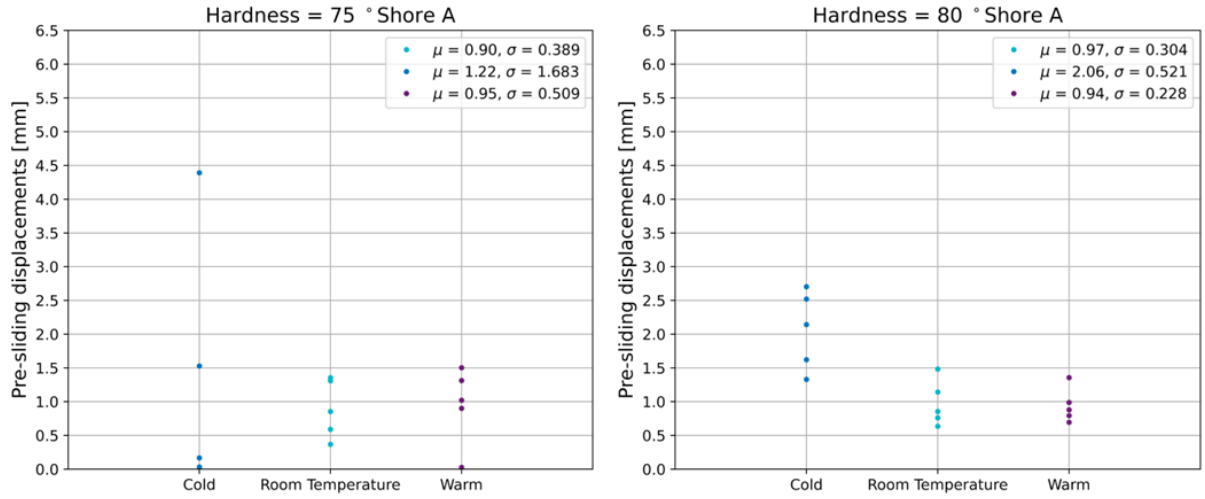

Figure 5.27. Influence of temperature on pre-sliding displacements (75 and 80° Shore A)

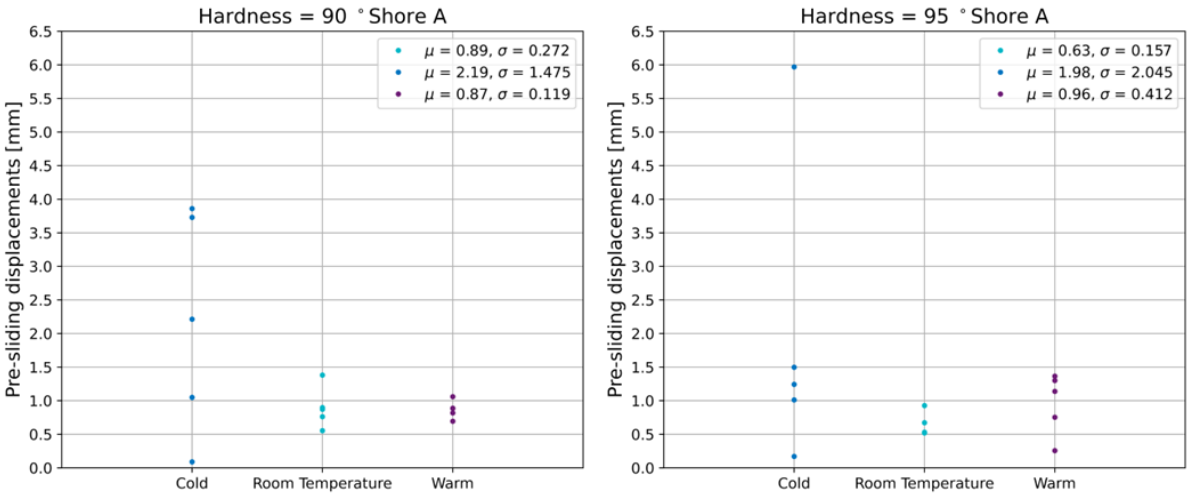

Figure 5.28. Influence of temperature on pre-sliding displacements (90 and 95° Shore A)

5.6 Conclusion

This Chapter shows that hardness, roughness and temperature should be considered in friction tests. An effect of viscoelastic properties on friction cannot be extracted from the performed tests. The hypotheses set in Section 5.1 are reviewed based on the results of the sensitivity tests.

Hypothesis 1: Static friction resistance increases with hardness.
Accepted: The static coefficient of friction increases with hardness.

Section 5.3.1 shows an increase of the static coefficient of friction with hardness. Hypothesis 1 is accepted. The effect can be explained by an increase of shear strength, which is dominant over the decrease in real contact area. A decrease in real contact area would decrease the friction resistance.

Hypothesis 2: Static friction resistance increases with monopile roughness.
Accepted: The static coefficient of friction increases with monopile roughness.

Section 5.3.2 observes that the static friction coefficient increases with roughness. This results in Hypothesis 2 being accepted. The increase in friction for an increase in roughness can be explained by the increase in real contact area.

Hypothesis 3: Static friction resistance increases with temperature.
Rejected: The static coefficient of friction does not clearly increase with temperature.

The sensitivity tests show that the static coefficient of friction decreases with temperature (section 5.5). Hypothesis 3 is not accepted. The differences in results can be due to the loose samples in the pad holders. It can also be caused by the different material properties of the polyurethane samples.

Hypothesis 4: Static friction resistance increases with decreasing viscoelastic properties.
Rejected: The static coefficient of friction does not clearly increase with viscoelastic properties.

Section 5.5 shows no correlation of viscoelastic properties and friction. Exact values for the viscoelastic properties cannot be determined due to the unknown surface temperature.

6 Modelling friction

A model is fit for the sensitivity tests performed in Chapter 5 in order to show the potential of friction models. The approach of fitting the model parameters, as well as the relation of model parameters with factors that affect friction is investigated.

6.1 Relevance of friction models

Monopile sea fastening cradles are designed to ensure the stability of monopiles during transport. The loads that are introduced on the cradles by the monopile, need to be transferred to the deck. The spread of the friction force between both cradles is unknown. The cradles are currently designed to resist a shear force that is relative to the normal force acting on the cradle and the maximum amount of friction generated by the support pad (Figure 6.1).

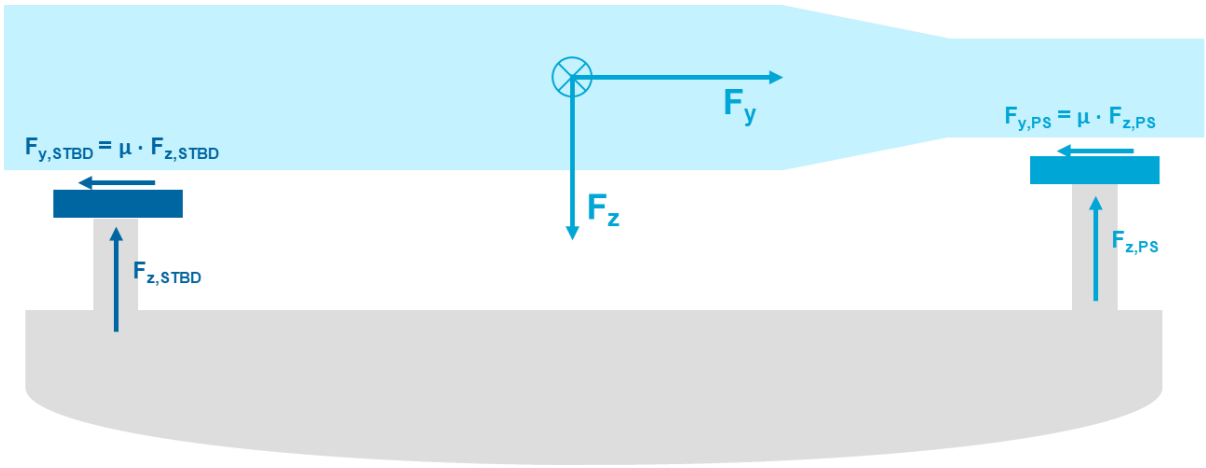

Figure 6.1. Currently assumed distribution of friction forces

In reality, the distribution of friction forces is probably related to friction displacements and the stiffness of the substructure. The location of contact points between monopiles and friction supports can change due to deformation of the cradle, deformation of the support pad and pre-sliding displacements. The Dahl model describes the relation between the friction force and pre-sliding displacements (Flores et al., 2016). This model will be used in this research. More information on the Dahl model and why it is chosen follows in Section 6.3. In Figure 6.2 two different Dahl models are plotted. If the distribution is based on F_C only, the distribution would be 58% to 42% in this example. By modelling the behavior of the friction interface a more realistic force distribution over the cradles might be deducted. At 0.5 mm pre-sliding displacements the force distribution would be 63% to 37% in the example of Figure 6.2. This can result in a more optimal design and thus reduction of material.

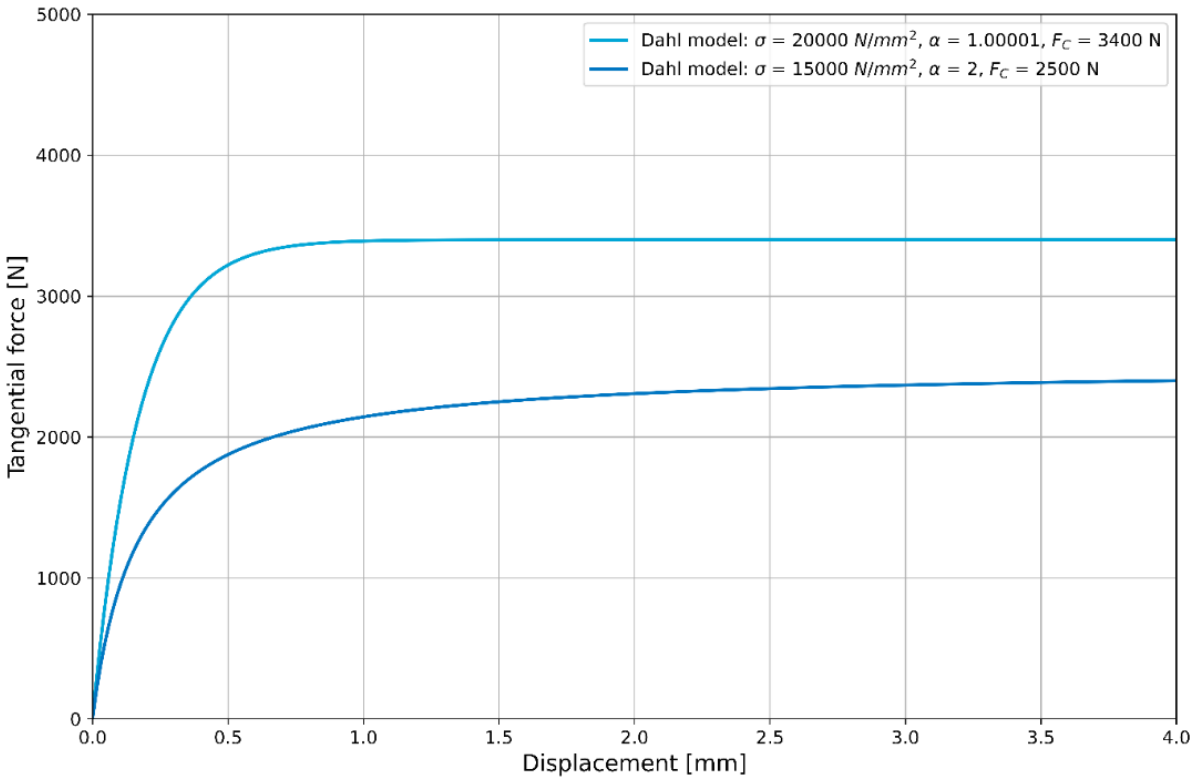

Figure 6.2. Example of two different Dahl models

6.2 Friction model comparison

Friction models use functions to describe friction with force-displacement or force-velocity graphs. The friction models range from simple (with one parameter) to complex (with over 8 parameters). The increase in complexity can result in an increase of phenomena captured in the model. This research compares five models that are used to describe friction. The models and their parameters are included in Table 6.1. The parameters are divided over phenomena that the parameters represent.

The phenomena over which the parameters are divided are stiffness, damping, hysteresis and other. Parameters that fall under stiffness, determine the slope of the force-displacement graph and represent the stiffness of the asperities (Aström & Canudas-De-Wit, 2008; Flores et al., 2016; Piatkowski, 2014; Swevers et al., 2000). The damping coefficient prescribes how fast the force reaches the kinetic friction level, after the static peak (Aström & Canudas-De-Wit, 2008; Flores et al., 2016; Piatkowski, 2014). Hysteresis adds non-local memory behavior. This means that the behavior of asperities not only depends on the previous state and what has happened after that, but also on the maxima and minima before that state (Swevers et al., 2000). This is mostly important when velocity reversals need to be modelled.

Table 6.1. Parameters of five friction models

Model	Force	Stiffness	Damping	Hysteresis	Other
Coulomb [a]	F_C	-	-	-	-
Bilinear [b]	F_C	σ	-	-	-
Dahl [c]	F_C	σ	-	-	α
LuGre [d]	F_C, F_s	σ_0	σ_1 , σ_2	-	$v_{Stribeck}$
Basic Maxwell Slip Element [e]	F_C, F_s, F_b	-	σ_1 , σ_2	W_i, k_i, ζ_i	$v_{Stribeck}$, n

[a] Information based on Olsson et al. (1997) and Pennestrì et al. (2016)

[b] Linear relation between force and displacement in both the static and the kinetic regime

[c] Information based on Olsson et al. (1997) and Pennestrì et al. (2016)

[d] Information based on Aström & Canudas-De-Wit (2008) and Piatkowski (2014)

[e] Information based on Lampaert et al. (2002) and Swevers et al. (2000)

A friction model will be used to describe the corrected static friction graphs obtained in Chapter 5. The graphs show an nonlinear increase in tangential force for an increase in displacement. It is required that the model can include this nonlinear stiffness as well as the pre-sliding displacements and static friction. The number of parameters should be as low as possible, since the amount of tests available to determine the parameters is limited. The criteria that the friction models needs to meet are:

1. The friction model must contain as less parameters as possible
2. The friction model must be able to model pre-sliding behavior
3. The friction model must be able to model nonlinear stiffness

In Table 6.2 the friction models are compared for describing the sensitivity tests from Chapter 5. The stiffness parameters capture the pre-sliding behavior of the asperities. The damping parameters and the curve shape parameter α include the nonlinear stiffness. Based on these findings, the Coulomb model and the bilinear model are not sufficient to describe the sensitivity tests. The Dahl model, the LuGre model and the Basic Maxwell Slip Element can be used to describe the sensitivity tests from Chapter 5. The Dahl model is preferred since this model has the least parameters, which makes the fitting process less extensive.

Table 6.2. Friction model comparison

	Criteria		
Model	**Number of parameters**	**Pre-sliding**	**Nonlinear stiffness**
Coulomb	1		
Bilinear	2		
Dahl	3		
LuGre	6		
Basic Maxwell Slip Element	9		

6.3 Dahl model

Section 6.2 showed that the Dahl model is the preferred model to describe the corrected static force-displacement graphs from Chapter 5. The Dahl model is a first order differential equation with four input parameters (Formula 6.1) (Flores et al., 2016; Olsson et al., 1997; Pennestrì et al., 2016). With these parameters the tangential friction force can be determined for a range of displacements.

$$\frac{dF}{dx} = \sigma\left(1 - \frac{F}{F_C} sgn(v)\right)^{\alpha} \qquad 6.1$$

One boundary condition is needed in order to solve the first order differential equation. The boundary condition which is used is that there is no tangential force at zero displacement (x = 0, F = 0). The derivation of the formula used for the model is included in Appendix D.

6.3.1 Parameter sigma, σ

Sigma is one of the input parameters in the Dahl model. The parameter has a stiffness unit, N/mm. Sigma determines the initial slope of the friction graph (Flores et al., 2016). For larger sigma's the initial slope of the friction graph is steeper. This effect is shown in Figure 6.3.

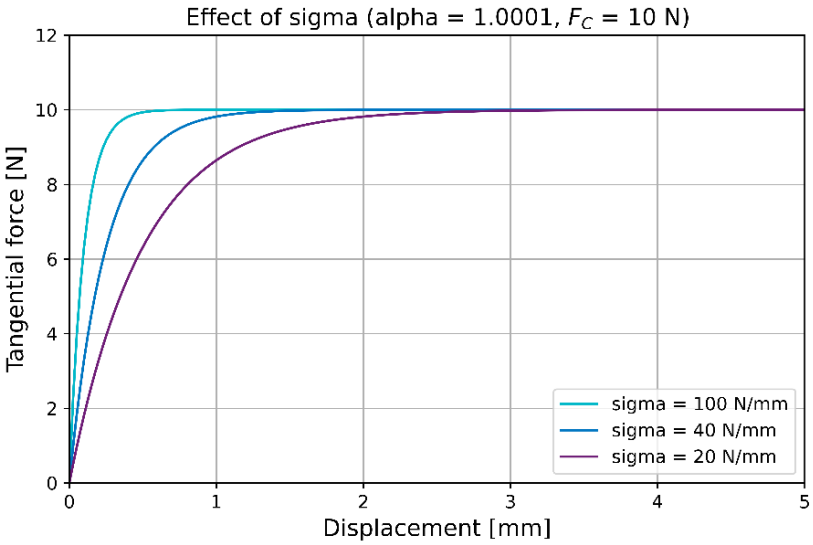

Figure 6.3. Effect of sigma parameter on Dahl model

6.3.2 Parameter alpha, α

Alpha is another input parameter in the Dahl model. This parameter determines how much displacement is needed for the graph to converge to the Coulomb friction force, F_C (Flores et al., 2016). This parameter must always be greater than 1 and smaller or equal to 2. Higher alphas require larger displacements to converges to F_C. This effect is shown in Figure 6.4.

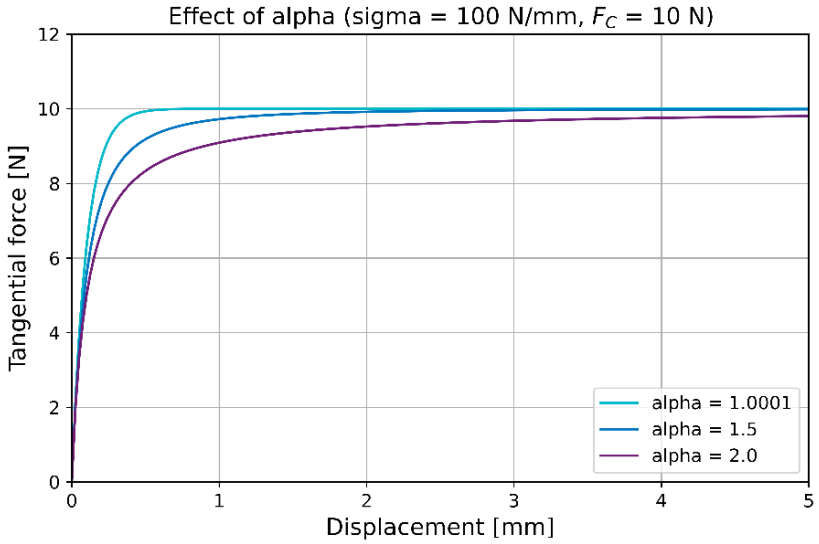

Figure 6.4. Effect of alpha parameter on Dahl model (sigma = 100 N/mm, FC = 10 N)

6.3.3 Parameter Coulomb friction force, F_C

F_C is the Coulomb friction force. This force describes the force to which the friction graph converges (Flores et al., 2016). The larger Fc, the larger the force to which the graph converges. This is visualized in Figure 6.5.

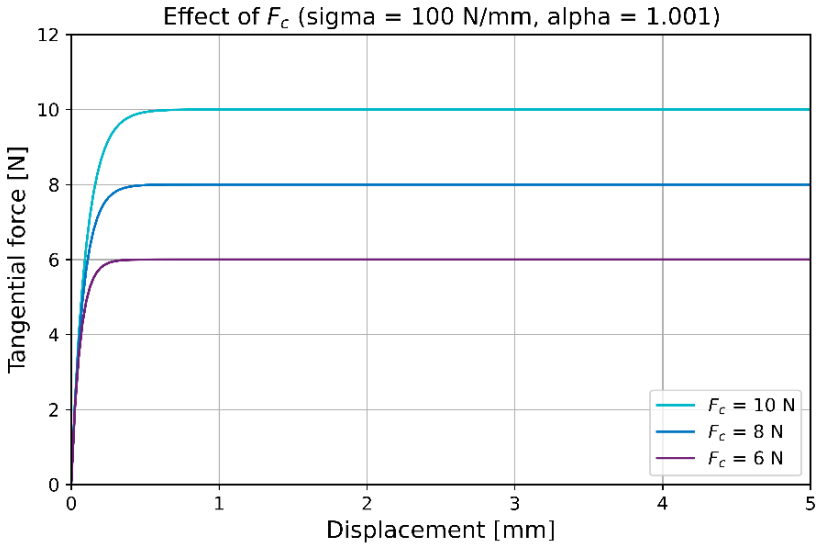

Figure 6.5. Effect of F_C on Dahl model (sigma = 100 N/mm, alpha = 1.0001)

6.3.4 Direction of the velocity, sgn(v)

The direction of the velocity determines whether the slope of the friction graph is positive or negative. In the friction tests, the direction of sliding (and thus the direction of the friction force) does not change. The direction of the velocity is thus chosen as positive.

6.4 Displacements correction

Friction measurements for this thesis are performed with the vertical plane testing method and testing procedure described in Section 4.4. Both force and displacement are measured by a load cell. The displacements measured, are disturbed by displacements that are not due to deformations at the friction interface. There are five deformations that disturb the displacement measurement: clearance pin and steel sample, pad deformation, pad in holder displacement, clearance sample holder and friction clamp, and pin clearance in friction clamp. Do fit the model for the friction displacements, the measured data is corrected.

6.4.1 Clearance pin and steel sample

Clearances are present between the pin and the steel sample. This pin connects the steel sample to the test bench. In Figure 6.6 this is visualized. The pin connection with clearance is chosen, because this ensures a moment free connection. This clearance is visible at the beginning of the force-displacement graph. Large displacements are measured, without an increase of the measured force (Figure 6.7). This corresponds to the first part of the friction test in which the pin is pulled up, without it being connected to the steel sample.

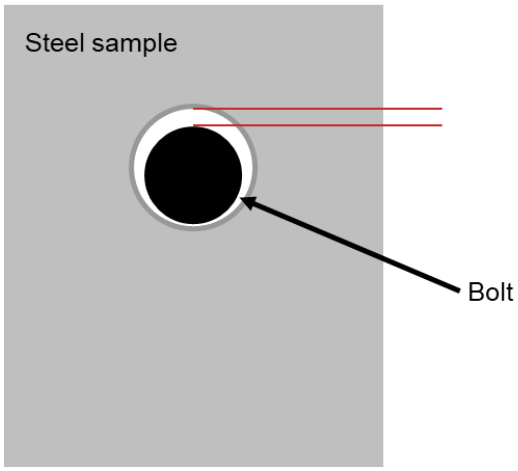

Figure 6.6. Schematic of bolt to steel sample clearances

The measured points contain forces and displacements. The measured force of each point is noted as F_0 and the measured displacement of each point is noted as d_0. All points for which F_0 is smaller than 12.5 N, are deleted. The clearance (d_{clear}) is the displacement corresponding to the displacement at the point for which F_0 is greater than or equal to 12.5 N for the first time. For each point after this point, the new displacement (d_1) is calculated with Formula 6.2. The force of all points after that point remains the same. The difference between the measured graph and the corrected graph can be seen in Figure 6.7.

$$F_0 \geq 12.5\ N: d_1 = d_0 - d_{clear} \qquad 6.2$$

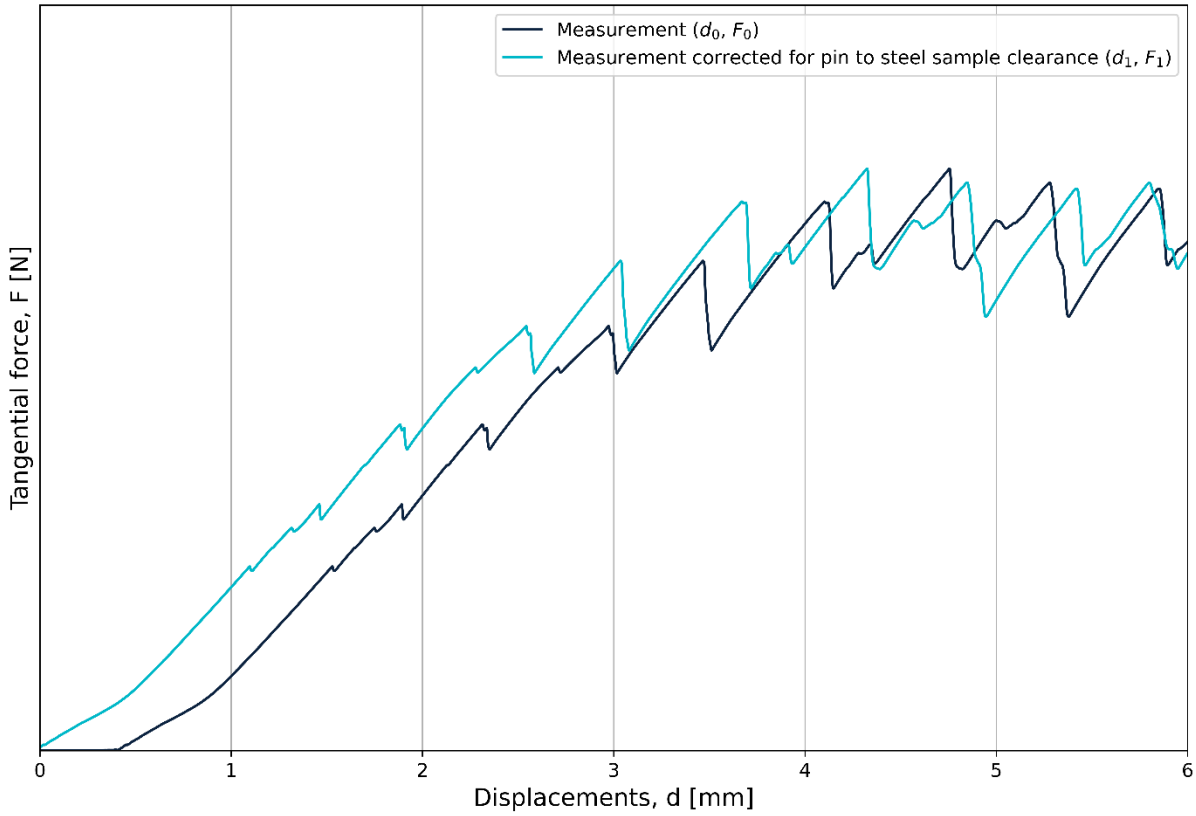

Figure 6.7. Force-displacement graph after correcting measurements for bolt to steel sample clearance (from temperature-viscoelasticity sensitivity tests, test 2, testing conditions in Section 5.2)

6.4.2 Shear pad deformation

Displacements are caused by shear deformation of the polyurethane pads (Figure 6.8. Schematic of shear pad deformation). The steel sample is pulled up and since the friction resistance is larger than the shear resistance, the pad deforms slightly. This is reason that the pad thickness must be as small as possible.

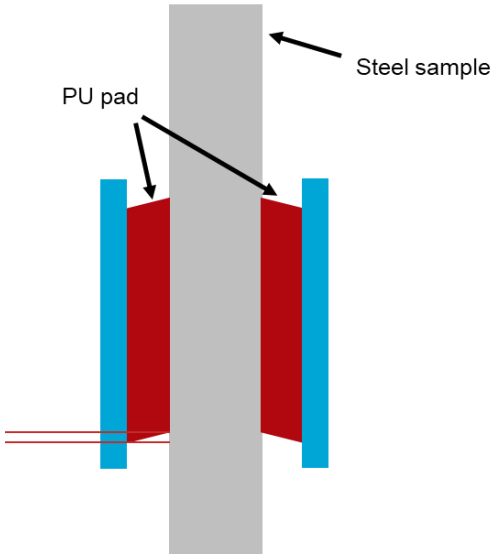

Figure 6.8. Schematic of shear pad deformation

The shear stiffness (τ) of the of the sample is required, to correct the force-displacement graph for the pad deformation. The forces and displacements of each point after adjusting it for the bolt to steel clearance, are denoted as F_1 and d_1 respectively. The displacements after correcting for the shear pad deformation are noted as d_2. Formula 6.3 shows how the displacements are corrected.

$$d_2 = d_1 - \frac{F_1}{\tau} \qquad 6.3$$

The shear stiffness of the pad samples can be determined with tests. These tests can be performed similar to friction tests, but with a glued interface between the steel sample and the polyurethane pad. By doing this, the pre-sliding displacements are reduced to 0. The slope of the measured graph is the shear stiffness of the PU sample. Figure 6.9 shows the measurements and determination of the shear stiffness of the four PU pad samples used in the tests in Chapter 5. These tests were performed at room temperature with the same rate of loading (180 kgf/min) and pressure (5 MPa) as in the tests of Section 5. This resulted in shear stiffnesses of 970, 1070, 1800 and 2040 N/mm^2 for hardness 75, 80, 90, 95 ° Shore A respectively (Figure 6.9).

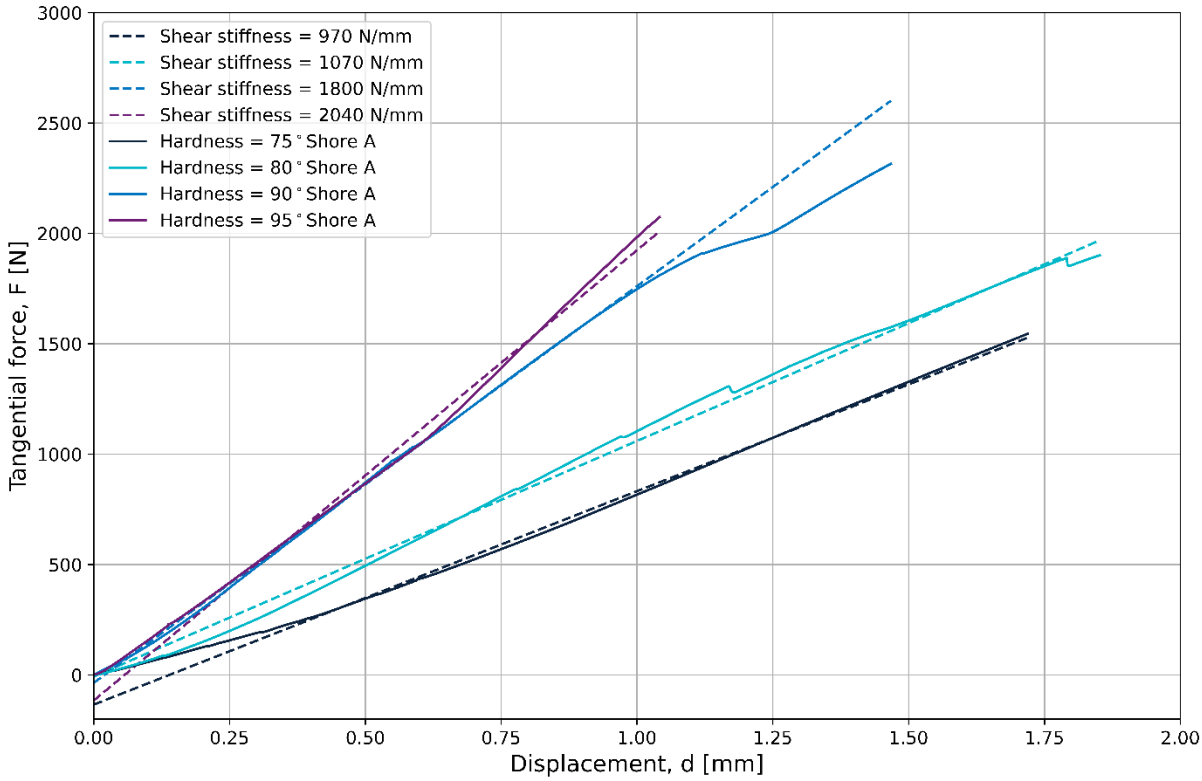

Figure 6.9. Shear stiffness determination

The force-displacement graph after correcting for the bolt-steel clearance and the pad deformation, is shown in Figure 6.10.

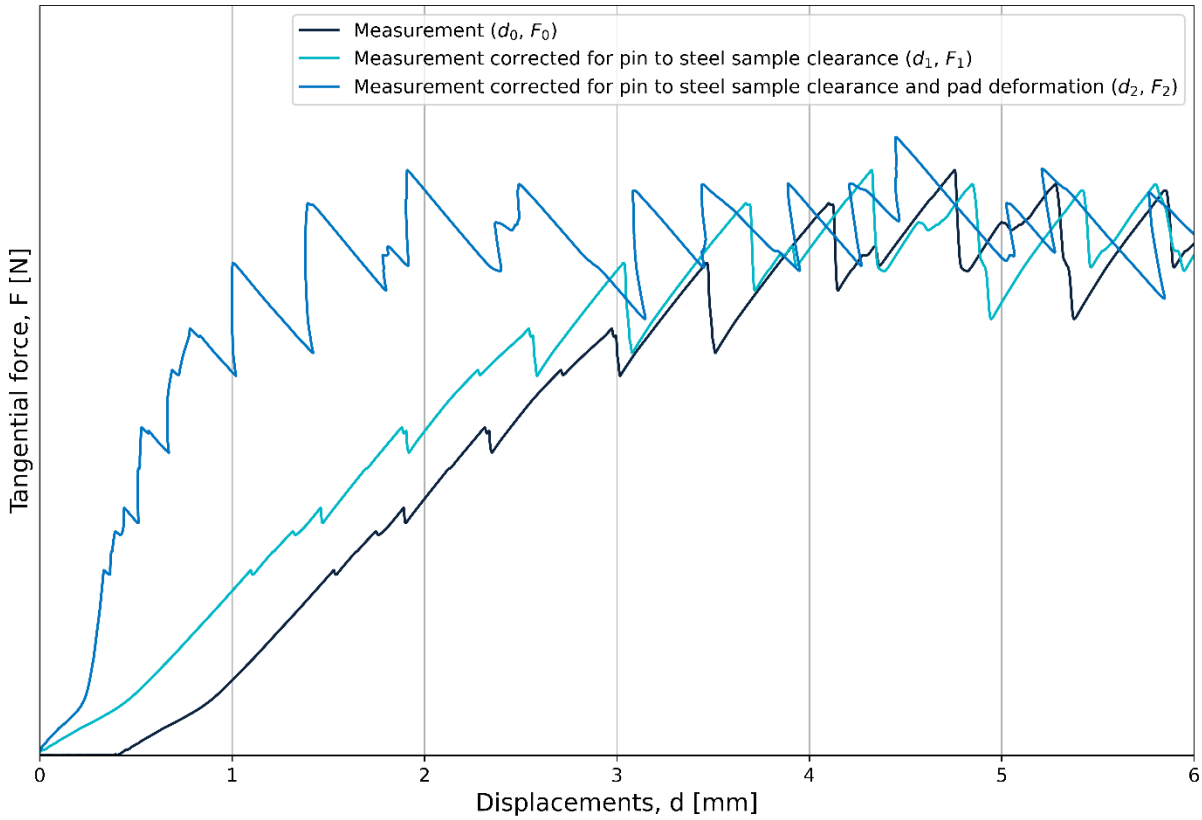

Figure 6.10. Force-displacement graph after correcting measurement for bolt to steel sample clearance and pad deformation (from temperature-viscoelasticity sensitivity tests, test 2, testing conditions in Section 5.2)

6.4.3 PU pad in holder displacement

In some tests, the polyurethane pad samples are placed in a holder and the polyurethane is not directly mold on a steel back plate. The diameter of the samples is 40 mm and the inner diameter of the pad holder is 41 mm. There is thus a possible clearance of 1 mm (Figure 6.11).

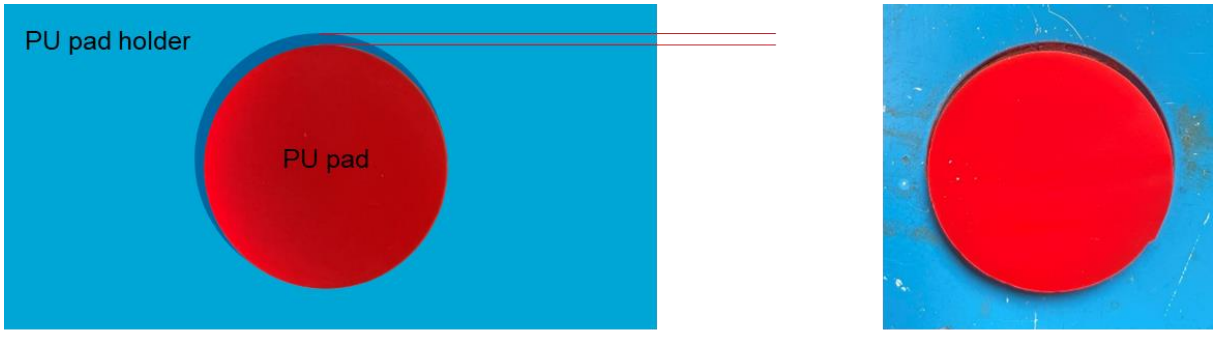

(a) *(b)*

Figure 6.11. PU pad in holder clearances: (a) Schematic, (b) Actual situation (Figure made on 28-6-2022)

In a small test campaign, it is proofed that the kink in the force-displacement graph is caused by this sample movement. The force-displacement graph of a test with the PU pad in a holder is compared to the force-displacement graph of a test with the PU pad casted directly on a steel back plate (Appendix E). In the force-displacement graph of the test with the PU pad in the holder the kink is observed. In the other force-displacement this kink is not observed.

The first step in adjusting the displacements is indicating the point of the kink. Then the displacements previously to this point are adjusted such that this slope equals the slope of 500 points after the point. Formula 6.4, 6.5 and 6.6 show how the measured data are corrected for these displacements.

$$slope = \frac{F_{kink+500} - F_{kink}}{d_{kink+500} - d_{kink}} \tag{6.4}$$

$$d_2 < d_{kink} : d_3 = \frac{F_2}{slope} \tag{6.5}$$

$$d_2 \geq d_{kink} : d_3 = \frac{F_{kink}}{slope} - d_{kink} + d_2 \tag{6.6}$$

In Figure 6.12 the difference is visible between the graph corrected for the bolt to steel clearance and the pad deformation and the graph corrected for all deformations and clearances.

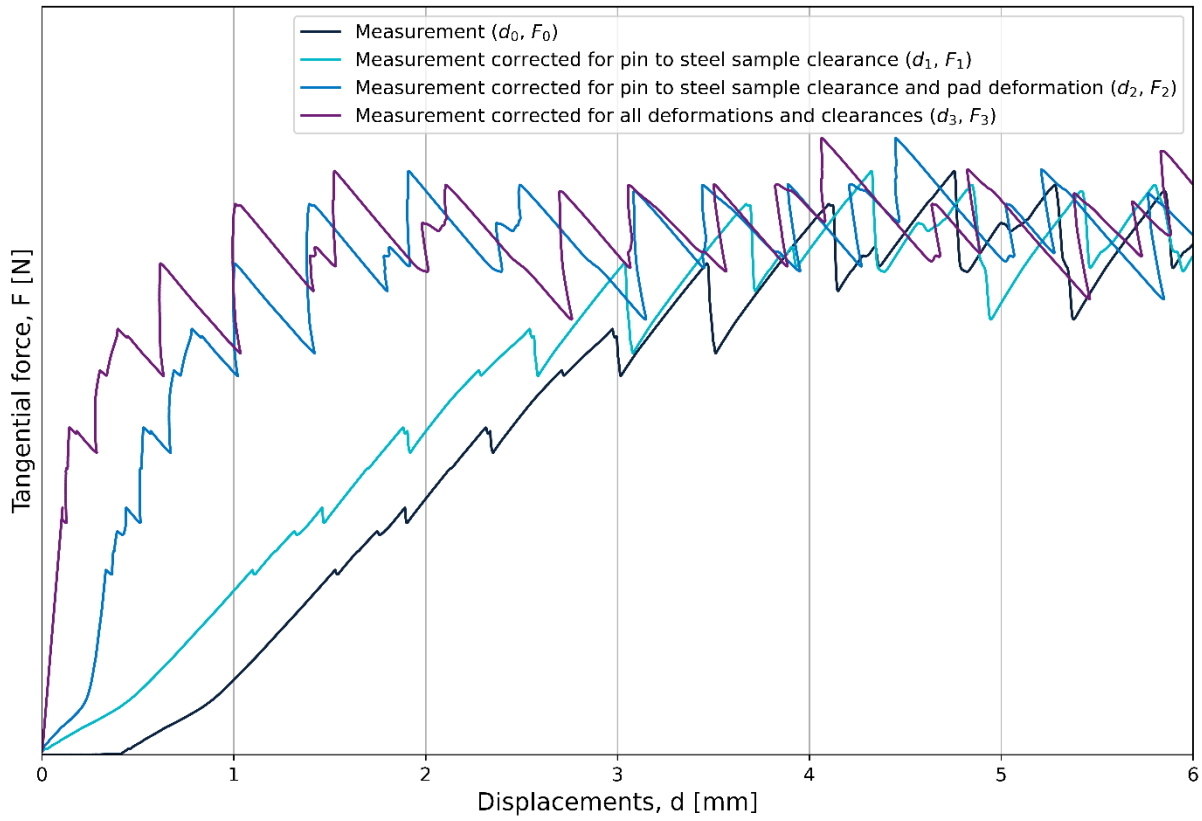

Figure 6.12. Force-displacement graph after correcting measurement for all deformations and clearances (from temperature-viscoelasticity sensitivity tests, test 2, testing conditions in Section 5.2)

6.4.4 Clearance of the sample holder with the friction clamp

The PU pad holders or in other cases the steel back plate is placed inside the friction clamp. There are bolts to prevent the pad holder or the back plate from displacing. There is still a possibility for the pad holder or the back plate to move, when these bolts are not fully fixing these samples (Figure 6.13).

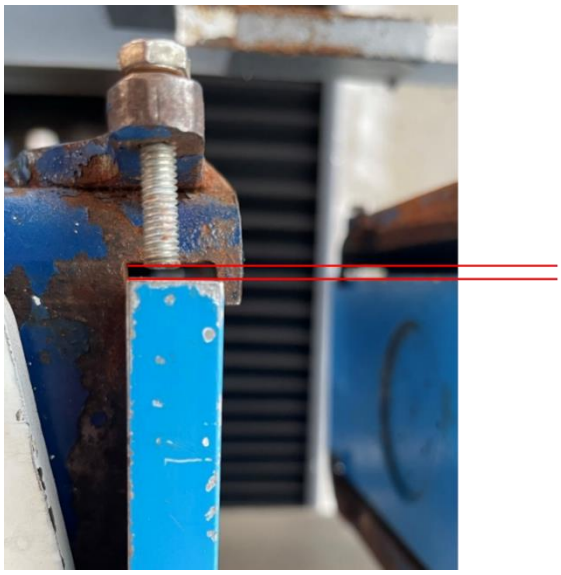

Figure 6.13. Clearance of the sample holder with the friction clamp (Figure made on 27-6-2022)

6.4.5 Clearance friction clamp to sub-structure

The friction clamp is connected to the substructure with four connections (Figure 6.14). These connections ensure the movement of both sides and to transfer possible moments to the sub-structure. The disturbance in the force-displacement graph can be due to the bolts, the bearings or the pins used in these connections.

Figure 6.14. Bolt clearance friction clamp (Figure made on 27-6-2022)

In Figure 6.15 the measured graph and the fully corrected graph are visualized. For some points the corrected displacement is almost 3 mm. Only the static part of these graphs is representative, since the correction for the shear displacement has also affected the stick-slip behavior. Correcting the force-displacement graph is required for modelling and has advantages for determining the transition point.

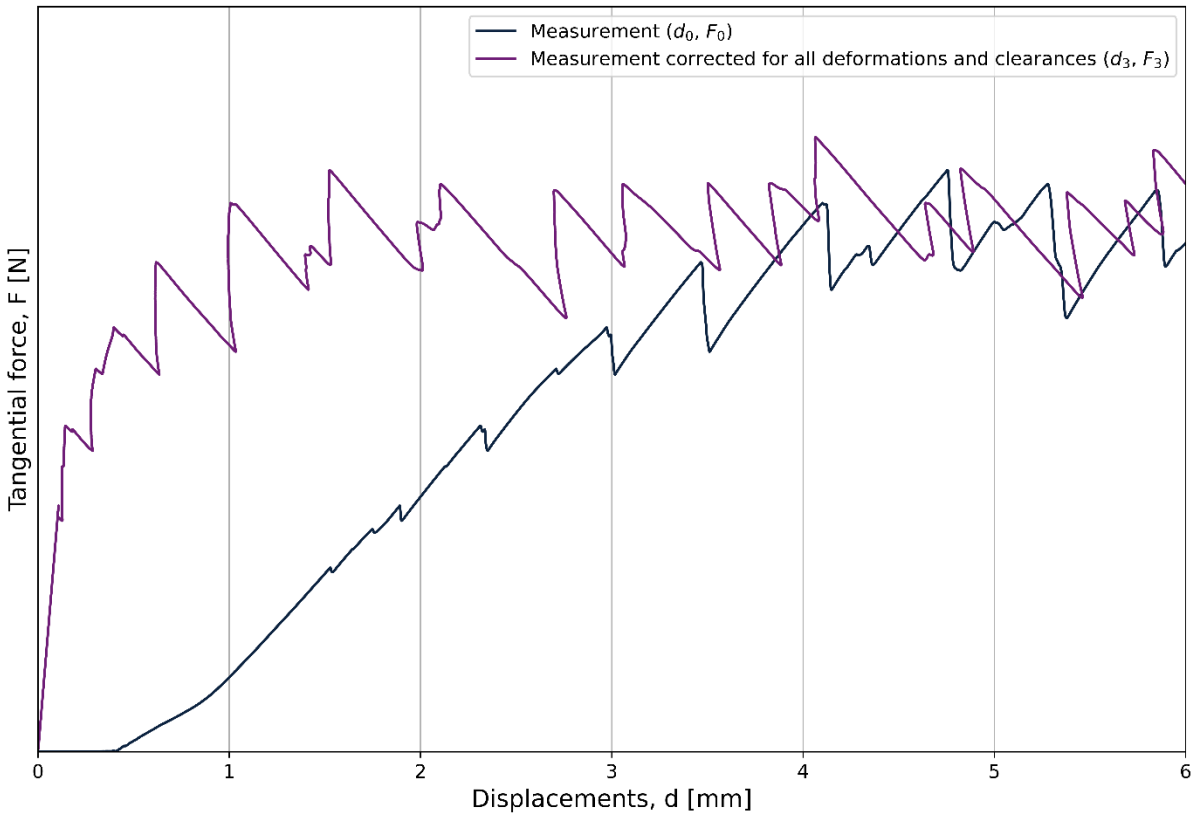

Figure 6.15. Measured force-displacement graph and corrected force-displacement graph (from temperature-viscoelasticity sensitivity tests, test 2, testing conditions in Section 5.2)

6.5 Modelling approach

To show the potential of modelling for the monopile sea fastening application, it is attempted to model the corrected static force-displacement graphs from the sensitivity tests in Chapter 5. The number of points per test is reduced since a large sampling frequency was used during tests. The data for which the models will be fitted exist of each 50th measurement point in the data sets per test.

Forces are calculated with the Dahl model in the fitting process. The displacements from the reduced test data functions as input for the model. Model parameters alpha and sigma are optimized in order to fit the Dahl model to the test data. The value of F_C is set to the tangential force at the transition point. To optimize the model parameters alpha and sigma a brute-force approach is used (Enqvist et al., 2011). A number of values for each parameter is used to compute the model and an optimal combination is given. The combination of model parameters with the lowest mean absolute error (MAE) (Chai & Draxler, 2014) is used as input for the second part of optimization, for which the BFGS algorithm is used (Yuan & Yao, 2013). The alpha range consists of 40 values between 1.000001 and 2, because this covers the possible range of alphas (Subsection 6.3.2). The sigma range consists of 40 values between 0 and 45,000 N/mm^2, because the initial slope of all corrected force displacement graphs is within these boundaries (Figure 6.16). The brute-force method is visualized in the Figure 6.17.

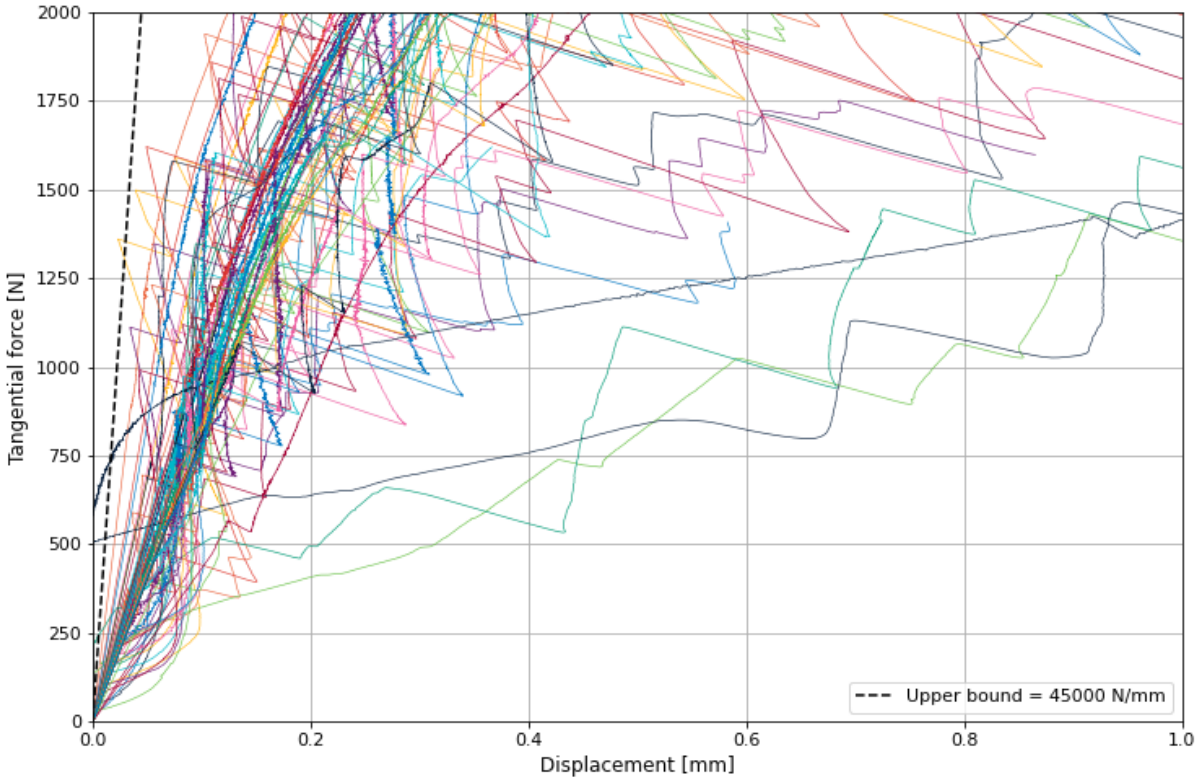

Figure 6.16. Corrected force displacement graphs to determine sigma range

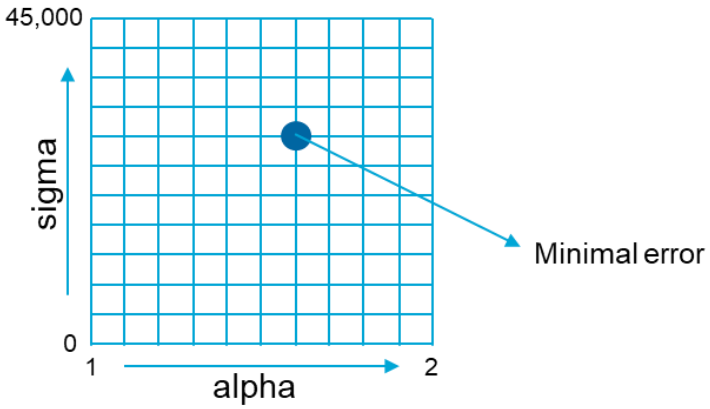

Figure 6.17. Visualization of brute-force approach for Dahl model optimization

In the second step the Broyden-Fletcher-Goldfarb-Shanno (BFGS) algorithm is used (Chai & Draxler, 2014). This algorithm uses a gradient-based approach to find a minimum for a formula. For the Dahl model the MAE is minimized with the BFGS algorithm. The starting point of this method is the optimal combination of model parameters from the brute-force approach. Both model parameters are bounded with the same boundaries that are used for the brute-force approach (alpha between 1.000001 and 2 and sigma between 0 and 45,000 N/mm^2). The details of both steps of the optimization per test are included in Appendix G.

6.6 Fitted models

An example of a model which fits well with the measurement points is given in Figure 6.18. The model does fit well for many measurements, but not for all measurements. The Dahl model is less suitable for describing the cold tests and the tests with hardness 80 °Shore A. After a few millimeters of displacement, the cold force-displacement graph shows a kink, after which the force increases again. The Dahl model fits worse for these measurements since this is not included (Figure 6.19). Stick-slip behavior causes the less good fit for the tests with hardness 80 °Shore A (Figure 6.20).

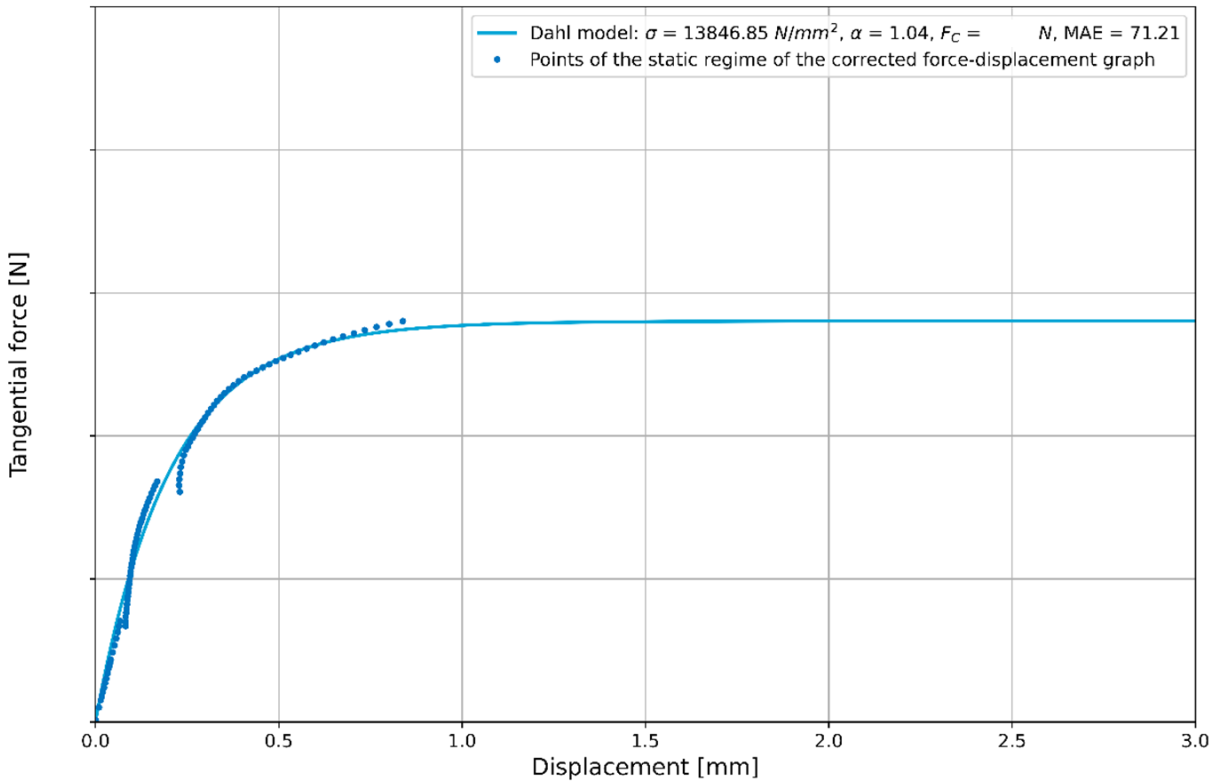

Figure 6.18. Dahl model fitted for points of static regime of the corrected force-displacement graph (roughness-hardness series, test 12), test conditions: hardness = 90° Shore A, R_a = 3 µm, room temperature

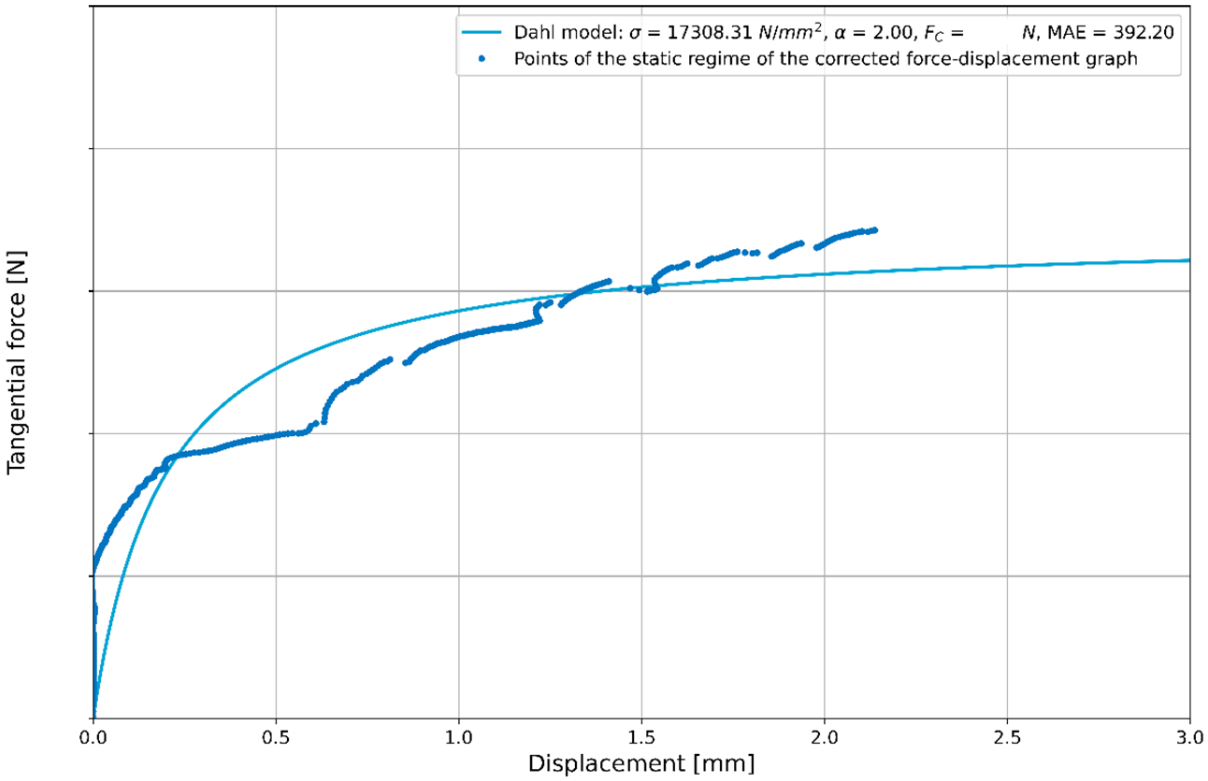

Figure 6.19. Dahl model fitted for points of static regime of the corrected force-displacement graph (temperature-viscoelasticity series, test 29), test conditions: hardness = 80° Shore A, R_a = 3 µm, cold conditions

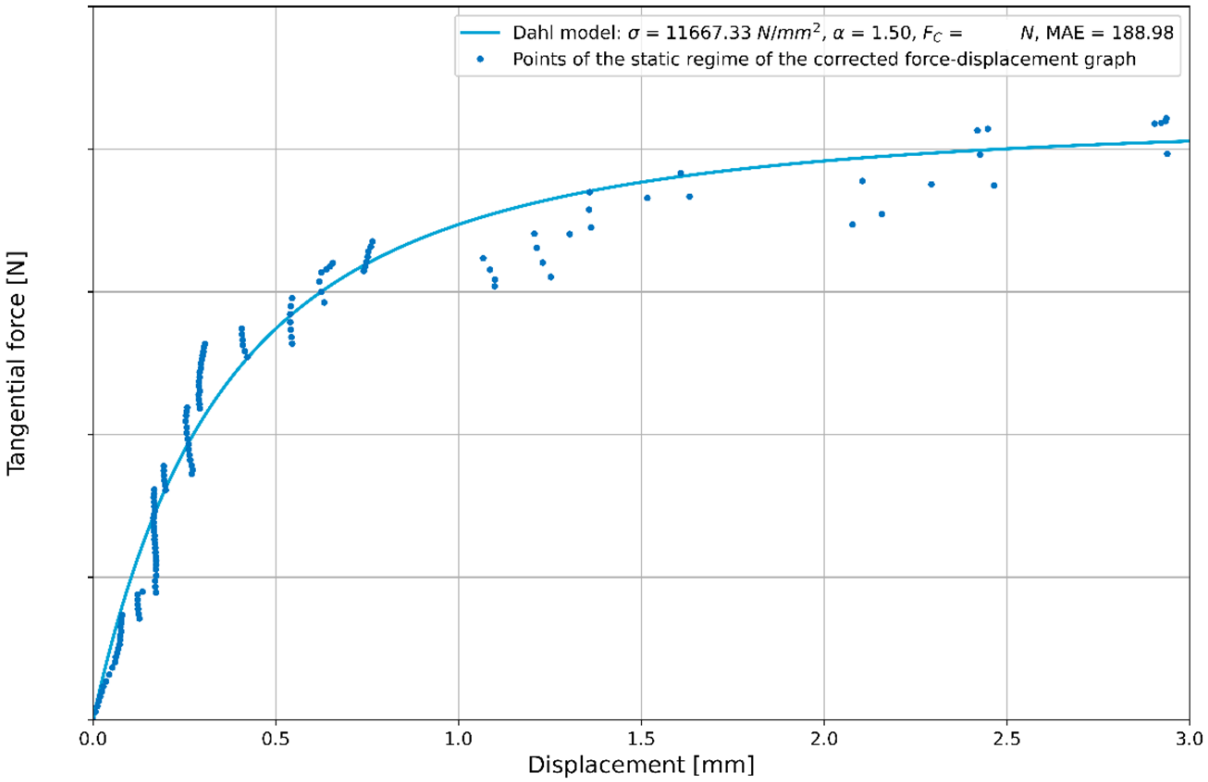

Figure 6.20 Dahl model fitted for points of static regime of the corrected force-displacement graph (roughness-hardness series, test 48), test conditions: hardness = 80° Shore A, Ra = 14 µm, room temperature

6.7 Modelling roughness-hardness tests

The process of modelling is applied for the monopile roughness-hardness tests of Section 5.2. This results in five sets of sigma and alpha per combination of hardness and roughness. It is investigated whether the model parameters relate to the factors that affect friction. All modelled graphs fitted for the measurements are included in Appendix J.

6.7.1 Relation hardness and sigma

The fitted values for sigma are plotted versus hardness in Figure 6.21. No relation is found from this Figure. It seems that hardness does not significantly affect sigma. This aligns with what is observed in the corrected force-displacement graphs in Figure 5.7.

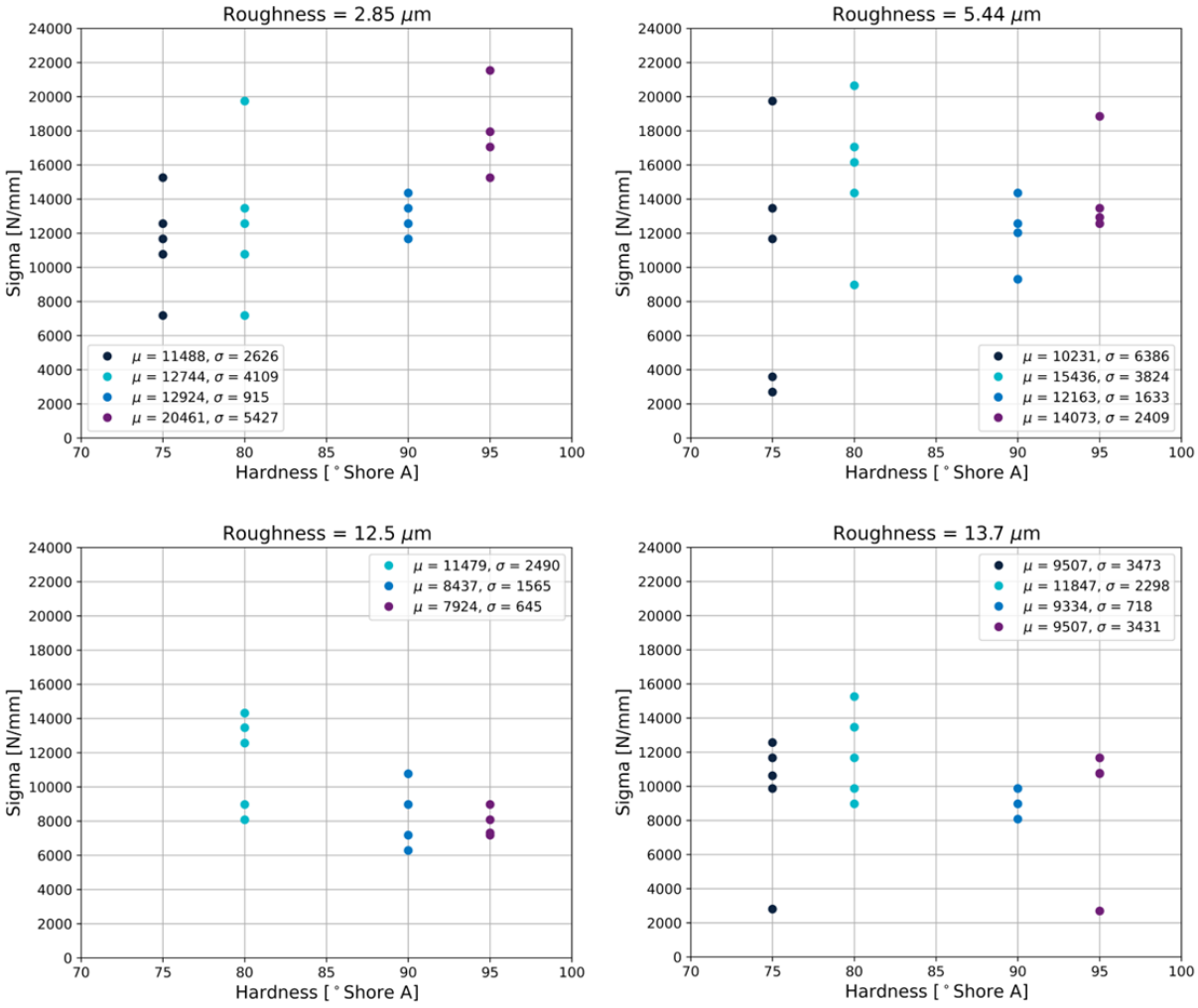

Figure 6.21. Influence of hardness on Dahl model parameter sigma (roughness-hardness sensitivity tests at room temperature)

6.7.2 Relation hardness and alpha

It is observed that alpha seems to reduce with the higher hardness materials. A possible correlation between hardness and alpha is found (Figure 6.22). A decrease of alpha means that the transition of the graph converges faster towards F_C (Subsection 6.3.2). An increase in hardness would thus result in a faster convergence towards F_C. This could be related to higher resistance of asperities and less deformation before reaching the kinetic regime. No relation between hardness and alpha is observed in the corrected force-displacement graphs in Figure 5.7.

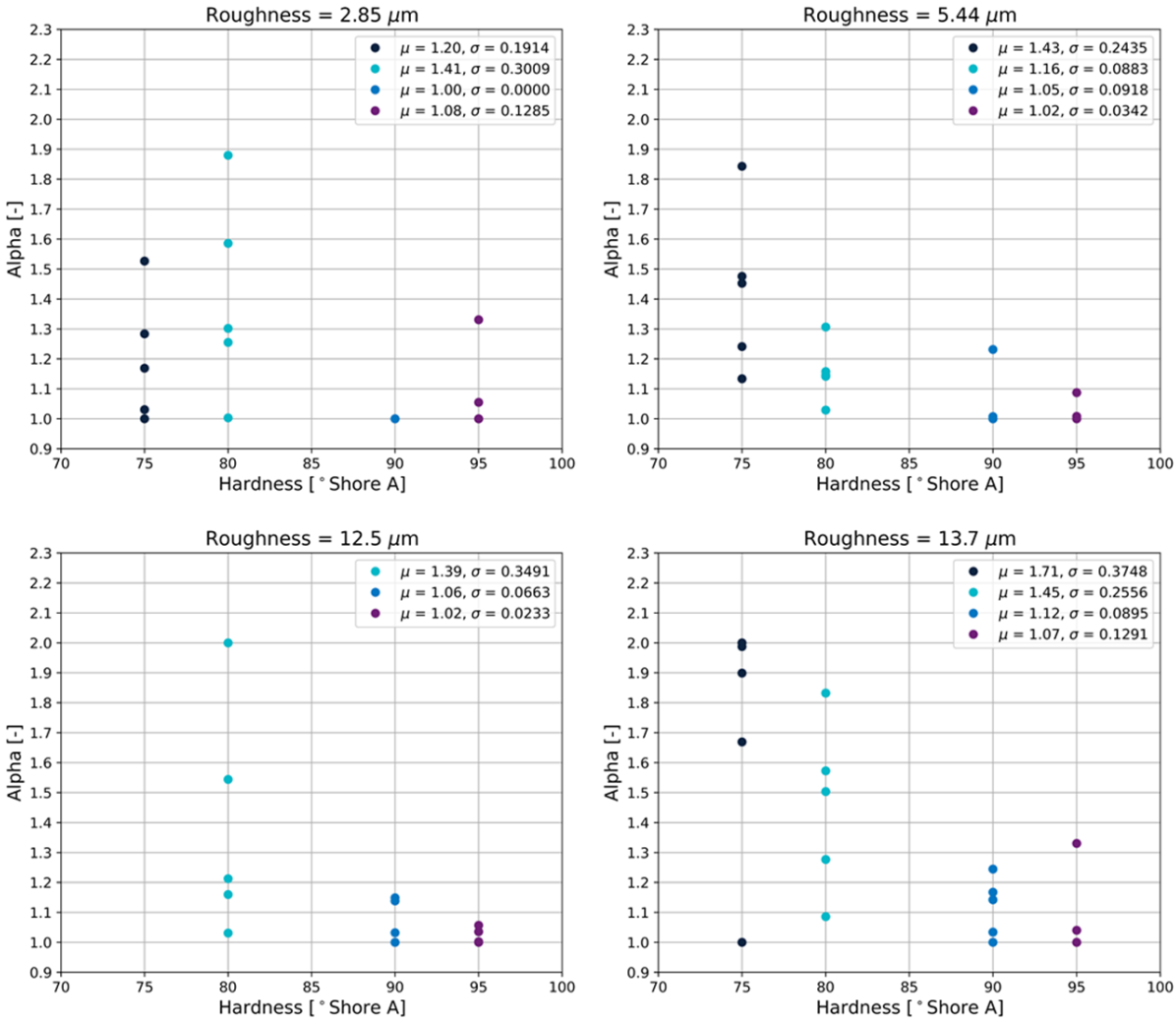

Figure 6.22. Influence of hardness on Dahl model parameter alpha
(roughness-hardness sensitivity tests at room temperature)

6.7.3 Relation roughness and sigma

Figure 6.23 shows the effect of roughness on model parameter sigma. No clear correlation is found between roughness and model parameter sigma for the lower hardness materials. The variability in the values for sigma is significant. For the higher hardness materials, there is correlation found between roughness and sigma. An increase in roughness results in decrease in sigma. This means that the initial slope of the force-displacement graph becomes less steep with higher roughness. This aligns well with the different initial slopes that are observed in the corrected force-displacement graphs in Figure 5.13.

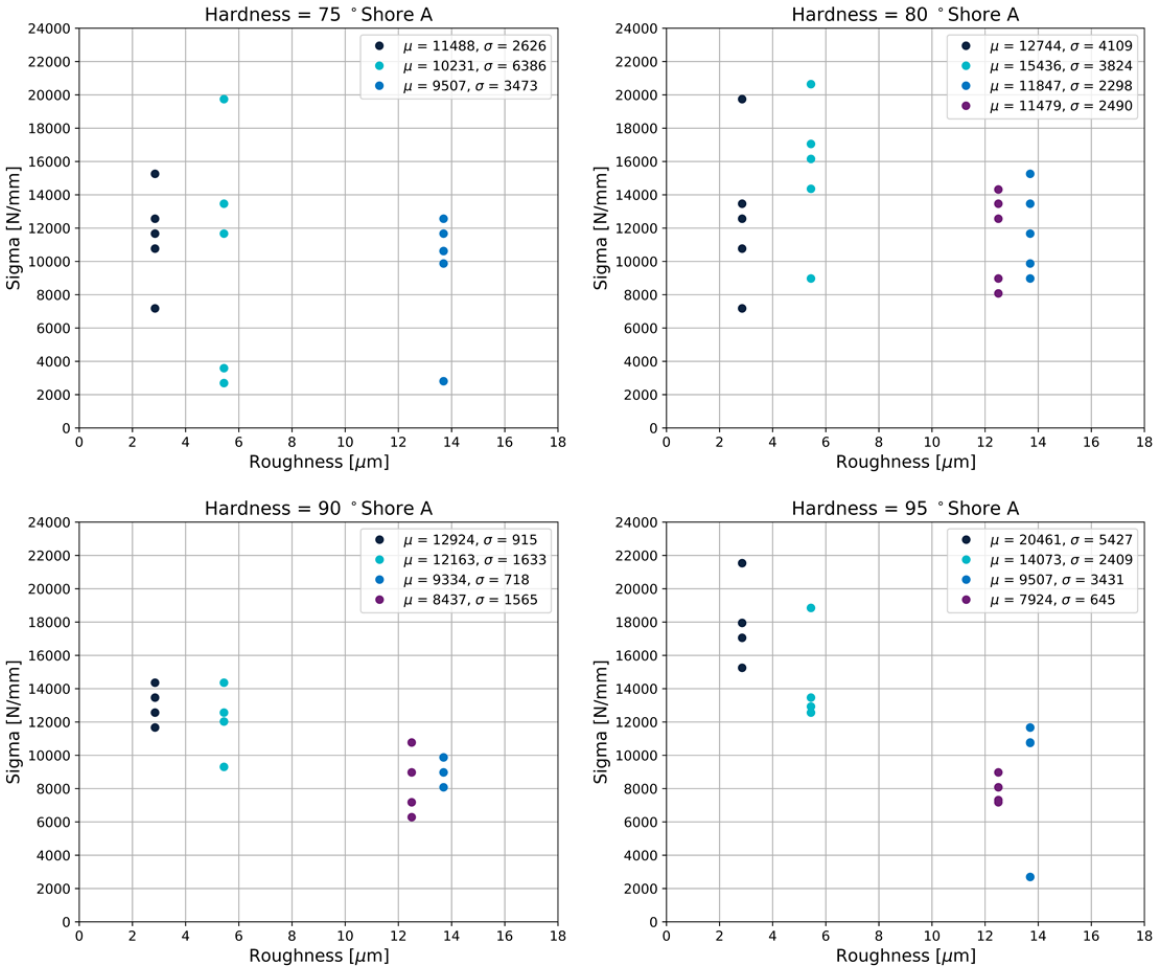

Figure 6.23. Influence of roughness on Dahl model parameter sigma (roughness-hardness sensitivity tests at room temperature)

6.7.4 Relation roughness and alpha

There is no general correlation observed between the roughness of the monopile and model parameter alpha (Figure 6.24). The alpha seems to increase with roughness for the tests with the lowest hardness samples. For the tests with higher hardnesses, no correlation is observed at all. This observation corresponds with the corrected force-displacement graphs in Figure 5.13 in which no correlation is observed for the increase to F_C.

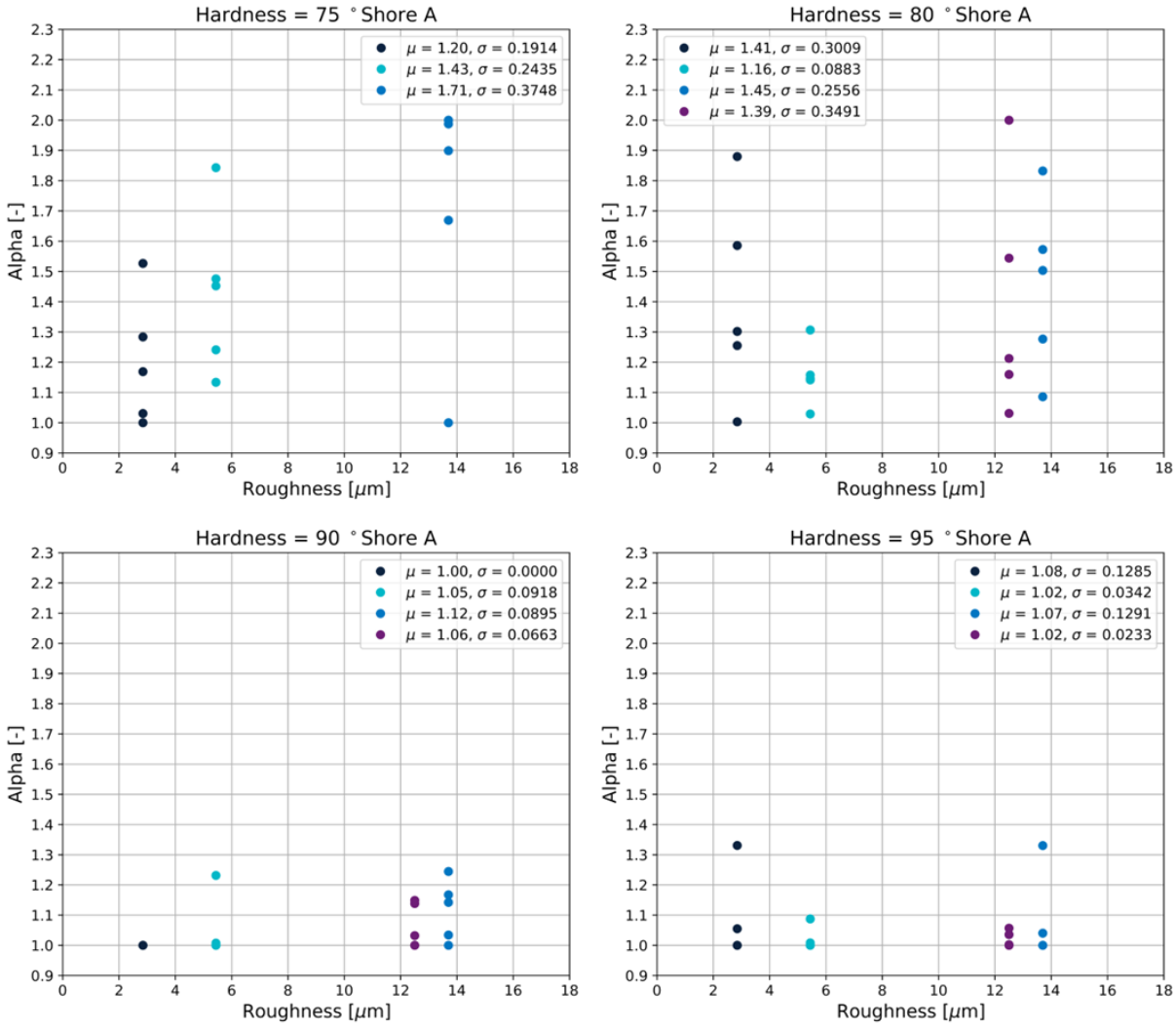

Figure 6.24. Influence of roughness on Dahl model parameter alpha

6.8 Modelling temperature-viscoelasticity tests

The process of modelling is also applied to the temperature-viscoelasticity tests. Per combination of temperature and hardness five values for sigma and five values for alpha are obtained. The fitted graphs and the MAE are included in Appendix J.

6.8.1 Correlation temperature and sigma

In Figure 6.25 sigma is plotted versus the different temperatures. The first thing to notice is that the variability in the values for the cold plots is large. This may be caused by the shape of the force-displacement graphs for these cold tests, which fits less good with the Dahl model. It seems that there may be a small correlation between temperature and sigma. This may also be caused by the corrections for the pad deformation. For the cold and the warm tests, the measurement data is corrected for the pad deformation measured at room temperature.

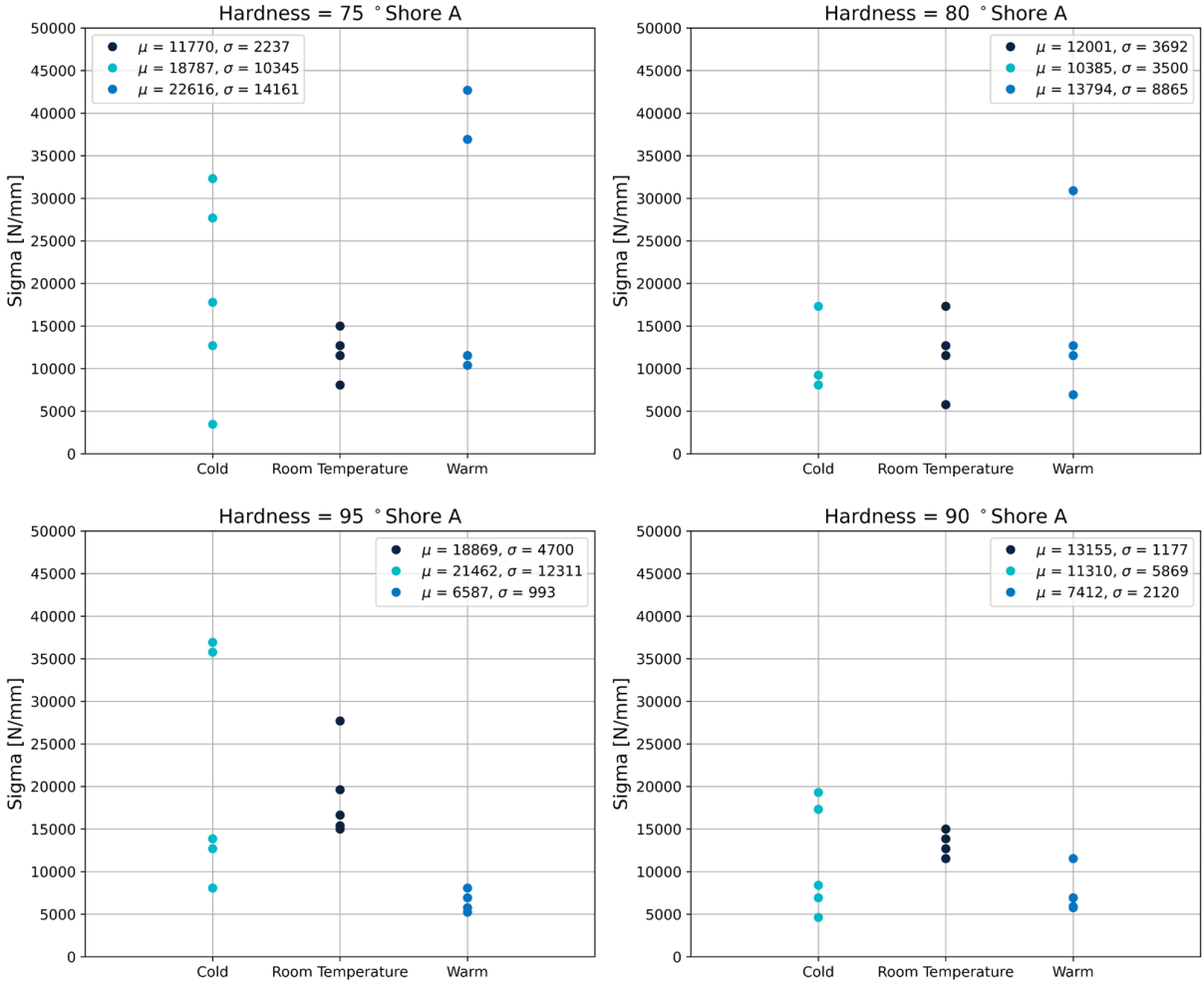

Figure 6.25. Influence of temperature on Dahl model parameter sigma

6.8.2 Correlation temperature and alpha

In Figure 6.26 the influence of temperature on Dahl model parameter alpha is visualized. For the higher hardness PU materials, it is observed that alpha is larger and varies more for the cold tests. This could also be due to the worse fits for the cold tests. Overall, there is no correlation found between roughness and alpha.

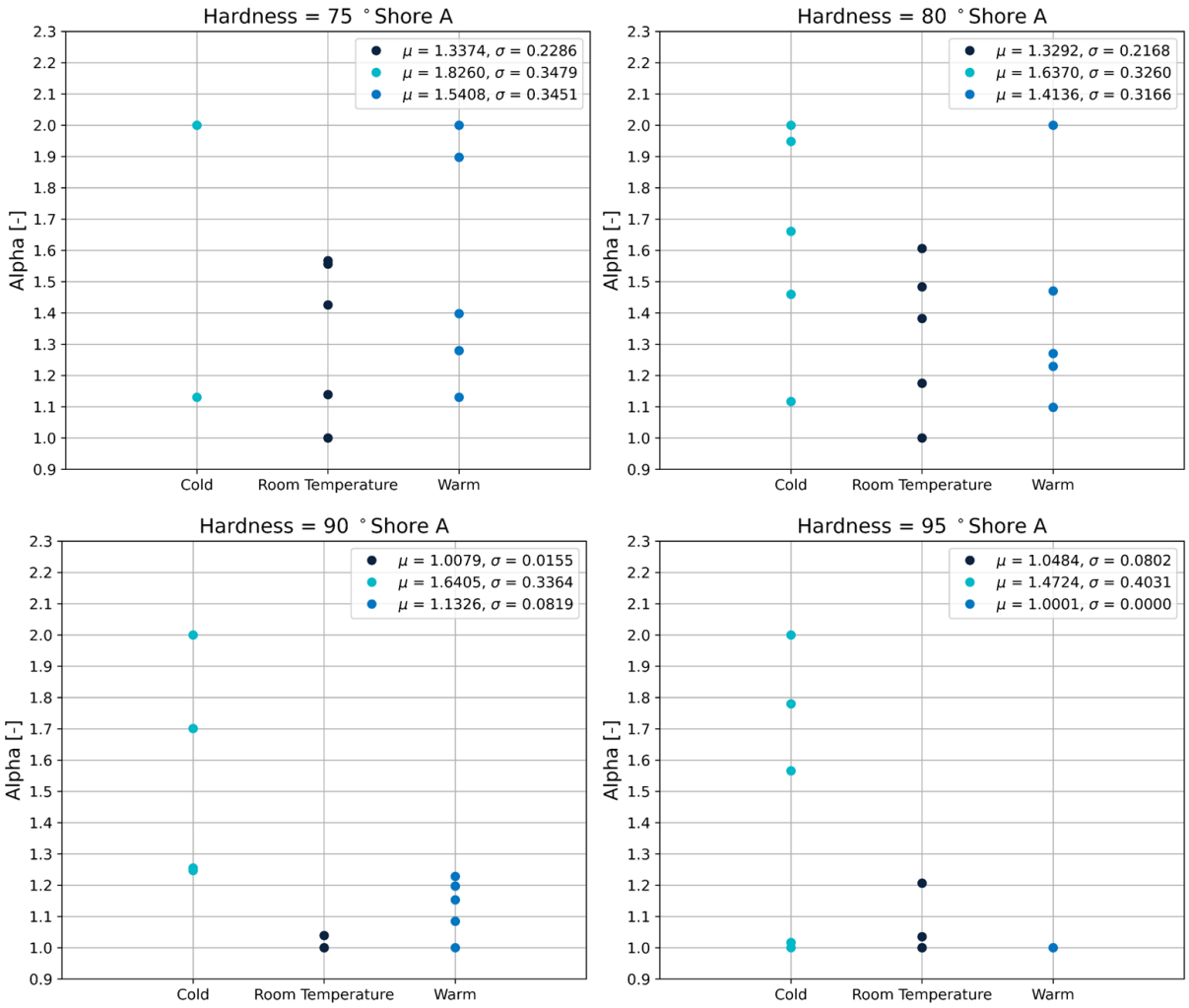

Figure 6.26 Influence of temperature on Dahl model parameter alpha

6.9 Conclusion

Friction modelling is relevant to increase the insight in the distribution of friction forces over the cradles. Disturbances in the measurements have to be filtered to apply a friction model on measurements. The Dahl model can be used to model pre-sliding displacements. It fits well with most measurements, but has troubles with describing cold tests and tests with 80 °Shore A PU. The cold tests show an kink after a few millimeters of displacement. The tests with 80 °Shore A PU show stick-slip, which is not included in the Dahl model. There are some relations present between the factors affecting friction and model parameters sigma and alpha. Hardness shows some correlation with alpha. Roughness shows some correlation with sigma. Predicting the friction behavior based on known conditions is not yet possible.

7 Safety

Safety is required in designs to account for variability and uncertainty. In friction-based monopile sea fastening designs, variability and uncertainty comes from wear, friction tests and unexpected effects. Therefore, the origin of variability in friction tests will be analyzed in Section 7.1. After identifying the origins of variability, the current way of dealing with the test variability is highlighted. Some alternatives to the current guidelines are studied and reviewed.

7.1 Total variability friction tests

The total test variability is divided over three elements. These three elements are treated separately in the following subsections. The variability sources are not estimated, because of limited available data. The three elements of the variability in friction tests are:

1. **Measurement system variability**
   The variability in executing measurements can be caused by actions taken differently by the operator. Measurement system variability might also be caused by deviations in the test setup (Igea & Cicirello, 2018). This can for example be the aligning of the two PU pads.
2. **Component-to-component variability**
   This includes variability caused by differences between tested samples. The surface of material properties of samples may vary locally from component to component due to manufacturing processes (Igea & Cicirello, 2018, 2020). Some PU pads might for example have a slightly higher hardness than indicated.
3. **Variability caused by conditions**
   The friction behavior can be less constant under some conditions. This is represented in variability caused by conditions. Adding lubrication can for example increase the variability caused by conditions.

7.1.1 Measurement system variability

The variability in the measurement system caused by the operator (reproducibility) is treated first. Some of the variability originates from the placement of the steel back plates in the friction clamp. The horizontal alignment can cause different loading conditions than aimed for. The impact of this misalignment is unknown. Insufficiently restraining the backing plates in the friction clamp might also cause some variability. This can impact the measured displacements and thus the determination of the transition point.

Operator variability may also be caused by the pressure which is applied by the compressor. Since a compressor based on air is used, applying an exact pressure and keeping it steady can be error sensitive. The variability that is caused by this is expected to be minimal for larger pressures.
The consolidation time is also a factor which can have some variability. When bringing the interfaces in contact and applying the load, some handling time is needed to start the countdown. The time between these handlings is approximately 5 seconds. On the standard consolidation time of 8 minutes, this is only 1%. This variability is insignificant (Section 3.8).

The setup can also cause some of the variability in measurements. Here the measured force, pressure and displacement have some variability. This variability is also limited since the measuring devices are calibrated regularly. The rate of loading could be affected by errors in measuring force.

7.1.2 Component-to-component variability

Three components are tested per monopile sea fastening friction test. Two PU samples and one steel sample are used in each test. When the PU samples that are tested in a test series are made by one supplier with the same manufacturing process and the same intended material properties, there is little variability. The PU samples might vary in roughness and might become rougher after testing. The scale and the effect of these roughness differences are not known. There is more possible variation at the steel interface. The steel might have variations in roughness, coating thickness and contaminations (corrosion). The scale of variability of these factors is unknown. In a test series multiple PU samples and steel samples are tested. This increases the component-to-component variability. For monopile sea fastening friction tests it is desirable to have component-to-component variability present in tests, since this represents the variability present in the friction interface at the sea fastening.

7.1.3 Variability caused by different testing conditions

Variability can also be caused by testing conditions. When water is present, more variability is expected because of the variation that comes with applying water. The amount of water that is applied is not the same in each test. A benefit of water being applied is that it mostly results in friction without stick-slip. This makes the determination of the transition point less critical.

Another thing that is noticed is that warm friction tests have less variation than the friction tests at room temperature and in cold conditions. This can be caused by the difference in viscoelastic properties, but also by the stable sliding behavior in the warm tests. Determining the transition point and the corresponding tangential force is more critical in cold conditions (Figure 7.1).

Performing friction tests at different temperatures is possible. However, it is difficult to determine the exact temperature of the friction interface. A different test temperature can result in a too high or too low coefficient of friction.

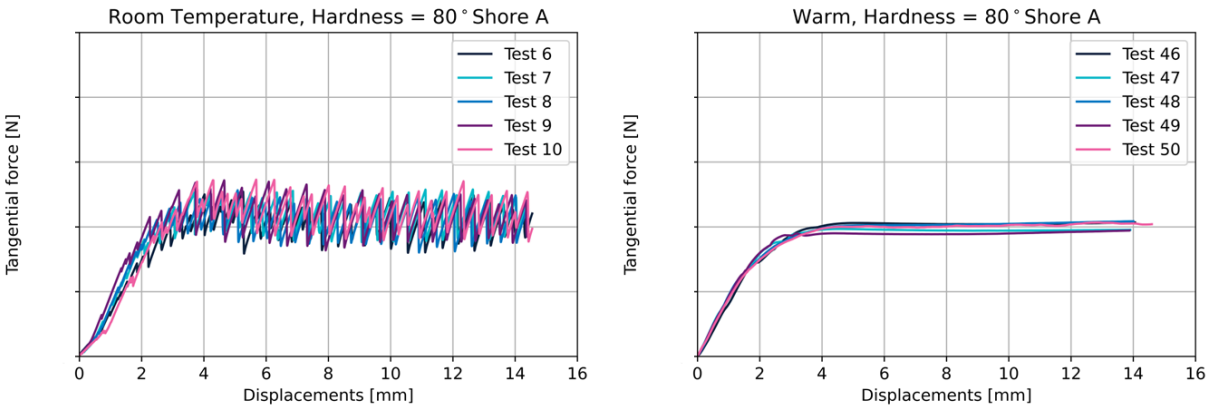

Figure 7.1. Force displacement graphs at room temperature and in warm conditions (sensitivity tests)

7.2 Current standard and variability

Variability is considered in the current standard on friction testing. The standard on friction tests itself exists approximately of one page and is not exhaustive (DNVGL-ST-N001 5.4.4, 2020). The statements from this standard are highlighted and discussed in this Section.

7.2.1 Representative friction interface and loading conditions

The friction testing standard states the following: “The testing conditions should represent the expected friction surface and load intensity as close as possible” (DNVGL-ST-N001 5.4.4, 2020). Testing for the expected friction interface may be interpreted as that the same PU samples and the steel samples used in testing are the same as in the intended application. This means the same type of material and for the steel this also means the same coating and coating thickness.

Testing for a representative temperature is not mentioned in the standards. It can however have significant impact on the friction. The difference of the mean coefficient of friction in cold conditions and at room temperature is a factor of 1.5 (Figure 7.2). Between room temperature and warm conditions this is a factor of 1.3.

Another example is the roughness of the steel sample. In the testing standard it is only stated indirectly that the steel roughness has to be taken into account in friction tests (DNVGL-ST-N001 5.4.4, 2020). The difference of the mean coefficient of friction between the least rough and the roughest steel sample is a factor of 1.45 (Figure 7.2).

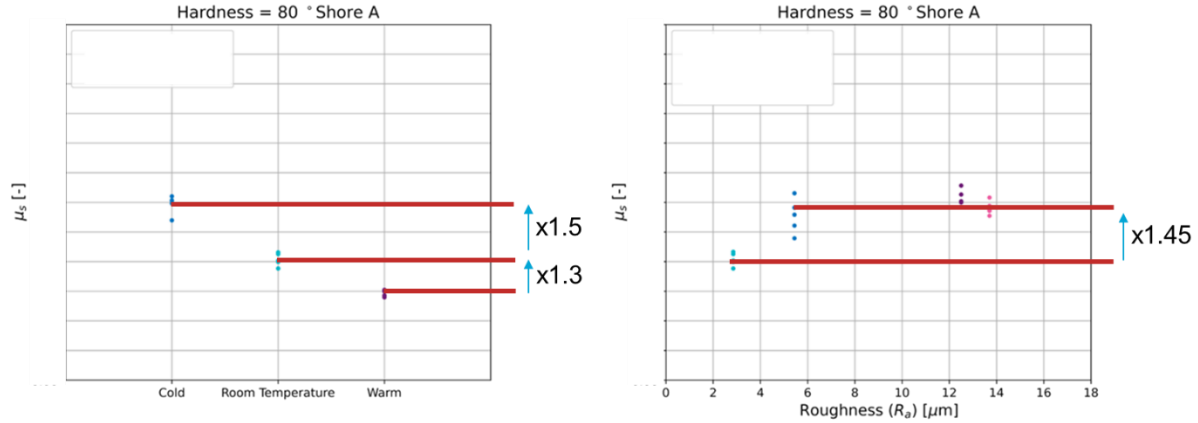

Figure 7.2. Effect of conditions on static coefficients of friction (from sensitivity tests), test conditions: 5 MPa, dry, blank steel (Ra = 3 µm) (temperature effect), room temperature (roughness effect)

7.2.2 Test five test samples twice

It is required to test five test samples at least twice (DNVGL-ST-N001 5.4.4, 2020). This results in component-to-component variability (Subsection 7.1.2). This variability could represent the variability of the material and surface properties that are also present in the friction interface of the monopile sea fastening. Reducing this variability is thus not required. The number of samples to be tested could even be increased to improve the representation of the monopile sea fastening friction interface in friction tests.

7.2.3 Design value (material factor & characteristic value)

The design value for the coefficient of friction is calculated by dividing the characteristic value by a material factor. In the current standard the characteristic value is the 5th percentile of the tests. The safety factor is based on the number of tests. A material factor of 1.4 is applied when 10 tests are performed. For an increasing number of tests, the material factor may be reduced, but not below 1.25. It has been agreed that a material factor of 1.25 can be used when 30 tests are performed, but this not specified in the standard. This material factor and the 5th percentile are measures that should account for wear, test variability and unexpected effects. Subsection 7.1.3 shows that a material factor of 1.4 is insufficient when conditions are not properly represent in tests.

The impact of the material factor and the number of tests which are performed is illustrated. For this example, a set of 60 coefficients of friction is used from tests that were performed in the same conditions. The tested materials were PU with a hardness of 87° Shore A blank steel. Salt water was applied as lubrication. The applied pressure was 3 MPa and the rate of loading was kgf/min. All tests were performed at room temperature. A bootstrap analysis is performed (Rabbi et al., 2022). 1000 times a random selection of 10 friction coefficients is made from the 60. For each selection of 10 tests, the 5th percentile was taken. The same has been done for selections of 30 tests from the 60 in total. In Figure 7.3 the 5th percentiles of the selections are plotted in a histogram. The mean 5th percentile of 10 selected friction coefficients is . For 30 selected friction coefficients, the mean 5th percentile is .

The 5th percentile for a selection of 30 tests is lower, since the probability is large to select extreme lows. Dividing the mean by the material factor that corresponds with the number of tests selected, results in both cases in a design coefficient of friction of . For this specific set of 60 friction coefficients, the design value for 10 and 30 tests is thus the same. This might be different for other sets of friction coefficients.

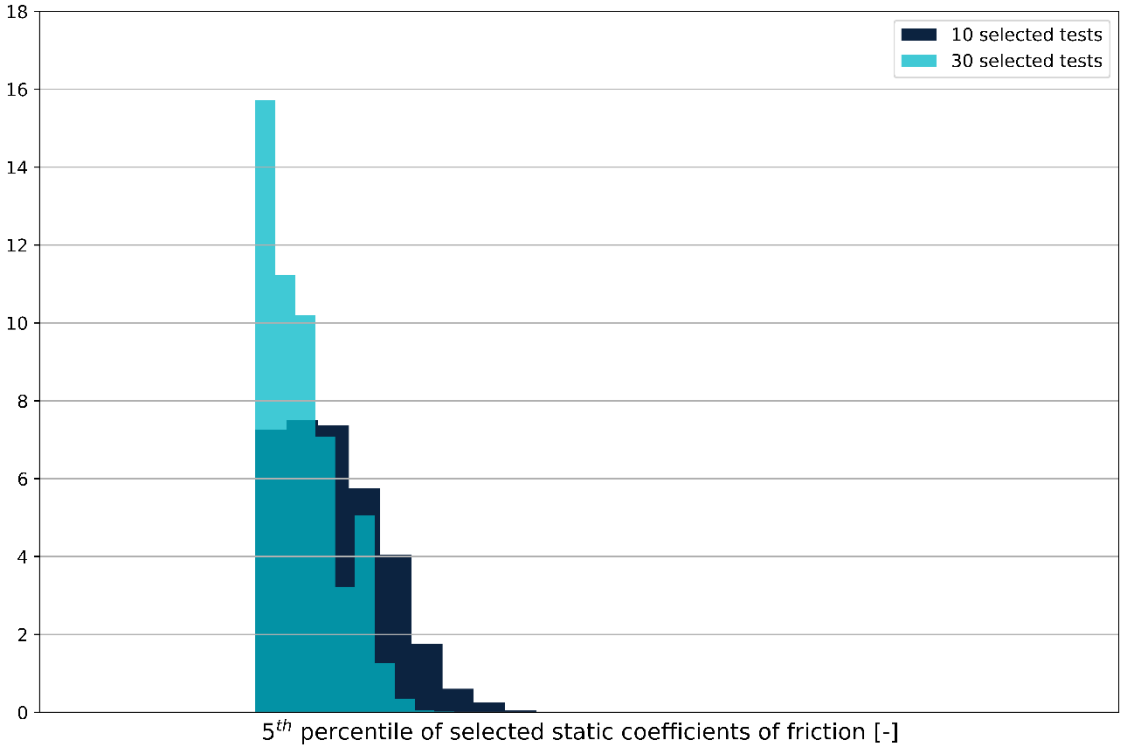

Figure 7.3. Distribution of 5th percentiles of 1000 selections of static coefficients of friction from test series of 60, test conditions: hardness = 87° Shore A, blank steel, wet (salt water), 3 MPa, room temperature

The characteristic value which is resembled by the 5th percentile of the coefficients of friction, might be too conservative. The characteristic value based on the mean value of the test set is studied as alternative. In this case taking the mean could account for the component-to-component variability. The component-to-component variability present in the test samples can resemble the variability at the support cradle and the monopile. The sea fastening cradle covers 15 m^2 compared to only 0.02 m^2 that is covered by the test samples. Taking the mean value would be more representative for the global behavior of the sea fastening.

To illustrate the difference between taking the 5th percentile and taking the mean, the set of 60 friction coefficient is used again. 1000 random sets are selected from the 60 values in total. Instead of taking the 5th percentile of these selected sets, the mean value is taken. From Figure 7.4 it can be observed that the mean value of the means is for all numbers of selected tests. The standard deviation increases for a fewer number of tests selected. The standard deviation for 10 selected tests is and for 30 selected tests it is . If the 5th percentile value is taken as the characteristic value, the material factor can be chosen based on the standard deviation.

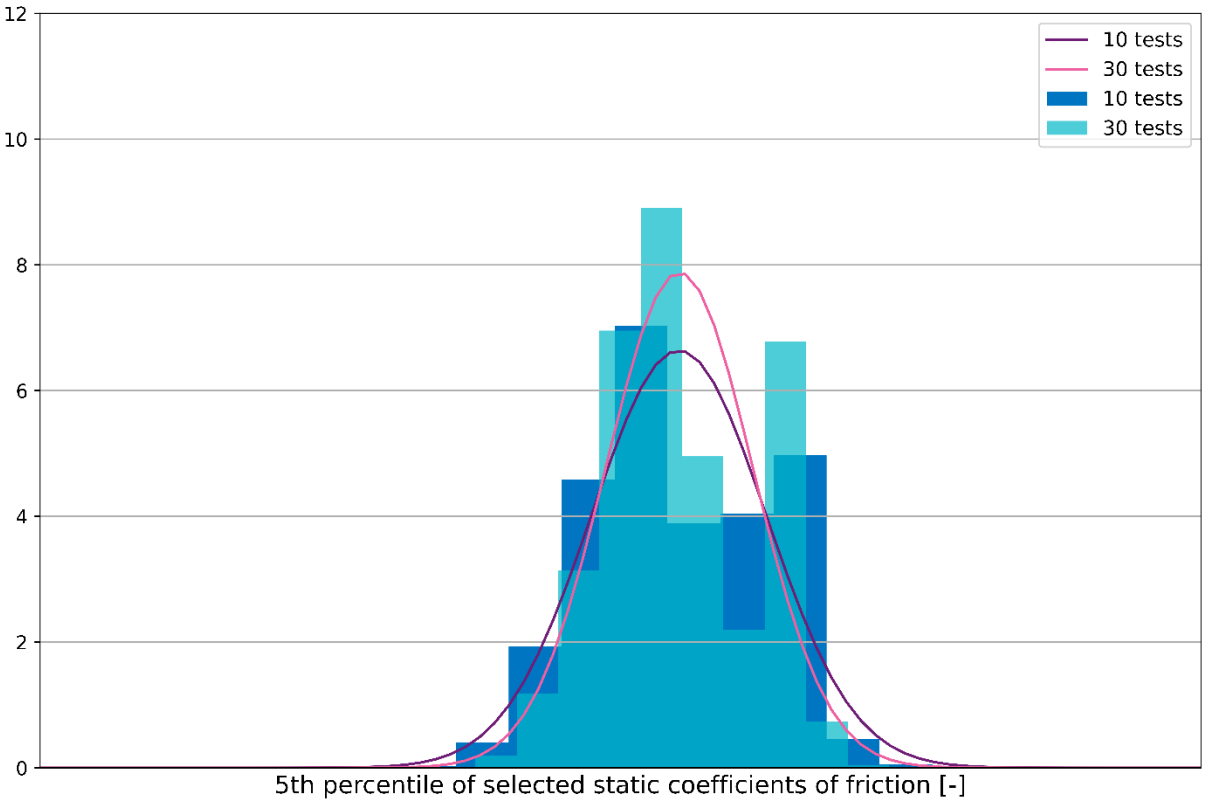

Figure 7.4. Normal distributions of means of 1000 selections of static coefficients of friction from test series of 60, test conditions: hardness = 87° Shore A, blank steel, wet (salt water), 3 MPa, room temperature

An option for determining the material factor could be based on the normal distribution of multiple bootstrap analysis. The standard deviation for the mean values reduces for the number of tests selected (Figure 7.4). Material factors could be determined based on multiple bootstrap analysis for different sets of conditions. A suggestion is to take the mean plus the two times the standard deviation as unwanted upper bound. The material factor can be deducted by dividing the unwanted upper bound by the mean value. An example for this approach is given in Table 7.1, based on the means and standard deviations in Figure 7.4.

Table 7.1. Material factors based on mean and standard deviations Figure 7.4

Number of tests	Mean μ	Upper bound $\mu + 2 \cdot \sigma$	Material factor = $(\mu - 2 \cdot \sigma)/\mu$
5			
10			
20			
30			
40			
50			

7.2.4 Unspecified test method and test conditions

The friction testing standard does not prescribe a friction testing method or setup that must be used in tests. The way of testing affects the coefficient of friction and the variability in measurements (Chapter4). Including a required test method or test setup, can increase insight in testing variability. With a required method or setup, it can be determined what variability is caused by the measurement system and what variability is caused by conditions or the different test samples. For the same reason it is beneficial to include guidelines for determining the static coefficient of friction.

Not all conditions that should be considered in friction tests are mentioned in the testing standard. Neglecting testing conditions can result in unsafe friction coefficients. Safety factors can be used to in case conditions are not considered. This could lead to and uneconomical design when multiple safety factors have to be applied for conditions that are neglected. The current safety factor of 1.4 is insufficient to cover unconsidered conditions.

7.3 Conclusion

The effect of wear, test variability and unexpected effects should be covered by safety measures in the test standard. The total test variability is divided over measurement system variability, component-to-component variability and variability caused by conditions. The measurement system variability of the friction tests used in this research can be caused by alignment of the samples, application of the pressure and the considering the consolidation time. The component-to-component variability is caused by different PU samples and steel samples that are used in test series. Lubrication and temperature are two conditions that add variability.

The current test standard prescribes a material factor of 1.4. This value is insufficient to cover the effect of unconsidered factors that affect friction. A bootstrap analysis showed that the 5^{th} percentile as characteristic value is very conservative, because of the size difference between the cradle and the tested samples. Prescribing the mean as characteristic value is shown to be a reasonable alternative. The material factor could then be composed of a factor for wear and unexpected effects and a factor considering test variability. This factor for test variability can be determined based on the standard deviation of the tests.

The test standard should include a safety factor that accounts for wear and unexpected effects. Another factor should be applied to cover the test variability. Prescribing all factors that must be considered in friction tests would reduce the test variability. A required test method can decrease variability as well.

8 Conclusion

This chapter presents the main conclusions of this research. The factors that affect friction, the friction test method, safety and friction modelling are treated.

Friction tests should be performed to determine the coefficient of friction for the interface on the monopile in contact with the sea fastening. All ten factors affecting friction should be represented in friction tests. The horizontal and vertical plane test method are able to take these factors into account. It is possible to describe the friction tests with the Dahl model, but it is not (yet) possible to predict the model parameters based on the known factors affecting friction. A characteristic coefficient should be divided by a material factor to determine the design coefficient of friction.

1. Factors that affect friction

This research shows ten factors that affect monopile sea fastening friction (Figure 8.1). These factors that affect friction follow from literature and results from previous tests. The effect of pressure, lubrication and consolidation time is known. The static friction coefficient of polymers decreases for an increase in pressure for pressures above 1 MPa. The presence of lubrication decreases the friction resistance. The lubrication layer reduces the real contact area and thus the friction. The consolidation time is the time that the friction surfaces are in contact before the introduction of forces parallel to the friction surface. The static friction coefficient increases for an increase in consolidation time, partially because of a growth in real contact area over time.

Additional tests have been carried out to investigate the effects of hardness, monopile roughness, temperature and viscoelasticity. An increase in hardness results in an increase of friction. This can be related to the increase in shear strength of the polymer asperities which is dominant over the reduction in real contact area. For an increase in monopile roughness an increase of friction is observed. This effect can be explained by an increase in real contact area. A decrease in friction is observed for an increase in temperature. No conclusions can be drawn for the viscoelastic properties.

Using prescribed friction values for specific sets of factors is not realistic, because of the multidimensionality of the problem, which is caused by the different factors affecting each other. Determining prescribed friction values for ranges of factors would also be an extensive process. This results in either too conservative or unsafe prescribed coefficients of friction. Project specific testing of friction is the best way to determine a friction coefficient. The tests should be performed with representative or conservative selected factors to obtain an optimal and safe design, since a change in the factors can result in a different friction coefficient.

An overview of the factors affecting monopile sea fastening friction is visualized in Figure 8.1. The factors affecting monopile sea fastening friction are:

- Hardness
- Viscoelastic properties
- Monopile roughness
- Roughness of support pads
- Coatings
- Applied pressure
- Lubrication
- Rate of loading
- Temperature
- Consolidation time

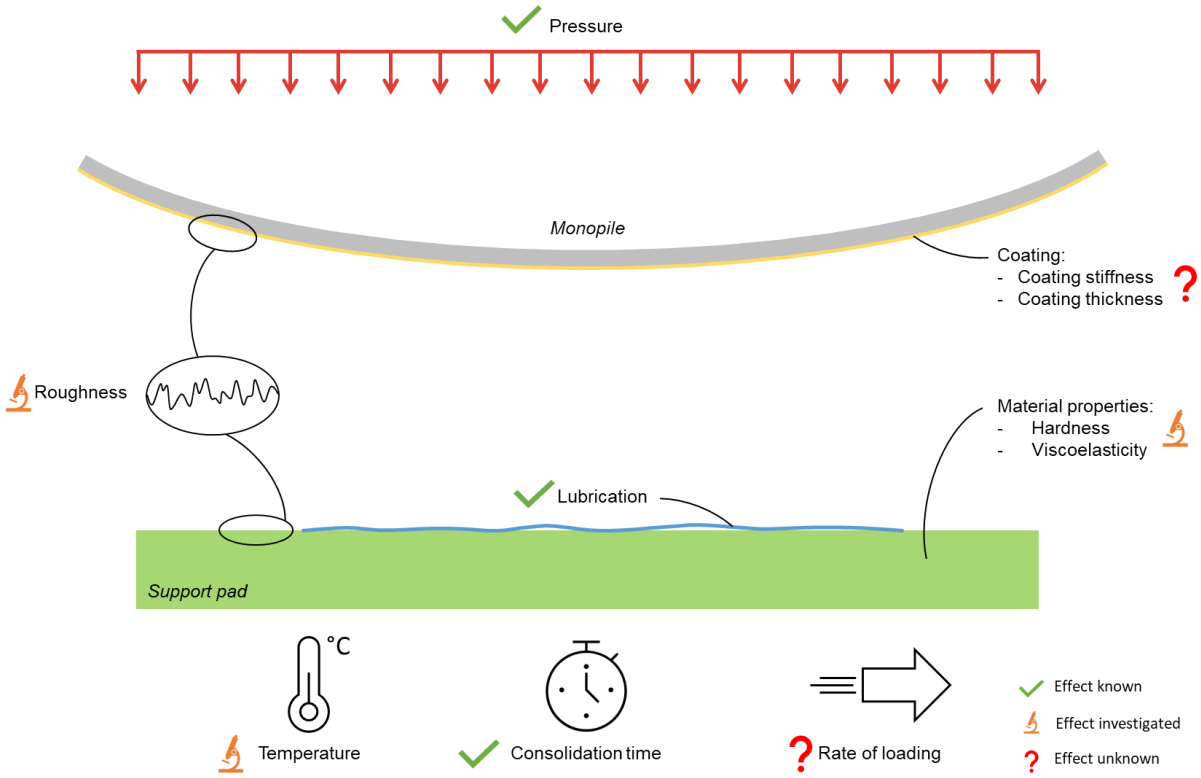

Figure 8.1. Overview of factors that affect friction

2. Friction testing

The horizontal plane, vertical plane, inclined plane and the pin-on-disk method are commonly used methods to test friction of flat surfaces in contact. A monopile sea fastening friction test should have a force-displacement graph and a static coefficient as outcome and it should be able to represent the factors that affect friction in friction tests as conditions. Monopile sea fastening friction tests should meet the following criteria:

- It is possible to calculate the static friction coefficient
- Force-displacement graphs for the static regime are obtained
- A constant pressure can be applied and can be controlled during testing
- Tests can be performed at different temperatures
- A consolidation time must be taken into account

- It is possible to test in wet and dry conditions
- Monopile surfaces and polymer materials can be tested, with different characteristics like roughness, coating thickness, and hardness
- The rate of loading can be controlled

The best methods for testing monopile sea fastening friction are the horizontal plane method and the vertical plane method. The horizontal plane method meets all criteria, provided that the high contact pressure can be applied. The vertical plane method also meets all criteria. The inclined plane method is not suitable, since the pressure during these tests is not constant. Since the pin-on-disk method focusses on kinetic friction and is not able to accurately measure static friction, this method is not applicable for testing monopile sea fastening friction.

High contact pressures are present in monopile sea fastening. These high pressures have to be represented in the friction tests. Introducing the pressures on the tested samples can result in moments occurring in the test setup. This must be avoided, because occurring moments will locally increase the contact pressure in the test samples and will disturb the measured forces. The test setup used for friction tests in this research is designed to be a moment-free setup. This setup is based on the vertical plane method. A test setup that uses the horizontal plane method has more challenges to avoid moments in the setup.

3. Modelling

Friction modelling is relevant to increase the insight in the distribution of friction forces over the sea fastening cradles. The Dahl model is able to describe static friction, with pre-sliding displacements and static friction forces. The model parameter sigma describes the initial slope of the force displacement graph (Figure 8.2). Alpha determines the rate in which the graph converges (Figure 8.2). F_C is the Coulomb friction force, the force to which the graph convergences (Figure 8.2). The Dahl model fits well for the measurements. However, no direct correlations between factors that affect friction and model parameters are present, but some relations do exist. Alpha is lower for tests with higher hardness PU samples. Higher monopile roughness results in a higher sigma value. Predicting friction behavior based on known factors affecting friction is not yet possible. A well fitted model to measurements can be used to describe friction behavior, instead of just using a coefficient of friction.

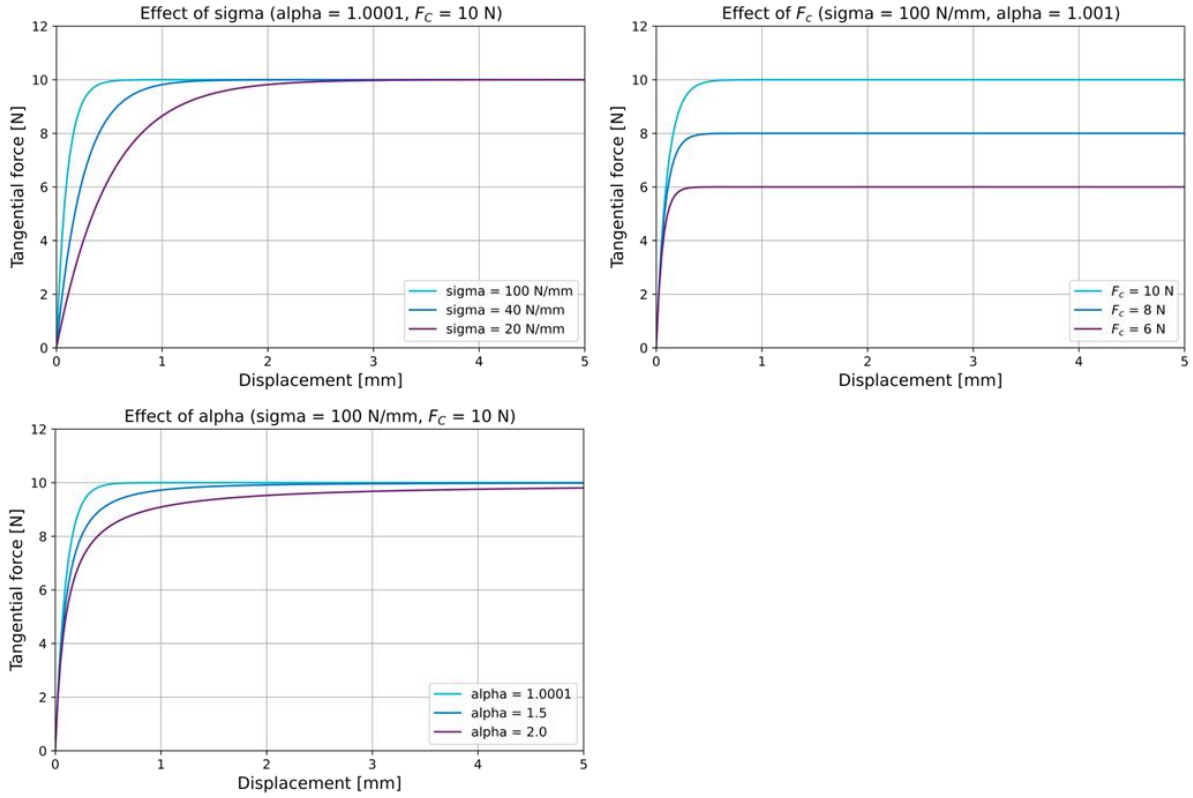

Figure 8.2. Effects of model parameters alpha, sigma and F_C in the Dahl model

4. Safety

The design friction coefficient is based on a characteristic friction coefficient and a material factor. These safety measures in the test standard should account for wear, test variability and unexpected effects. The variability in the friction tests used in this thesis is divided over variability caused by conditions, measurement system variability and component-to-component variability. Lubrication and temperature are the main conditions that add variability. Measurement system variability is mainly due to the operator. The sample placement and applying the pressure are the processes that could cause the measurement system variability if performed incorrectly. The component-to-component variability represents the variability that is present over the monopile sea fastening supports as well and is thus not undesirable.

The current friction testing standard prescribes that tests have to be performed with the representative friction surface, lubrication if representative and representative loading conditions (DNVGL-ST-N001 5.4.4, 2020). The standard does not mention factors that affect friction like rate of loading and temperature as test conditions. A material factor of 1.4 must be applied according to the standard. This would be insufficient if the temperature and the roughness is not considered, since these difference can be more than 1.4. The effect of wear and unexpected effects should be added as well, which makes the material factor incorrect. Applying material factors to compensate for the unconsidered conditions is uneconomical or unsafe. It is recommended to test for the representative conditions and apply material factors to just cover wear and unexpected effects.

A bootstrap analysis shows that the characteristic value as 5th percentile is very conservative. The mean 5th percentile of the bootstrap analysis (selecting 30 measurements out of 60) is . For the average mean of the bootstrap analysis is in that case . The mean value would be more representative for the monopile sea fastening, because of the scale of the tests compared to the scale of the sea fastening. The sea fastening cradle is approximately 15 m^2 and the test samples are approximately 0.02 m^2. The test samples are more than 750 times smaller than the cradles.

9 Discussion & Recommendations

1. Factors that affect friction

This research focused on obtaining an overall overview of factors that affect friction. For each factor, literature and previously performed test exercises are analyzed. Four factors that affect friction are studied in more detail, because literature and previously performed test exercise were unconclusive about their effect on friction. More in-depth knowledge on these factors can improve test and design choices. The factors hardness, monopile roughness, temperature and viscoelasticity were studied in more detail in sensitivity tests. Similarities between the results of the sensitivity tests and literature results is found for hardness and monopile roughness. For temperature the findings were contradictory. The following paragraphs describe the results of the sensitivity tests and why they might differ from literature and test exercises performed previously to this research.

Hardness effect on friction

In the sensitivity tests an increase of hardness results in an increase of friction resistance. This does not align with the findings of Capanidis & Sokolska (2020). Reason for this contradiction could be the lower pressure at which was tested in Capanidis & Sokolska (2020) (maximum 0.7 MPa) compared to the pressure in the sensitivity tests (5 MPa). A small test series is performed with the same conditions as in the sensitivity tests, but at a lower pressure (1 MPa). These tests show the same effect as Capanidis & Sokolska (2020) (Figure 9.1). An average friction coefficient of is measured for the two tests on samples with a hardness of 75 °Shore A. The samples with hardness 95 °Shore A resulted in a friction coefficient of . In Capanidis & Sokolska (2020) the inclined plane method is used for testing, which could be another reason for deviating results.

The increase in friction resistance for increasing hardness aligns with the theory of Briscoe & Tabor (1978) (Figure 9.1). There are some assumptions made, since the real contact area and the shear strength cannot be measured. The shear strength is assumed to increase for increasing hardness, because of the overall increase in stiffness. The real contact area is assumed to decrease, because the polymer shows more resistance to deformation. The deformation component is assumed to be constant. If the shear strength increase is dominant over the decrease in real contact area, this indeed results in an increase of friction.

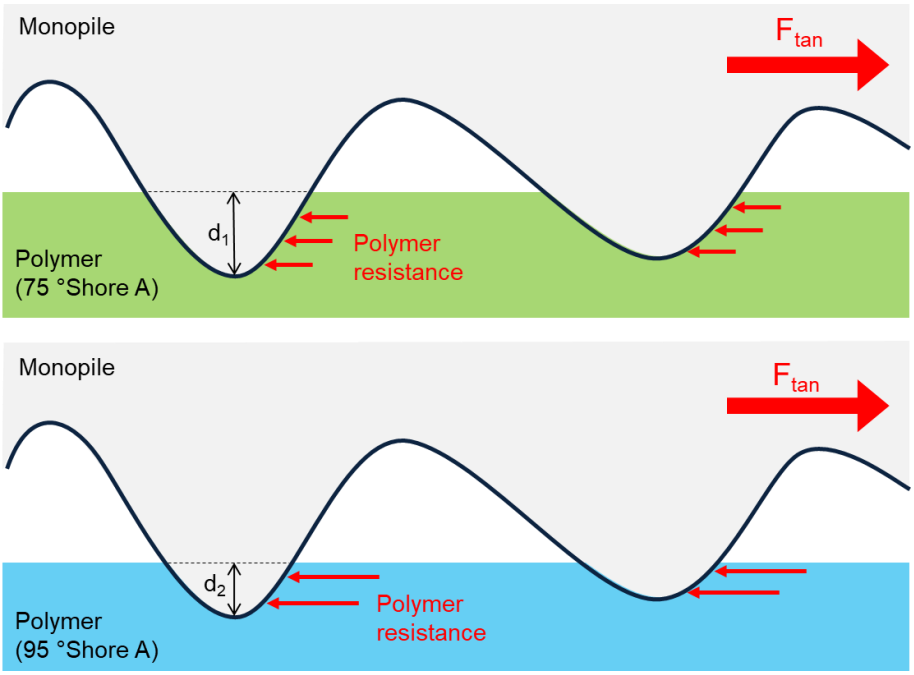

Figure 9.1. Visualization of the effect of hardness on friction

Monopile roughness effect on friction

The static friction coefficient increases for an increase in roughness. The sensitivity tests and literature align on this. Ivkovic et al. (2000) states that for solids in general it is valid that an increase in roughness results in an increase of friction resistance. The sensitivity tests prove this effect of roughness on friction for polymers. The increase in friction for an increase in roughness can be explained with the theory of Briscoe & Tabor (1978). The friction resistance increases, because of an increase of real contact are. It is assumed that the real contact area increases with roughness and that the other components remain constant. The higher roughness results in larger variation in surface heights and the real contact are increases. The surface height variations that form the roughness are measured on a millimeter scale. The difference between roughness on a larger or smaller scale could be investigated further.

Temperature effect on friction

The results of the sensitivity tests on temperature and viscoelasticity do not align with expectations. Based on previous performed tests by (TWD, 2021d), an increase in friction resistance was expected for an increase in temperature. The sensitivity tests showed opposite effects. The sensitivity tests were performed with loose PU samples in pad holders (Figure 9.2a) and in the other tests the samples were on a steel back plate (Figure 9.2b). The loose sample can deform more, as shown in Figure 9.2c. The tests were also performed rates of loading, namely kgf/min in the previous tests and kgf/min in the sensitivity tests. The different PU samples that were used, were from different suppliers with different hardnesses and could have different viscoelastic properties. This shows once again that specific tests are required, due to the amount of factors involved and their interdependencies. The different pressures at which was tested were 0.5 MPa (previous tests) and 5 MPa (sensitivity tests). Additional research could be performed to investigate the effect of temperature and viscoelasticity for more conclusive results.

Based on the observed deformation in Figure 9.2c and the possible differences it causes, it is recommended to test with a similar pad to steel connection as in the monopile sea fastening. The PU in the monopile sea fastening installations is often molded on a steel back plate (Figure 9.2b).

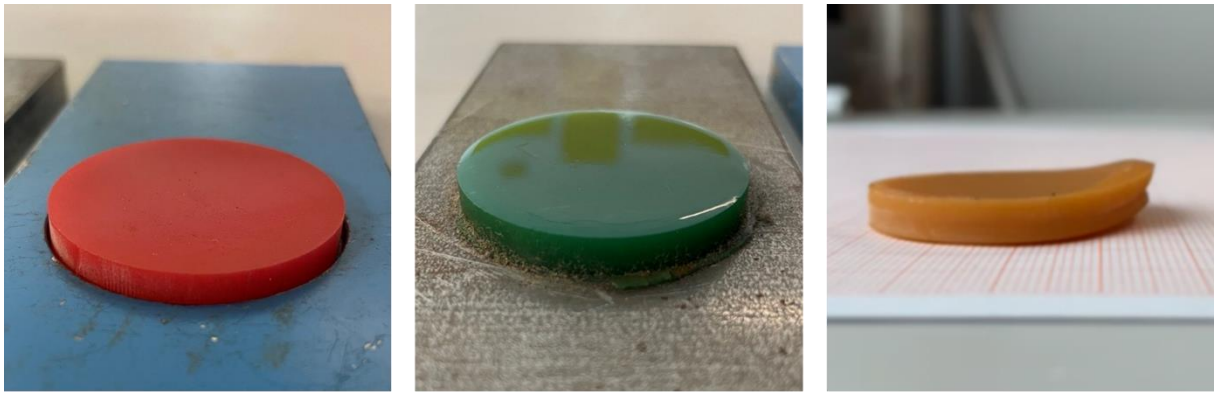

(a) (b) (c)

Figure 9.2. Difference between temperature tests: (a) PU sample in pad holder, (b) PU pad on steel back plate, (c) Possible PU sample deformation for PU sample in pad holder

Coating, rate of loading and support pad roughness

Coating (stiffness and thickness), rate of loading and support pad roughness proved to have an effect on friction from literature and previous test exercises. Therefore, these factors have to be considered when testing friction and comparing test results performed with other testing methods. Rate of loading is a factor that can differ significantly between different tests, which results in different results. This research did not study these factors. Additional research could be performed to investigate the effect of coating, rate of loading and support pad roughness on friction and reasons for the effects.

Theory of Bowden & Tabor (1978)

The explanations of the effects on friction of hardness and monopile roughness are based on the theory from Briscoe & Tabor (1978). The real contact area, the shear strength of asperities and the deformation component are used in this explanation. Therefore, quantifying these components would be of great value. The real contact area might be determined by applying paint or other visual tools. A 3D profile scan of both surfaces might also be helpful. Relating the shear strength of asperities to other stiffness properties (hardness) could be possible.

Multidimensionality

It is important to note that friction is a multidimensional problem. When one of the factors changes this might affect other factors. Obtaining more knowledge on the dependencies between factors can increase the predictability of friction. Dependencies might be:

- Roughness – lubrication, because rougher surfaces have more height variations and the lubrication might be contained in pits between peaks. This can reduce the impact of lubrication on friction, since the real area of contact is less affected. On the other hand, the increase in

roughness might lead to storage of lubrication, instead of the lubrication being pushed out of smoother contacts.

- Pressure – lubrication, since a higher pressure might result in the loss of lubrication. This can reduce the impact of lubrication on friction.
- Pressure – consolidation time, because a stable contact surface might be reached faster when subjected to higher pressures. In this way the consolidation time during testing could be reduced.
- Temperature – coating, since coatings can also be polymer-based and do have viscoelastic properties that change at different temperatures. These changes can effect friction.
- Temperature – consolidation time, since the temperature effects the material response of polymers. This can result in a stable contact surface that is reached in a different time.

Roughness scale

The roughness that is considered in monopile sea fastening friction tests should represent the roughness of the monopile. Roughness is influenced by steel treatment, corrosion and coating. The roughness of coatings can be implemented in tests by applying the exact same coating on the tested steel samples. Determining a representative monopile roughness for friction tests is more difficult for the uncoated side of the monopile. The surface can be smooth blank steel, but also rough and heavily corroded steel. Friction tests can be performed conservatively with smooth blank steel, but the design could be more economical when testing with a more representative surface. It would thus be interesting to investigate the uncoated monopile surface on site. Developing corrosion classes, from smooth blank steel to rough and heavily corroded steel, would be helpful to translate the conditions at the monopile surface to test conditions.

2. Testing friction

Scale effect

The scale effect of friction was not investigated in this research. Several studies mention that friction and contact area are independent (Gao et al., 2004; Hutchings, 2016; Popova & Popov, 2015). Therefore it is assumed that the small scale tests are representative for the large scale monopile sea fastening designs. The small scale samples used in the friction tests should represent the monopile sea fastening interface. It is unknown whether the adhesion and deformation components on a local scale are comparable to a global scale. This study does not investigate the differences in properties between the small scale samples and the elements in monopile sea fastening. Additional research is required on the scale effect of friction. This effect can be investigated testing by samples with different sizes. The PU samples used in this research are circular and have a diameter of 40 mm.

Cyclic loading

Monopile sea fastening friction is exposed to cyclic loading, because of vessel motions. In the friction tests performed in this research the tangential force was applied in one direction. Increasing the

tangential force to a certain limit and then reducing it and applying the force in the other direction might lead to different results. To investigate this effect, an initial test should be performed to compare the effect of cyclic loads. Cyclic loads can be applied force-based. When a certain force is reached, the movement is reversed. This can be repeated several times before increasing the load until kinetic friction is reached.

An initial test series shows slightly different behavior between a test without cyclic loading and a test with cyclic loading (Figure 9.3). The test without cyclic loading is performed by increasing the tangential load with a specific rate of loading (kgf/min) until a displacement of 15 mm is reached. In the test with cyclic loading, the tangential force was increased with kgf/min until a force of 500 N was reached. At that moment the force was reduced until 0 N, before increasing again until 500 N. This cycle was executed 4 times before increasing the tangential force until 15 mm displacement. Further research is required to study the effect of cyclic loading.

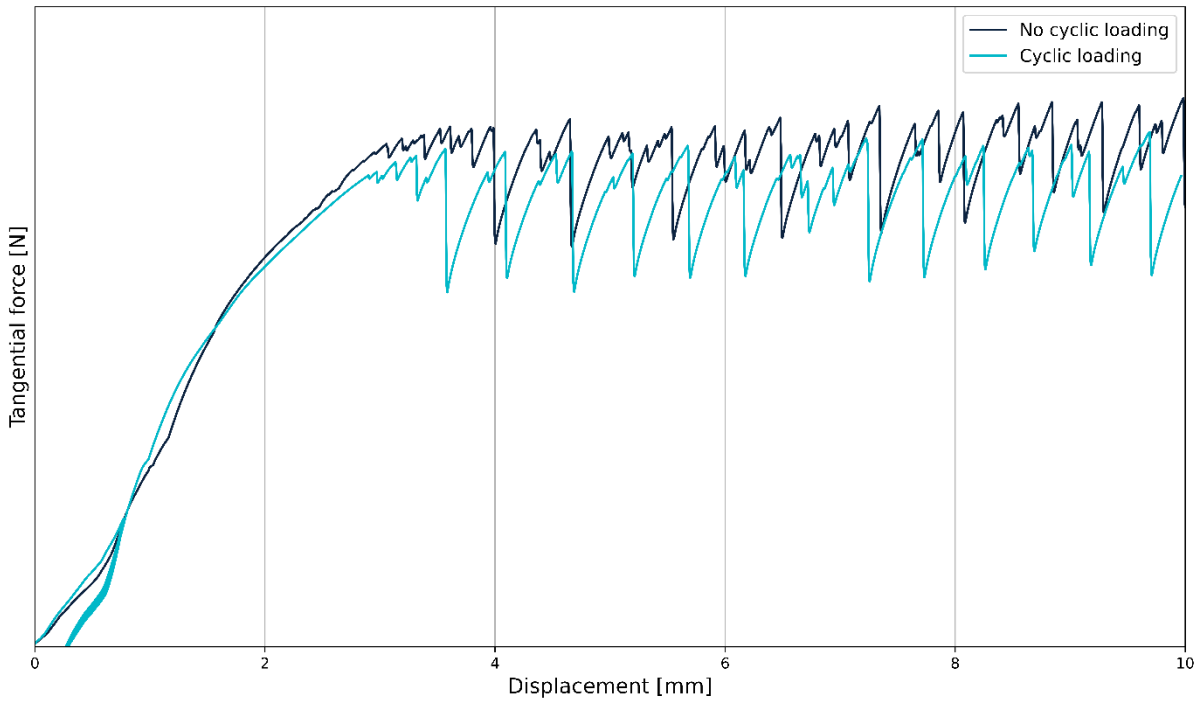

Figure 9.3. Effect of cyclic loading on friction (performed on 25-7-2022), test conditions: hardness = 87° Shore A, R_a = 3 µm, 1 MPa, room temperature, consolidation time = 7 min, dry

Vibrations

The monopile sea fastening might be subject to vibrations. These vibrations can be caused by the vessel engine or engine motions. Vibrations could cause differences in the real contact area, because of deforming asperities and pressure differences. The effect of vibrations on monopile sea fastening friction is not known and requires further investigation.

Different testing setups

There might be a relation between testing with the different testing setups. With known relations between testing setups, conversion rates might be used to determine the friction coefficient for another setup. Results from different studies could be compared in a more easy way. The relations between test methods are not investigated since this research focused on the best setup for testing monopile sea fastening friction. The same conditions should be present in all tests. One of the conditions that varies significantly in current practice is the rate of loading. The different rates of loading can significantly affect the measured friction coefficients.

Transition region

Currently the friction coefficient is determined from a single point, the transition point. Based on the measured displacements, the transition point and thus the static friction coefficient can be determined. It is noticed that the transition from static to kinetic for these viscoelastic polymers can be smoothly, so it is difficult to determine a clear transition point. It would also be an option to determine a transition region, in which the transition between static and kinetic friction takes place. This is less critical than determining one single point. This research mainly focusses on qualitative relations between friction and factors that affect friction. The transition points in all tests are determined in the same manner. For five tests per set of conditions relations between investigated factors and friction were visible. For this study it was thus not required to determine a transition region instead of a transition point. When quantification of friction is required, a transition region or even a force-displacement graph would be more relevant.

3. Modelling

Disturbances measured displacements

The measured displacements of the sensitivity tests proved to be slightly disturbed. The shear pad deformation is one of the components that caused the disturbances. In this research the shear stiffness was determined by testing glued samples. It could also be possible to determine the shear stiffness with comprehensive finite element models with multiple material parameters that must be estimated. This would introduce model uncertainty in the problem. A finite element model that describes the PU pad deformation in the friction tests can be used to confirm the shear stiffness measured in tests and it can increase insight in the behavior of the pad during friction tests. The PU sample should be modelled as a circular disk that is fixed at one flat side. A surface load is applied at the other side of the disk. Material properties that are provided by suppliers can be included in a Finite Element Method software as properties for a solid.

Model modification

The Dahl model does not perform well on the tests performed in cold conditions. The Dahl model can be extended or modified such that the kink in the force-displacement graph can be described properly (Figure 9.4). Another model that is able to describe this kink could be used as well. In the sensitivity tests performed in this research the PU samples were tested in contact with steel. Monopile coating is

thus not included in these tests. The presence of coating might affect the corrected static force-displacement graphs, because of its material properties. These coatings can also made of polymers and are expected to show viscoelastic behavior as well.

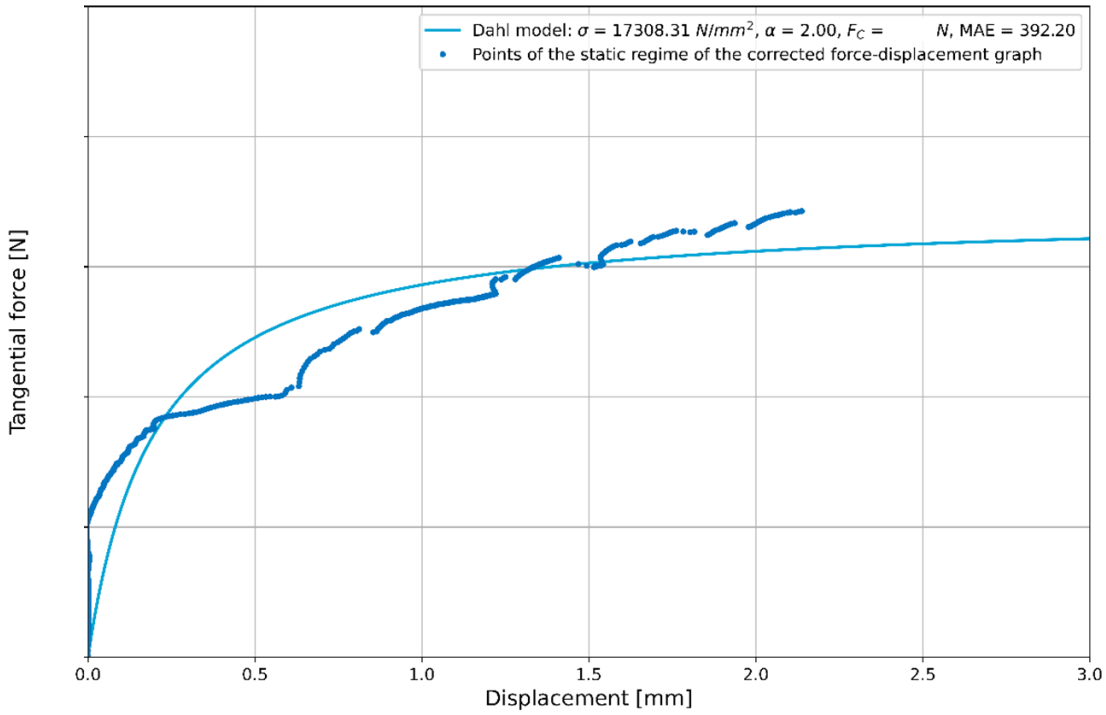

Figure 9.4. Dahl model fitted for points of static regime of the corrected force-displacement graph (temperature-viscoelasticity series, test 29), test conditions: hardness = 80° Shore A, R_a = 3 µm, cold conditions

4. Safety

Safety factor and number of tests

This study has not focused on quantifying new safety factors. It does prove that the current safety factor is unsafe when not considering representative or conservative conditions. The amount of tests that should be performed in a test campaign to determine the design value for the static friction coefficient is not studied in detail. The amount of tests and that have to be performed and the material factors can be determined based on bootstrap analysis for different sets of conditions.

Wear

The effect of wear and tear is not studied in this research. During operations, the polyurethane support pads are exposed to processes that change the friction interface and leave corrosion residues (Figure 9.5). Loading and unloading of the monopile are examples of processes that can cause wear and tear. Wear and tear might impact the friction performance (Bartenev et al., 1981; Briscoe & Tabor, 1978; Popov, 2010). Investigating the effect of wear and tear on the static friction coefficient can increase safety over the lifetime of the support pad. In case of a reduction of friction due to wear and tear, the material factor can be revisited and adjusted according to the amount of reduction. Treatments of the surface can be investigated to recover the initial friction resistance and increase the lifetime of the support pads.

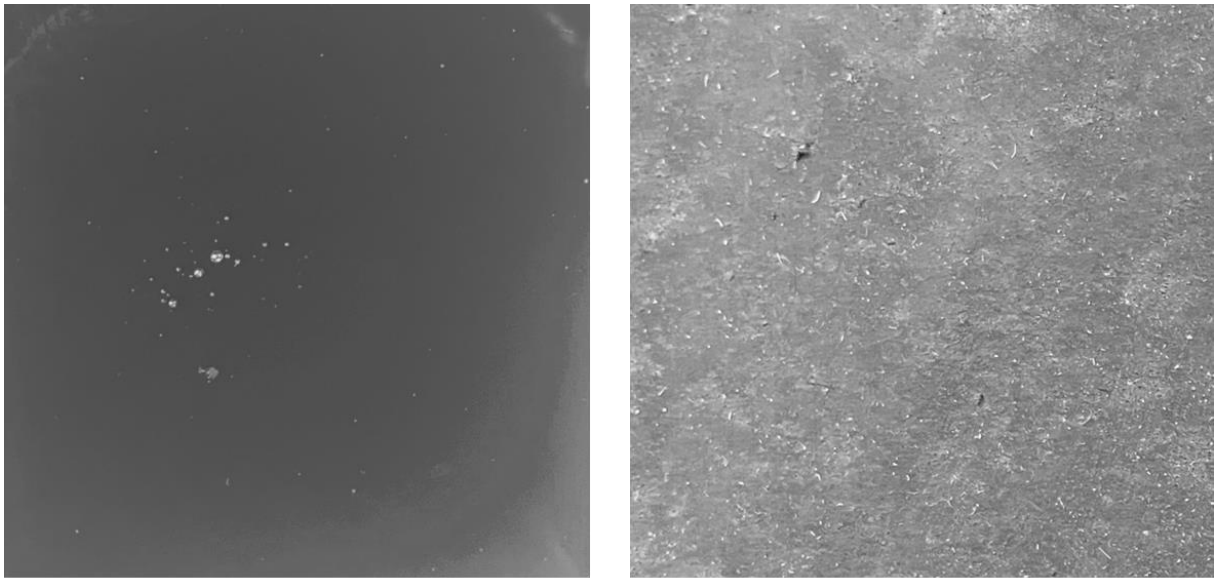

(a) (b)

Figure 9.5. Effect of wear: (a) New support pad surface, (b) Weared support pad surface

Probabilistic design

Probabilistic design could be an alternative to the characteristic value and safety factors. The probability density function of coefficients of friction can be determined from a number of tests. The probability density function of friction coefficients required results from the structural analysis. The allowed probability of failure, the probability that the required friction coefficient is higher than the tested friction coefficient, should be satisfied.

References

Amaral, M. M., Raele, M. P., Caly, J. P., Samad, R. E., Vieira, N. D., & Freitas, A. Z. (2009). *Roughness Measurement Methodology according to DIN 4768 Using Optical Coherence Tomography (OCT)*.

ANSI B46.1. (1985). *Surface Texture (Surface Roughness, Waviness, and Lay)*.

Archard, J. F. (1974). *Surface topography and tribology*.

ASTM D2240. (2000). *Standard Test Method for Rubber Property - Durometer Hardness*.

ASTM G115. (1998). *Standard Guide for Measuring and Reporting Friction Coefficients*.

Aström, K. J., & Canudas-De-Wit, C. (2008). *Revisiting the LuGre Model: Stick-slip motion and rate dependence*.

Atkins, P. W. (2021, September 24). *chemical bonding*. Encyclopedia Britannica. https://www.britannica.com/science/chemical-bonding

Balci, M. N. (2021). Implementation of Dahl's dynamic friction model to contact mechanics of elastic solids. *SN Applied Sciences*, *3*. https://doi.org/10.1007/s42452-020-03989-0

Bartenev, G. M., Lavrentev, V. V., Payne, D. B., Lieng-Huang Lee, & Ludema, K. C. (1981). Wear of polymers. In *Friction and wear of polymers* (Vol. 6, pp. 202–205).

Berman, A. D., Ducker, W. A., & Israelachvili, J. N. (1996). *Origin and Characterization of Different Stick-Slip Friction Mechanisms*. https://pubs.acs.org/sharingguidelines

Berthoud, P., Baumberger, T., G'sell, C., & Hiver, J.-M. (1999). *Physical analysis of the state- and rate-dependent friction law: Static friction*.

Bowden, F. P., & Tabor, D. (1966). *Friction, lubrication and wear: a survey of work during the last decade* (Vol. 17).

Brinson, H. F., & Brinson, L. C. (2015). Dynamic Properties: Steady State Oscillation Testing. In *Polymer Engineering Science and Viscoelasticity* (2nd ed., pp. 191–208). Springer. https://doi.org/10.1007/978-1-4899-7485-3

Briscoe, B. J., & Tabor, D. (1978). *Friction and Wear of Polymers: The Role of Mechanical Properties*.

Capanidis, D., & Sokolska, J. (2018). Effect of contact pressure and sliding speed on the friction of polyurethane elastomer (EPUR) during sliding on steel under water wetting conditions. *Open Engineering*, *8*(1), 545–551. https://doi.org/10.1515/eng-2018-0064

Capanidis, D., & Sokolska, J. (2020). The effect of pressure and time of stationary contact under load on the static friction coefficient of polyurethane elastomers (EPUR) during friction on steel in various lubricating conditions. *Tribologia*, *289*(1), 21–29. https://doi.org/10.5604/01.3001.0014.0835

Chai, T., & Draxler, R. R. (2014). Root mean square error (RMSE) or mean absolute error (MAE)? - Arguments against avoiding RMSE in the literature. *Geoscientific Model Development*, *7*(3), 1247–1250. https://doi.org/10.5194/gmd-7-1247-2014

DEME. (2016). *Internal image friction support interface of monopile sea fastening [Image]*.

DEME. (2018). *Internal image friction-based monopile sea fastening [Image]*.

Dillavou, S., & Rubinstein, S. M. (2019). *Shear Destruction of Frictional Aging and Memory*. https://doi.org/10.1103/PhysRevLett.124.085502

DIN 53505. (2000). *Shore A and Shore D hardness testing of rubber*.

DNVGL-RU-SHIP-Pt3Ch4. (2018). *Rules for Classification: Ships*. http://www.dnvgl.com,

DNVGL-ST-0358 5.2.1. (2021). *Offshore gangways: Functional requirements*.

DNVGL-ST-0378 1.1.7. (2019). *Offshore and platform lifting appliances: Design temperature*.

DNVGL-ST-N001 3.1.1. (2020). *Marine operations and marine warranty: Environmental conditions and criteria*.

DNVGL-ST-N001 3.2.1. (2020). *Marine operations and marine warranty: Environmental conditions and criteria*.

DNVGL-ST-N001 5.4.4. (2020). *Marine operations and marine warranty: Testing of friction*.

DNVGL-ST-N001 11.9.2. (2020). *Marine operations and marine warranty: Friction - general*.

Dong, C., Shi, L., Li, L., Bai, X., Yuan, C., & Tian, Y. (2017). Stick-slip behaviours of water lubrication polymer materials under low speed conditions. *Tribology International*, *106*, 55–61. https://doi.org/10.1016/j.triboint.2016.10.027

DT Hydraulics. (n.d.). *Specialist in hydraulische aandrijvingen [Online Image]*. Retrieved December 21, 2021, from https://www.dt-hydraulics.nl/projecten-hydrauliek/hydraulisch-systeem-seafastening-en-upend-frame-/

Duerst, A. (2016, March 7). *The world's largest monopile to date is being moved out of production hall 5 in Rostock [Online image]*.

Dutch Government. (2019). *Climate Agreement*.

Enqvist, O., Jiang, F., & Kahl, F. (2011). A brute-force algorithm for reconstructing a scene from two projections. *Proceedings of the IEEE Computer Society Conference on Computer Vision and Pattern Recognition*, 2961–2968. https://doi.org/10.1109/CVPR.2011.5995669

European Commission. (2020). *Offshore renewable energy for a climate-neutral Europe*. https://ec.europa.eu/environment/nature/natura2000/management/pdf/guidance_on_energy_transmission_infrastr

Flores, P., Lankarani, H. M., & Marques, F. (2016). *Study of Friction Force Model Parameters in Multibody Dynamics*. https://www.researchgate.net/publication/303677516

Gao, J., Luedtke, W. D., Gourdon, D., Ruths, M., Israelachvili, J. N., & Landman, U. (2004). Frictional forces and Amontons' law: From the molecular to the macroscopic scale. *Journal of Physical Chemistry B*, *108*(11), 3410–3425. https://doi.org/10.1021/jp036362l

Hutchings, I. M. (2016). Leonardo da Vinci's studies of friction. *Wear*, *360–361*, 51–66. https://doi.org/10.1016/j.wear.2016.04.019

IDM instruments. (n.d.). *Coefficient of friction tester - standard [Online image]*.

Igea, F., & Cicirello, A. (2018). A vibro-acoustic quality control approach for the elastic properties characterisation of thin orthotropic plates. *Journal of Physics: Conference Series*, *1106*(1). https://doi.org/10.1088/1742-6596/1106/1/012031

Igea, F., & Cicirello, A. (2020). Part-to-part variability assessment of material properties for flat thin orthotropic rectangular panels using Chladni patterns. *Mechanical Systems and Signal Processing*, *139*. https://doi.org/10.1016/j.ymssp.2019.106559

ISO 8295. (1995). *Plastics - Films and sheeting - Determination of the coefficients of friction*.

ISO 19840. (2012). *Paints and varnishes — Corrosion protection of steel structures by protective paint systems — Measurement of, and acceptance criteria for, the thickness of dry films on rough surfaces*.

Ivkovic, B., Djurdjanovic, M., & Stamenkovic, D. (2000). *The Influence of the Contact Surface Roughness on the Static Friction Coefficient*.

JIS B 0601. (1994). *Surface Roughness*.

Johannes, V. I., Green, M. A., & Brockley, C. A. (1973). The role of the rate of application of the tangential force in determing the static friction coefficient. In *Wear*. Elsevier Sequoia S.A.

Kaynia, A. M. (2019). Seismic considerations in design of offshore wind turbines. *Soil Dynamics and Earthquake Engineering*, *124*, 399–407. https://doi.org/10.1016/j.soildyn.2018.04.038

Kennedy, F. E., Lu, Y., & Baker, I. (2015). Contact temperatures and their influence on wear during pin-on-disk tribotesting. *Tribology International*, *82*(PB), 534–542. https://doi.org/10.1016/j.triboint.2013.10.022

KNMI. (n.d.). *Waarneemstations op de Noordzee [Online image]*.

KNMI. (2020a). *Uurgegevens van station 201 - D15-FA-1 [Data set]*.

KNMI. (2020b). *Uurgegevens van station 206 - F16-A [Data set]*.

KNMI. (2020c). *Uurgegevens van station 212 - Hoorn-Alfa [Data set]*.

KNMI. (2020d). *Uurgegevens van station 321 - Euro Platform [Data set]*.

Laber, A. (2012). *Selection of polyurethane for the fiction pair of a drilling machine due to tribological properties*.

Lampaert, V., Swevers, J., & Al-Bender, F. (2002). Modification of the Leuven Integrated Friction Model Structure. *IEEE Transactions on Automatic Control*, *47*(4), 683–687. https://doi.org/10.1109/9.995050

Ludema, K. C., & Tabor, D. (1966). *The friction and visco-elastic properties of polymeric solids*.

Lundgren, V. (2016). *Stick-Slip Friction in Polymer-Polymer Contacts*.

Malvern Instruments Limited. (2016). *A Basic Introduction to Rheology*.

Myshkin, N. K., & Kovalev, A. v. (2009). Adhesion and friction of polymers. In *Polymer Tribology* (pp. 3–37). Imperial College Press. https://doi.org/10.1142/9781848162044_0001

Myshkin, N. K., Petrokovets, M. I., & Kovalev, A. v. (2005). Tribology of polymers: Adhesion, friction, wear, and mass-transfer. *Tribology International*, *38*(11-12 SPEC. ISS.), 910–921. https://doi.org/10.1016/j.triboint.2005.07.016

Negro, V., López-Gutiérrez, J. S., Esteban, M. D., Alberdi, P., Imaz, M., & Serraclara, J. M. (2017). Monopiles in offshore wind: Preliminary estimate of main dimensions. *Ocean Engineering*, *133*, 253–261. https://doi.org/10.1016/j.oceaneng.2017.02.011

NEN-EN-ISO 868. (2003). *Plastics and ebontie - Determination of indentation hardness by means of a durometer (Shore hardness)*.

NEN-EN-ISO 12944. (2018). *Paints and varnishes - Corrosion protection of steel structures by protective paint systems*.

NEN-EN-ISO 21920-2. (2022). *Geometrical product specifications (GPS) - Surface textures: Profile - Part 2: Terms, definitions and surface texture parameters*.

Olsson, H., Aström, K. J., Canudas de Wit, C., Gäfvert, M., & Lischinsky, P. (1997). Friction Models and Friction Compensation. *European Journal of Control*, 176–196.

Pennestrì, E., Rossi, V., Salvini, P., & Valentini, P. P. (2016). Review and comparison of dry friction force models. In *Nonlinear Dynamics* (Vol. 83, Issue 4, pp. 1785–1801). Springer Netherlands. https://doi.org/10.1007/s11071-015-2485-3

Petkov, P. v., & Radoev, B. P. (2014). Statics and dynamics of capillary bridges. *Colloids and Surfaces A: Physicochemical and Engineering Aspects*, *460*, 18–27. https://doi.org/10.1016/j.colsurfa.2014.03.038

Piatkowski, T. (2014). Dahl and LuGre dynamic friction models - The analysis of selected properties. *Mechanism and Machine Theory*, *73*, 91–100. https://doi.org/10.1016/j.mechmachtheory.2013.10.009

Popov, V. L. (2010). Contact mechanics and friction: Physical principles and applications. In *Contact Mechanics and Friction: Physical Principles and Applications*. Springer Berlin Heidelberg. https://doi.org/10.1007/978-3-642-10803-7

Popova, E., & Popov, V. L. (2015). The research works of Coulomb and Amontons and generalized laws of friction. *Friction*, *3*(2), 183–190. https://doi.org/10.1007/s40544-015-0074-6

Rabbi, F., Khalil, A., Khan, I., Almuqrin, M. A., Khalil, U., & Andualem, M. (2022). Robust model selection using the out-of-bag bootstrap in linear regression. *Scientific Reports*, *12*(1), 10992. https://doi.org/10.1038/s41598-022-14398-1

Rabinowicz, E. (1951). The nature of the static and kinetic coefficients of friction. *Journal of Applied Physics*, *22*(11), 1373–1379. https://doi.org/10.1063/1.1699869

Ren, Y., Zhang, L., Xie, G., Li, Z., Chen, H., Gong, H., Xu, W., Guo, D., & Luo, J. (2021). A review on tribology of polymer composite coatings. *Friction*, *9*(3), 429–470. https://doi.org/10.1007/s40544-020-0446-4

Richardson, R. S. H., & Nolle, H. (1976). Surface friction under time-dependent loads. In *Wear* (Vol. 37). Elsevier Sequoia S.A.

Sakaguchi, R., Ferracane, J., & Powers, J. (2019). Chapter 4 - Fundamentals of Materials Science. In *Craig's Restorative Dental Materials (Fourteenth Edition)* (pp. 29–68).

Shi, L., Sikavitsas, V. I., & Striolo, A. (2011). Experimental friction coefficients for bovine cartilage measured with a pin-on-disk tribometer: Testing configuration and lubricant effects. *Annals of Biomedical Engineering*, *39*(1), 132–146. https://doi.org/10.1007/s10439-010-0167-3

Sif Group. (2021, March 10). *Sif Rolls Out First Hollandse Kust Zuid TP-Less Monopiles [Online image]*.

Stachowiak, G. W., Batchelor, A. W., & Stachowiak, G. B. (2004a). Measurement of Friction and Wear. In *Experimental Methods in Tribology* (Vol. 44, pp. 79–102).

Stachowiak, G. W., Batchelor, A. W., & Stachowiak, G. B. (2004b). Tribometers. In *Experimental Methods in Tribology* (Vol. 44, pp. 25–78).

Swevers, J., Al-Bender, F., Ganseman, C. G., & Prajogo, T. (2000). An Integrated Friction Model Structure with Improved Presliding Behavior for Accurate Friction Compensation. *IEEE Transactions On Automatic Control*, *45*(4), 675.

Tabor, D. (1970). *The hardness of solids*. http://iopscience.iop.org/0034-6683/1/3/I01

TNO. (n.d.). *Design limitations for large monopiles*. Retrieved December 22, 2021, from https://www.tno.nl/en/focus-areas/energy-transition/roadmaps/renewable-electricity/wind-energy/support-structure-wind-turbine/design-large-monopiles/

Tonazzi, D., Massi, F., Baillet, L., Culla, A., di Bartolomeo, M., & Berthier, Y. (2015). Experimental and numerical analysis of frictional contact scenarios: from macro stick–slip to continuous sliding. *Meccanica*, *50*(3), 649–664. https://doi.org/10.1007/s11012-014-0010-2

TWD. (2019). *Internal data set lubrication effect: unpublished [Data set]*.

TWD. (2020a). *Internal data set hardness effect: unpublished [Data set]*.

TWD. (2020b). *Internal data set pressure effect: unpublished [Data set]*.

TWD. (2021a). *Internal data set coating thickness effect: unpublished [Data set]*.

TWD. (2021b). *Internal data set monopile roughness effect: unpublished [Data set]*.

TWD. (2021c). *Internal data set PU roughness effect: unpublished [Data set]*.

TWD. (2021d). *Internal data set temperature effect: unpublished [Data set]*.

TWD. (2022). *Internal data set rate of loading effect: unpublished [Data set]*.

Viswanathan, K., Sundaram, N. K., & Chandrasekar, S. (2016). Stick-slip at soft adhesive interfaces mediated by slow frictional waves. *Soft Matter*, *12*(24), 5265–5275. https://doi.org/10.1039/c6sm00244g

Wahlström, J., Lyu, Y., Matjeka, V., & Söderberg, A. (2017). A pin-on-disc tribometer study of disc brake contact pairs with respect to wear and airborne particle emissions. *Wear*, *384–385*, 124–130. https://doi.org/10.1016/j.wear.2017.05.011

Wang, L., Zhou, J., Duszczyk, J., & Katgerman, L. (2012). Friction in aluminium extrusion - Part 1: A review of friction testing techniques for aluminium extrusion. *Tribology International*, *56*, 89–98. https://doi.org/10.1016/j.triboint.2012.01.012

Windenergie Nieuws. (n.d.). *Eerste lading funderingen voor Hollandse Kust Zuid is onderweg | Windenergie Nieuws*. Retrieved December 21, 2021, from https://windenergie-nieuws.nl/05/eerste-lading-funderingen-voor-hollandse-kust-zuid-is-onderweg/

Ying, S., & Yupeng, Y. (2017). Temperature field analysis of pin-on-disk sliding friction test. *International Journal of Heat and Mass Transfer*, *107*, 339–346. https://doi.org/10.1016/j.ijheatmasstransfer.2016.11.047

Yoshizawa, H., Chen, Y.-L., & Israelachvili, J. (1993). Fundamental Mechanisms of Interfacial Friction. 1. Relation between Adhesion and Friction. In *J. Phys. Chem* (Vol. 97). https://pubs.acs.org/sharingguidelines

Yuan, G., & Yao, S. (2013). A BFGS algorithm for solving symmetric nonlinear equations. *Optimization*, *62*(1), 85–99. https://doi.org/10.1080/02331934.2011.564621

Zhou, Y. J., Wang, D. G., & Guo, Y. B. (2017). The reduction of static friction of rubber contact under sea water droplet lubrication. *Lubricants*, *5*(12). https://doi.org/10.3390/lubricants5020012

Zuleeg, J. (2015). How to measure, prevent, and eliminate stick-slip and noise generation with lubricants. *SAE Technical Papers*, *2015-June*. https://doi.org/10.4271/2015-01-2259